Performance of Discrete Fractional Fourier Transform Classes in Signal Processing Applications

A thesis submitted
in fulfillment of the requirement for the award of degree
of
Doctor of Philosophy

Submitted by

KULBIR SINGH

Supervisor

Prof. RAJIV SAXENA
Head, Department of Electronics Engineering
Madhav Institute of Technology and Science, Gwalior (M.P.)
India

[*Formerly: Head, Department of Electronics and Communication Engineering*
Thapar Institute of Engineering and Technology, Patiala (*Punjab*) *India*]

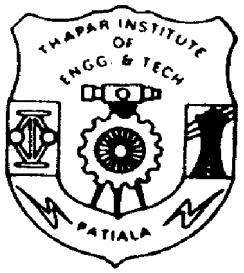

DEPARTMENT OF ELECTRONICS AND COMMUNICATION ENGINEERING
THAPAR INSTITUTE OF ENGINEERING AND TECHNOLOGY, PATIALA
(Deemed University)

CERTIFICATE

Certified that the thesis entitled "***Performance of Discrete Fractional Fourier Transform Classes in Signal Processing Applications***" being submitted by **Mr. Kulbir Singh** to the **Department of Electronics and Communication Engineering, Thapar Institute of Engineering and Technology, Patiala** in fulfillment of the requirements for the award of degree of **"Doctor of Philosophy"** is a record of bonafide research work carried out by him. He has worked under my guidance and supervision and fulfilled the requirements for the submission of this thesis which has reached the requisite standard. The matter presented in this thesis does not incorporate any material previously published or written by any other person except where due reference is made in the text.

The results contained in this thesis have not been submitted in part or full to any other institute or university for the award of degree or diploma.

(Dr. Rajiv Saxena)
Professor and Head,
Department of Electronics Engineering
Madhav Institute of Technology and Sciences,
Gwalior (M.P.) - 474005
India

ACKNOWLEDGEMENT

Walking on the trail blazed by an exemplary phenomenon Baba Ji – the Supreme Commander of my life, I humbly and earnestly would like to thank one and all who acted as building material in the citadel of my success.

Although the Knowledge like electricity pervades everywhere yet the Teacher is the point where it shines as light. I am extremely lucky to have an opportunity to blossom under the supervision and guidance of Dr. Rajiv Saxena, Professor, Department of Electronics Engineering, Madhav Institute of Engineering and Sciences, Gwalior who helped me to grow like Phoenix out of the ashes of my shortcomings and failures. His charismatic personality delves in knowledge to bring zeal and enlightenment in the lives of not only his students but also the humanity. To me, he is not mere a man but a current of love who treaded with me through thick and thin.

Dr. S.C. Saxena, Director, TIET, Patiala, Prof. R.S. Kaler Head of Department, Electronics and Communication Engineering and my colleagues supported me in this endeavour to the best of their possibilities. I am modestly bowing my head in the feet of divine Lord to thank them all for their love, support and sacrifices.

Of course, I thankfully acknowledge my fellow research scholars Mr. S. N. Sharma, Mr. Alok Jain and Mr. Rajesh Khanna who helped with their discussions to have clearer conceptions in this study.

A boat held to its moorings will see the floods pass by; but detached of its moorings, may not survive the flood. The support of all the members of family enthused me to work even while facing the Blues. I take pride of myself in being the son of ideal parents who sacrificed their little joys to bring me to the realization of my dreams and

their hopes. It is said that realization comes to those who are immersed in love. It is undoubtedly a rare bliss to be a son of compassionate and affectionate parents who priortise you above everything in their lives. Lady luck has graced me with loving wife, brothers, sisters and little Gurshabd - my son all of whom acted as props to my success.

My maternal uncle Mr. Raminderjit Singh Randhawa is the ocean of support who uplifted my consciousness by touching the highest recesses of my heart. No word in this universe can help me to acknowledge his role as a Comforter. This work would never have started without Master Puran Singh –a paragon of '*sewa*' who firstly asked me to strive to look for my potential in this field.

I am laying before you the result of numerous sleepless nights, strenuous hard work, determined and gritty solutions of the fights with my own self but everything is possible only with Almighty's grace as:

"What you make me know,
That alone I know,
What you make me see,
That alone I see."

Kulbir Singh
(Kulbir Singh)

ABSTRACT

Given the widespread use of ordinary Fourier transform in science and engineering, it is important to recognize this integral transform as the fractional power of FT. Indeed, it has been this recognition, which has inspired most of the many recent applications replacing the ordinary FT with FrFT (which is more general and includes FT as special case) adding an additional degree of freedom to problem, represented by the fraction or order parameter *a*. This in turn may allow either a more general formulation of the problem or improvement based on possibility of optimizing over *a* (as in optimal wiener filter resulting in smaller mean square error at practically no additional cost). The FrFT has been found to have several applications in the areas of optics and signal processing and it also lead to generalization of notion of time (or space) and frequency domains which are central concepts of signal processing. In every area where FT and frequency domain concepts are used, there exists the potential for generalization and implementation by using FrFT.

With the advent of computers and enhanced computational capabilities the Discrete Fourier Transform (DFT) came into existence in evaluation of FT for real time processing. Further these capabilities are enhanced by the introduction of DSP processors and Fast Fourier Transform (FFT) algorithms. On similar lines, so there arises a need for discretization of FrFT. Furthermore, DFT is having only one basic definition and nearly 200 algorithms are available for fast computation of DFT. But when FrFT is analysed in discrete domain there are many definitions of Discrete Fractional Fourier Transform (DFrFT). These definitions are broadly classified according to the methodology of computation adopted.

In the current study the various class of DFrFT algorithms are studied and compared on the basis of computational complexity, deviation factor, properties of FrFT retained by particular class and constraints on the order or fraction parameter *a* etc.

As discussed earlier, the FrFT has found a lot of applications in signal processing, so the DFrFT is used for some of the one-dimensional and two-dimensional applications in the present work. The one dimensional applications discussed include filtering using window functions, optimal filtering of faded signals, beamforming for the mobile antenna and optimal beamforming in faded channels. In the two dimensional applications the image processing for compression and encryption are discussed.

Window functions have been successfully used in various areas of filtering, beam forming, signal processing and communication. The role of windows is quite impressive and economical from the point of view of computational complexity and ease associated with its application. An attempt has been made to evaluate the window functions in FrFT domain. The study of side lobe fall of rate (SLFOR), main side lobe level (MSLL) and half main lobe width (HMLW) for window functions are done for different values of *a*.

A new FrFT based Minimum Mean Square Error (MMSE) filtering technique is also suggested and it is also established that the results are much better as compared to FT. The signals in real life are non-stationary random processes. This may be attributed to the randomness of signals due to variation in amplitude and phase and associated Doppler shift, delay spread etc (as in the case of mobile sources and receivers). The multipath environment of mobile communication also makes the signal non-stationary due to changing spatial position with time. In these type of applications, where signal and noise both are non-stationary (time–frequency varying) FrFT is a powerful tool in

designing an optimal filter. The proposed filter is compared with time and frequency domain filtering. This algorithm is also used as an optimal beamformer for mobile and wireless communication, as in this is also an example of non-stationary signal and noise. This beamforming technique also works more efficiently for faded signals.

The FrFT and FrCT are used for image compression and the results are much better than FT. It is also shown that in compression the FrFT gives better results than FrCT. The image encryption is also done using FrCT and phase masking. This technique gives an advantage of additional keys i.e. order parameter of the transform. The number of these additional keys can be further enhanced by using repetition the FrCT with various orders.

The merits of FrFT are that it is not only richer in theory and more flexible in application but the cost of implementation is also low as it can be implemented with same complexity as that of conventional Fast Fourier transform. The FrFT provides additional degree of freedom to the problem as parameter *a* gives multidirectional applications in various areas of optics and signal processing in particular and physics and mathematics in general. The most important aspect of the FrFT is its use in time varying signals for which the FT fails to work.

In past few years researchers are trying to fractionalize every transform so as to formulate a more general problem. It is obvious this that an era has been opened up for a generalization of the problems to get better results in every area of engineering by using Fractional Domains of a Transform opening up a new signal processing technique may be referred as FRACTIONAL SIGNAL PROCESSING.

The advances in FrFT are multidimensional but still it is interesting to note that the algebra of Fractional Fourier domain is far from complete at present and there are several unforeseen identities and results to be derived.

TABLE OF CONTENTS

LIST OF TABLES

LIST OF FIGURES

ACRONYMS AND ABBREVIATIONS

FT	Fourier Transform
FrFT	Fractional Fourier Transform
LCT	Linear Canonical Transform
DFT	Discrete Fourier Transform
FFT	Fast Fourier Transform
DFrFT	Discrete Fractional Fourier Transform
TFD	Time–Frequency Distributions
FrCT	Fractional cosine Transform
DFrCT	Discrete Fractional cosine Transform
DAFT	Discrete Affine Fourier Transform
MSE	Mean Square Error
CFrFT	Chirp Fractional Fourier Transform
WFrFT	Weighted Fractional Fourier Transform
CT	cosine Transform
WDF	Wigner distribution function
DRFT	Discrete Rotational Fourier Transform
IDFrFT	Inverse Discrete Fractional Fourier Transform
FIR	Finite Impulse Response
MSLL	Main Side Lobe Level
HMLW	Half Main Lobe Width
SLFOR	Side Lobe Fall Off Rate
SAR	Selectivity Amplitude Ratio
MLW	Main Lobe width
AWGN	Additive White Gaussian Noise
MMSE	Minimum Mean Squared error
SNR	Signal to Noise Ratio
PSNR	Peak Signal to Noise Ratio
DCT	Discrete cosine Transform
CR	Compression Ratio

GLOSSARY OF SYMBOLS

$f(x)$	Function $f(.)$ of independent variable x
$F(x_1)$	Fourier transform of $f(x)$
a	Fractional order parameter
$K^a(x, x_a)$	FrFT kernel, a function of x and x_a
$K^{-a}(x, x_a)$, $[K^a(x, x_a)]^{-1}$	Inverse FrFT kernel
$[K^a(x, x_a)]^*$	Complex conjugate of FrFT kernel
$F^a[f(x)]$	FrFT of a function $f(x)$ in a^{th} domain
$f^a(x_a)$	Function $f^a(.)$ in a^{th} domain of indepent variable x_a
$f(t)$	Function $f(.)$ of independent variable t (time domain)
$f(f)$	Function $f(.)$ of the independent variable f (frequency domain)
A_α	$\sqrt{1-i\cot\alpha}$
$\delta(x-x_a)$	Impulse function
π	Pi
α	Fractional order parameter in terms of angle $\alpha = a\pi/2$
I	Identity operator
F	Fourier operator
P	Time inversion operator
F^{-1}	Inverse Fourier operator
F^a	FrFT operator of order a
F^{-a}	Inverse FrFT operator of order a
j	An integer variable
sgn(.)	Signum function
ε	infinitesimal interval
$\psi_l(x)$	Hermite-Gaussian function
λ	Eigenvalue
Σ	Summation

W_f	Wigner distribution of a signal
M	Two-dimensional rotation matrix in the time-frequency plane
C_l	Coefficients of Hermite-Gaussian Polynomials
ξ	$\xi = \gamma = \cot\alpha$
β	$\csc\alpha$
U	Coordinate multiplication operator
D	Differentiation operator
U^a	Multiplication by the coordinate variable in the a^{th} order fractional Fourier domain
D^a	Differentiation with respect to the coordinate variable in the a^{th} order fractional Fourier domain
H	Quadratic Hermitian operator
K^{-a}	Inverse FrFT kernel
l	Order of Hermite-Gaussian Function
C^M	Linear canonical transform operator
$C^M(x, x')$	Linear canonical transform kernel
Γ	$\Gamma(z)$ is a complex variable whose polynomial series is defined as $\Gamma(z) = \sum_{n=0}^{\infty} \Gamma_n z^n$
mod	Modulus operator
$\|f\|$	Energy of signal
$\langle\ \rangle$	Ensemble average
τ	Delay
Im	Imaginary part of complex number
Re	Real part of complex number
F_s^a	Fractional sine transform of order α
F_c^a	Fractional cosine transform of order α
ν	Scaled frequency domain variable
$\lvert f(x)\rvert$	Absolute value of $f(x)$
$g(x)$	Function $g(.)$ of independent variable x
c_n	Coefficient of n^{th} point

n	Discrete time domain variable
N	Number of points of a variable in discrete domain
Δt	Small time period
t	Continuous time domain variable i.e. when domain $a = 0$
S	Scaling parameter
f	Continuous frequency domain variable i.e. when $a = 1$
Δf	Small frequency bandwidth
Δx	Length of signal in all domains
$h(x)$	Function $h(.)$ of independent variable x
$\mathbf{f}$	column vectors with N elements containing the samples of $f(x)$
$\mathbf{f}^a$	column vectors with N elements containing the samples of $f^a(x_a)$
$\mathbf{D}$	Matrix representing decimation operation
$\mathbf{J}$	Matrix representing interpolation operation
	Diagonal matrix that corresponds to chirp multiplication
H_{lp}	Convolution operation
W_{nk}	Discrete Fourier transform matrix
W	Discrete Fourier transform operator
$R(\theta)$	A matrix
θ	Angle
A^{γ}	Sympletic transformation corresponding to rotation
Δ_0	Period in time domain
Δ_{α}	Period in a^{th} domain
$\bar{\delta}^a[f(x)]$	FrFT of uniform impulse train in a^{th} domain
$\#(.)$	A multiplicity function
m	Multiplicity of eigenvalues of DFT
E_0–E_3	Eigenspaces of eigenvectors of DFT i.e. (1,-j,-1,j) respectively
ω	Angular frequency
S	A matrix

$\bar{u}_n$	Eigenvector of DFT corresponding to the n^{th} order discrete Hermite function
T_s	Sampling interval
$\phi_n(k)$	Sampled n^{th} order Hermite polynomial
U	Matrix of the normalized eigenvector corresponding to the n^{th} order Hermite function
u_n	Continuous Hermite samples vector
$\overline{u}_n$	DFT Hermite eigenvectors (projections of u_n in its DFT eigensubspace)
$\tilde{u}_n$	Non-orthogonalised Hermite eigenvectors
$\hat{u}_n$	Orthogonalised Hermite eigenvectors
$\| \ \|_F$	Frobenius norm of a matrix
fft(i)	i^{th} sample of FFT of a function
Dfrft(i)	i^{th} sample of DFrFT of a function
$\eta(x)$	Additive white Gaussian noise
$h_d(x, x_a)$	The kernel of the linear system that distorts or blurs the desired signal $f(x)$
Λ_h	Operator corresponding to multiplication by the filter function $h(x)$
$f_{\mathbf{est}}(x)$	Estimation of $f(x)$
σ^2_{err}	Mean square error
$R_{fg}(x, x_a)$	Cross-correlation of $f(x)$ and $g(x_a)$
$R_{gg}(x, x_a)$	Auto-correlation of $g(x)$
$R_{\eta\eta}(x, x_a)$	Auto-correlation of $\eta(x)$
G	Column vector of *N* elements corresponding to $g(x)$
η	Column vector of *N* elements corresponding to $\eta(x)$
$\mathbf{R}_{\mathrm{ff}}$	Correlation matrix of **f**
$\mathbf{R}_{\eta\eta}$	Cross-correlation matrix of η
$\mathbf{R}_{\mathrm{fg}}$	Cross-correlation matrix of **f** and **g**
$\mathbf{R}_{\mathrm{gg}}$	Correlation matrix of **g**

$\mathbf{f}_{\text{est}}$	Estimation of **f**
$\mathbf{g}^a$	Column vector of *N* elements corresponding to $g^a(x_a)$
$\mathbf{R}_{\mathbf{f}^a\mathbf{g}^a}$	Cross-correlation of $\mathbf{f}^a$ and $\mathbf{g}^a$
$\mathbf{R}_{\mathbf{g}^a\mathbf{g}^a}$	Correlation of $\mathbf{g}^a$
x_c	Frequency of unmodulated carrier
x_d	Doppler shift in frequency
R_D	Redundancy of data
$f(x, y)$	Function of two variables *x* and *y* used for analog image
$f(i, j)$	Function of two variables *i* and *j* used for digital image
$g(i, j)$	Function of two variables *i* and *j* used for digital decompressed image
$f(x_0, y_0)$	Real valued two-dimensional data for image
$H_1(x, y)$	Random phase masks
$\phi_2(x, y)$	randomly generated homogeneously distributed functions

CHAPTER 1

INTRODUCTION

1.1 PREAMBLE

Fourier analysis, given by Jean-Baptiste-Joseph Fourier (1768-1830), is a frequently used tool in signal processing and analysis. Fourier Transform (FT) finds applications in many areas of science and engineering. Optics, physics, acoustics, statistics, heat conduction and diffusion, electrical engineering, antenna and array processing are some areas where this transform is widely applicable. It is a linear transform used to solve linear system problems. Impressed by the capability of this transform Wittaker placed it amongst the three most important mathematical advances of the last quarter of the 19^{th} century. However, the FT is unable to solve certain classes of ordinary and partial differential equations of optics, signal processing and quantum mechanics [1].

Looking into the applicability of FT the concept of fraction was introduced in the FT in the year 1929 [2] and lead to the development of fractional Fourier transform (FrFT). On tracing the history of fractional concept it is found that in 17^{th} century Bernoulli (1695) formulated a question about the meaning of a non-integer order derivative. This was the beginning of the fractional calculus which is the base of the continuous time fractional systems described by the fractional

differential equations. Since then, the concept of fractional calculus has evolved in pure mathematics and developed by famous mathematicians. Inspite of the progress in pure mathematics this concept had been applied in applied sciences only in 1920's. Furthermore, it is only in the last three decades that the applications of fractional calculus have emerged in engineering field which lead to a significant impact in several areas and attracted the scientific and technical community to the fractional objects. Presently, the related themes of active research are Brownian motion, discrete time fractional linear systems, fractional delay filtering, fractional splines and wavelets.

Also, worth mentioning is the fact that earlier most of the reported applications on FrFT were in the field of optics. Recently, the FrFT has also made inroad in the digital signal analysis and processing with filtering, encoding, watermarking, phase retrieval being the key application arenas [3].

1.2 HISTORICAL PERSPECTIVE OF FrFT

The generalization of FT called FrFT was first introduced in 1980 by Namias [4], apparently unaware of the previous work done by various researchers which dates back to 1929. All the authors discussed the FrFT in a broader context and not by the same name, although the idea was same. Mustard in 1987 [5]-[7] did a lot of work taking Condon [8] and Bargmann [9] as his base without citing the Namias work. Moreover, FrFT is a special case of linear canonical transform (LCT) and all the work previously done on LCT covers FrFT in some sense. In some cases FrFT

has not been given any special attention but in other cases the authors have commented on it as a one-parameter sub-class with the FT as a special case. Many variant, relatives or essentially equivalent forms of FrFT can be found under different guises but it is practically impossible to trace all of them [3].

A lot of work is done by Mendlovic, Ozaktas and Lohmann in years 1993 [10]-[13], 1994 [14], 1995 [15]-[16] and they established that various definitions of FrFT are equivalent to each other. Almedia, in 1993 [17], independently reintroduced the transform as 'angular' FT. Pei *et al.* also did a lot of work in 1990's to consolidate FrFT [18]-[27]. Furthermore, a general definition of FrFT for all classes of signals (one-dimensional and multidimensional, continuous and discrete, periodic and non-periodic) is given by Cariolario *et al.* in [28]. With the advent of computers the discrete Fourier transform (DFT) came into existence to evaluate FT of discrete time signals. This capability has been further enhanced by the introduction of DSP processors and fast Fourier transform (FFT) algorithms. On similar lines, there aroused a need for discretization of FrFT. DFT is having only one basic definition and nearly 200 FFT algorithms are available for fast computation of DFT. But when FrFT is analyzed in discrete domain there are many definitions of discrete fractional Fourier transform (DFrFT) [18]-[23], [27], [29]-[35]. It has also been established that none of these definitions satisfy all the properties of continuous FrFT [24]. Santhanam and McClellan first reported the work on DFrFT in 1995 [30]. Thereafter, within a short span of time many definitions of DFrFT came into existence and these definitions are classified according to the methodology used for calculations in 2000 by Pie *et al.* [24].

The FrFT has been found to have several applications in the areas of optics [10]-[12], [36]-[50] and signal processing [51]-[70] and it also leads to generalization of notion of space (or time) and frequency domains, which are central concepts of signal processing. Applications of FrFT have been reported in the solution of differential equations[3], [4], [71], optical beam propagation and spherical mirror resonators [40], optical diffraction theory [49], quantum mechanics [4], statistical optics [3], [38], [39], [47], optical system design and optical signal processing [42]-[45], signal detectors [64], [68], correlation [38], [64] and pattern recognition [52], space or time variant filtering [54], [56], [59], [63], [67], [70], multiplexing [72], signal and image recovery [51], [57]-[58], image restoration and enhancement [60], study of space or time–frequency distributions (TFD's) [26], [51], [56], etc. Thus, it can be said that the FrFT can replace the FT and related concepts.

1.3 FRACTIONAL OPERATIONS

Breaking up an entity into fractions represents a relatively major conceptual leap. For example, the fourth power of 3 can be defined as $3^4 = 3\times3\times3\times3$, but it is not obvious from this definition that how $3^{3.5}$ is defined. It must have taken sometime before the common definition $3^{3.5} = 3^{7/2} = \sqrt{3^7}$ emerged. Similarly, the first and second derivatives of the function $f(x)$ are commonly denoted by: $\frac{df(x)}{dx}$ and $\frac{d^2 f(x)}{dx} = \frac{d}{dx}\left[\frac{df(x)}{dx}\right] = \frac{d[df(x)/dx]}{dx} = \left(\frac{d}{dx}\right)^2 f(x)$, respectively.

Similarly, higher order derivatives can be defined in the same way. But what is meant by the 2.5^{th} derivative of a function is not clear from the above definition. Let $F(x_a)$ denote the FT of

$f(x)$. The FT of the nth derivative of $f(x)$ [i.e., $\frac{d^n f(x)}{dx^n}$] is given by $(i2\pi x_a)^n F(x_a)$, for any positive integer *n*. The generalized property is obtained by replacing n with the real order *a* and take it as the a^{th} derivative of $f(x)$. Thus to find $\frac{d^a f(x)}{dx^a}$, the a^{th} derivative of $f(x)$, calculate the inverse Fourier transform of $(i2\pi x_a)^a F(x_a)$.

Above examples deal with the fractions of an operation performed on an entity, rather than fractions of the entity itself. The $3^{0.5}$ is the square root of the integer 3. The function $[f(x)]^{0.5}$ is the square root of the function $f(x)$. But $\frac{d^{0.5} f(x)}{dx^{0.5}}$ is the 0.5th derivative of $f(x)$, with $\left(\frac{df(x)}{dx}\right)^{0.5}$ being the square root of the derivative operator $\frac{d}{dx}$. Bracewell [1] has shown that the fractional derivatives can be used to characterize the discontinuities of certain functions used in optics and signal processing. During the last two decades, the process of going from the whole of an entity to fractions of it underlies several interesting applications such as fractal objects, fuzzy logic and fractional signal processing. The fractional signal processing leads to a more general formulation of the problems that were solved by the integral transforms in the early days, because of the additional degree of freedom available with the designers. This in turn allows better performance or greater generality based on possibility of optimization over a fractional variable parameter *a*. The FrFT founds several applications in signal processing. Particularly, windowing, filtering, optimal filtering are the key areas in one-dimensional signal processing [59]-[60], [73]. Now, researchers are trying to get better results using FrFT as a tool. The capability of the FrFT is to significantly reduce the error as compared to FT for specific nature of degradation and noise

especially in Doppler shift and chirp signals [55], [67], [72]. A fast algorithm for computation of FrFT of order ($N \log_2 N$) is available so that real time implementation can easily be made without additional cost [24], [29].

One-dimensional fractional signal processing can be further extended to two-dimensional and multi-dimensional fractional signal processing. Their application includes image compression [74], image encryption [75], beamforming [55], digital watermarking [76], tomography [56], [62], image restoration [60] etc. The properties and implementation of two-dimensional FrFT has been reported by Sahin *et al.* [36]-[37], [77] and Edren *et al.* [45], [63]. Sahin *et al.* have generalized the two-dimensional FT into the two-dimensional separable FrFT and two-dimensional separable canonical transform. In another reported work Sahin *et al.* also generalized it into the two-dimensional non-separable FrFT with four parameters. Pei and Ding have introduced the two-dimensional affine generalized FrFT [25].

The FrFT has been used efficiently in image compression with better results in comparison to FT [74]. The image encryption is also done using FrFT and phase masking [75]. This technique gives an advantage of additional keys, i.e., order parameter of the transform. The number of additional keys can be further enhanced by repetition of the FrFT with various orders which leads to the multi-dimensional fractional signal processing.

From the implementation point of view discretized version of FrFT known as DFrFT is used in all of the above mentioned one- and two-dimensional FrFT signal analysis. A good review work regarding different types of DFrFT is reported by Pei *et al.* [24]. In this article a new type of DFrFT which is unitary, reversible, flexible and has closed form analytical current DFrFT's that

were similar to the continuous FrFT but it puts certain constraints on the signal [24].With this brief presentation of chronological development of FrFT and its vast application expression was introduced. But, this DFrFT looses an important property of additivity. They also extended the DFrFT into the discrete affine Fourier transform (DAFT) and derived two types of DFrFT and DAFT. The closed form expression has the lowest complexity among all domain, the problems, attempted and included, in this study are formulated in the next section.

1.4 PROBLEM FORMULATION

The work in this thesis focuses on following aspects and applications of DFrFT:-

1. The available FrFT definitions are studied and equivalence between them has been verified with simulation studies. The properties of FrFT are also confirmed and demonstrated graphically.
2. The available classes of DFrFT have been studied and their comparative study has been carried out.
3. DFrFT has been applied and analysed in one dimensional time-frequency varying signal applications. Optimal filtering of faded signals, beamforming for the mobile antenna and optimal beamforming in faded channels have been selected as particular applications.
4. Applications of DFrFT in image compression and image encryption are discussed.
5. Two-dimensional signal processing applications using discrete fractional cosine transform (DFrCT) have been attempted and their performance with DFrFT is compared. Also a comparison has been done with wavelet transform.

1.5 ORGANISATION OF THE THESIS

The first chapter gives the historical perspective of FrFT and an introduction to fractional operations. The limitation of FT to solve certain classes of ordinary and partial differential equations of quantum mechanics, optics and signal processing is discussed. It is also established that FrFT is a powerful tool for the analysis of time varying signals with applications in one- and two-dimensional signal processing. In second chapter so far reported definitions of FrFT are reviewed with their brief introduction. The properties of FrFT are discussed and illustrated using Riemann function. In third chapter the description of DFrFT and its historical development is given. The various classes of the DFrFT are discussed and a comparative study is done. It is established that the eigenfunction of DFrFT is the best one, although it lacks closed form expression for precise calculations. Characterization of window functions in fractional Fourier domain is also done in this chapter. Applications of DFrFT in one dimensional signal processing are discussed in chapter four. Optimal filtering of faded signals, beamforming for the mobile antenna and optimal beamforming in faded channels are the applications included in this chapter. The optimal filtering in time and frequency domain becomes a special case of optimal filtering in the FrFT domain. This method is extremely useful for the signals having Doppler shift because of moving source or receiver. It has also been shown that using FrFT domain filtering the mean square error (MSE) gets reduced in case of moving sources and receivers. Chapter five contains the two dimensional applications of DFrFT and DFrCT. Compression and encryption of images are the applications undertaken. The performances of the two transforms for these applications are compared. Also a comparison with wavelet transform is accomplished. The DFrFT and DFrCT

give better results for image compression and image encryption respectively. It has also been shown that for very high compression ratios, FrFT gives better results for compression than wavelet transform. The last chapter concludes with critical discussion of results of the investigations carried out. Important observations are made and useful conclusions are drawn along with a discussion on future scope of this work.

CHAPTER 2

FRACTIONAL FOURIER TRANSFORM

2.1 INTRODUCTION

The FrFT is a generalization of FT, which is richer in theory, flexible in application, and implementation cost is at par with FT. With the advent of FrFT and related concept, it is seen that the properties and applications of the conventional FT are special cases of those of the FrFT. However, in every area where FT and frequency domain concepts are used, there exists the potential for generalization and implementation by using FrFT. In this chapter, the basic concept and properties of FrFT are described.

In 1929, Wiener, discussed a transformation kernel whose eigenfunctions are Hermite-Gaussian functions and it has eigenvalues which are of more general form than of ordinary FT eigenvalues [2]. The work by Wiener motivated Weyl to develop the integral transform relationship for providing a basis of developments in group theory and quantum mechanics. In 1937, Condon, discussed the generalization of FT to a continuous group of Functional transformation. Kober, in 1939, discussed Fractional Fourier and Hankel transform. He also provided general framework for consideration of other transforms in the same manner. In 1956, Gujnand, worked on the relationship between fractional transform and matrices. Bragmann in 1961 citing the work by Condon, and Bruijn in 1973 referred to Kober, briefly discussed the transform in a much broader context. Khare, in 1971, gave a generalized transform in a physical context,

which includes FrFT [3]. All these authors discussed the FrFT in a broader context and not by the same name, although the idea was same. In 1980, Namias discussed FrFT as the fractional powers of classical FT and gave several of its properties [4]. Mustard, in 1987, did a lot of work taking Condon and Bragmann as his base without citing Namias [5]-[7]. He discussed the relationship of FrFT to time-frequency distribution (Wigner distribution) and new classes of uncertainty relationships which are invariant under FrFT. Many variants, relatives or essentially equivalent forms of FrFT are found under different guises but it is practically impossible to trace all of them. In 1990's a lot of work is done by Mendlovic, Ozaktas, Lohmann, Almedia, Pei, Yeh, and Tseng to consolidate FrFT [3].

2.2 DEFINITIONS OF FrFT

As discussed earlier, FrFT is defined in many different ways. To have a complete understanding of the transform all definitions are discussed in detail, and thereafter established that they are equivalent to each other. All definitions have different physical interpretations which is very useful in a variety of applications. These definitions of FrFT are discussed below.

2.2.1 Linear Integral Transform

It is the most concrete and direct form of FrFT and is specified as a linear transform kernel. The a^{th} order FRFT of a function $f(x)$ is a linear operation defined by the integral [78]

$$F^{a}[f(x)] = \int_{-\infty}^{\infty} K^{a}(x, x_a) f(x) dx = f^{a}(x_a) \qquad (2.1)$$

where,

$K^{a}(x, x_a) = A_{\alpha} \exp[i\pi(x^2 \cot\alpha - 2xx_a \csc\alpha + x_a{}^2 \cot\alpha)]$ is FrFT kernel that transforms the function $f(x)$ in a domain x to a function $f^{a}(x_a)$ in another domain x_a and $\alpha = \frac{a\pi}{2}$. $f(x)$ is a

function of independent variable x and $f^{a}(x_a)$ is the function of independent variable x_a. F^{a} is the FrFT operator which acts on $f(x)$ to transform the function from an arbitrary domain to arbitrary plus a^{th} domain.

$A_\alpha = \sqrt{1 - i\cot\alpha}$ when $a \neq 2j$.

$K^{a}(x, x_a) = \delta(x - x_a)$ when $a = 4j$ and

$K^{a}(x, x_a) = \delta(x + x_a)$ when $a = \pm 2j$, where j is an integer.

In case the arbitrary domain is $a = 0$, i.e. $F^{0}[f(x)] = f(x) = f(t)$, the variable x becomes t (time variable) and $f(x)$ becomes $f(t)$. In case the arbitrary domain is $a = 1$, $F^{1}[f(x)] = F[f(x)] = f(f)$, the variable x becomes f (frequency) and $f(x)$ becomes $f(f)$ i.e. $f(.)$ is a function of f frequency.

The a^{th} order transform is also referred as α^{th} order transform. The square root is defined so that the argument of the result lies in the interval $(-\pi/2, \pi/2)$. The A_α can be written for the interval $0 < |a| < 2$ $(0 < |\alpha| < \pi)$ without any ambiguity as [71]

$$A_\alpha = \frac{e^{-i[\pi\,\mathrm{sgn}(\alpha)/4 - (\alpha/2)]}}{\sqrt{|\sin\alpha|}} \qquad (2.2)$$

where, sgn(.) is the signum function.

This definition is a one parameter sub-class of LCT. The transform is linear but not shift invariant (unless $a = 4j$), since the kernel is not the function of $(x - x_a)$ only. First of all the cases are examined when a is an integer. As j is an arbitrary integer, it is noted that $F^{4j} = F^{4j\pm 2}$ corresponds to an identity operator and the parity operator, where F^{a} is FrFT operator. The several cases of varying j are discussed below:

i) When $\alpha = 0$, i.e., $a = 0$, the transform kernel reduces to identity operation. This is attributed to the fact that as α approaches 0, $\sin\alpha$ approaches α and $\cot\alpha$ approaches $1/\alpha$. Using the fact that in sense of generalized functions [71]

$$\lim_{\varepsilon \to 0} \frac{1}{\sqrt{i\pi\varepsilon}} e^{(-x^2/i\varepsilon)} = \delta(x) \tag{2.3}$$

so that the (2.1) reduces to

$$F^0[f(x)] = \int_{-\infty}^{\infty} \delta(x - x_a) f(x) dx = f(x) \tag{2.4}$$

ii) When $\alpha = \pi/2$, i.e., $a = 1$

$$F^1[f(x)] = \frac{1}{\sqrt{2\pi}} \int_{-\infty}^{\infty} f(x) \exp(-ixx_a) dx \tag{2.5}$$

i.e., the ordinary FT.

A similar procedure can be applied to case

iii) When $\alpha = \pi$ i.e., $a = 2$ and the result turns out to be

$$F^2[f(x)] = \int_{-\infty}^{\infty} \delta(x + x_a) f(x) dx = f(-x) \tag{2.6}$$

So, for an angle from 0 to 2π, the value of a varies from 0 to 4 and the transform kernel is periodic with a period equal to 4. Table-2.1 gives the different kernels of FrFT for variation of a from 0 to 4. Thus, most of the attention is limited in the interval $a \in (-2,2]$ (or $\alpha \in (-\pi,\pi]$) and sometimes $a \in [0,4)$ (or $\alpha \in [0,2\pi)$) [29].

Table-2.1: Various kernels available with FrFT.

Value of parameter a	$\alpha = a\,\pi/2$	Kernel	Fractional operator	Operation on signal
$a = 0$ or $a = 4$	$\alpha = 0$ or $\alpha = 2\pi$	$\delta(x - x_a)$	$F^0 = F^4 = I$	Identity operator
$a = 1$	$\alpha = \pi/2$	$\exp(ixx_a)$	$F^1 = F$	Fourier operator
$a = 2$	$\alpha = \pi$	$\delta(x + x_a)$	$F^2 = P$	Time inversion operator
$a = 3$	$\alpha = 3\pi/2$	$\exp(-ixx_a)$	$F^3 = FF^2 = FP = PF = F^{-1}$	Inverse Fourier operator

2.2.2 Fractional Powers of Fourier Transform

The a^{th} order FrFT operation is defined as the fractional power of the FT operation. Let ψ_l (or $\psi_l(x)$) denote the Hermite-Gaussian signal (or function) which are eigensignals (or eigenfunctions) of the ordinary FT operation with respective eigenvalues λ_l. These eigenvalues are known to constitute an orthogonal basis for the space of well-behaved finite-energy signals (functions). The FrFT operation defined is linear and satisfies [71]

$$F^a[\psi_l(x)] = \lambda_l^a \psi_l(x) = \left(e^{-il\pi/2}\right)^a \psi_l(x) = e^{-ial\pi/2}\psi_l(x) \qquad (2.7)$$

This definition completely defines the FrFT by specifying its eigenfunctions and eigenvalues. It depends on the particular set of eigenfunctions chosen as well as on the particular way in which the a^{th} power of the eigenvalues are chosen. Several properties of FrFT (like special cases, index additivity property) are deduced easily from this definition in comparison to the linear integral transform definition [4], [71].

The given signal (function) is first expanded as a linear superposition of eigenfunctions of the FrFT, to calculate the fractional transform of a function $f(x)$ as:

$$f(x) = \sum_{l=0}^{\infty} C_l \psi_l(x) \tag{2.8}$$

where, $C_l = \int \psi_l(x_a) f(x_a) dx_a$

By taking the a^{th} order Fourier transform on both sides of (2.8)

$$F^a[f(x)] = \sum_{l=0}^{\infty} e^{-ial\pi/2} C_l \psi_l(x) = \int \sum_{l=0}^{\infty} e^{-ial\pi/2} \psi_l(x) \psi_l(x_a) f(x_a) dx_a \tag{2.9}$$

Comparing (2.9) with (2.1), yields

$$K^a(x, x_a) = \sum_{l=0}^{\infty} e^{-ial\pi/2} \psi_l(x) \psi_l(x_a) \tag{2.10}$$

The equation (2.10) is known as singular value decomposition (or spectral expansion) of the kernel of FrFT [3]. It is one of the properties of the Hermite-Gaussian functions. Hence, it can be said that the Hermite–Gaussian functions are indeed the eigenfunctions of the transform defined by (2.1) with the eigenvalues given by (2.7). It is also known that $\psi_0(x)$ and $\psi_1(x)$ are eigenfunctions with eigenvalue 1 and $\exp(-ia\pi/2)$. Then by using the recurrence relations of Hermite-Gaussian polynomials [11]

$$H_{l+1}(x) = 2xH_l(x) - 2lH_{l-1}(x), \tag{2.11}$$

$$\frac{dH_l(x)}{dx} = 2lH_{l-1}(x) \tag{2.12}$$

By assuming that the same result holds for (*l - 1*), *l* and (*l + 1*), therefore,

$$\psi_{l+1}(x) = 2\sqrt{2\pi}\,\frac{A_{l+1}}{A_l} x\psi_l(x) - 2l\frac{A_{l+1}}{A_{l-1}}\psi_{l-1}(x), \tag{2.13}$$

$$\frac{d\psi_l(x)}{dx} = \frac{A_l}{A_{l-1}} 2l\sqrt{2\pi}\psi_{l-1}(x) - 2\pi x\psi_l(x) \tag{2.14}$$

where, $A_l = 2^{1/4}/\sqrt{2^l l!}$.

From the above discussion it can be stated that Hermite-Gaussian functions are eigenfunctions of FrFT as defined in (2.1). It is also clear that sinusoidal functions are special case of Hermite-Gaussian functions, as FrFT reduces to ordinary FT, when $a = 1$.

2.2.3 Rotation in the Time-Frequency plane

The FrFT is directly defined as a special case of one-parameter sub-class of LCT. The a^{th} order FrFT is defined by the transform matrix

$$M = \begin{bmatrix} A & B \\ C & D \end{bmatrix} \equiv \begin{bmatrix} \cos\alpha & \sin\alpha \\ -\sin\alpha & \cos\alpha \end{bmatrix} \tag{2.15}$$

where, $\alpha = a\pi/2$.

The defining matrix is seen as the two-dimensional rotation matrix in the time-frequency plane. This corresponds to rotation of the Wigner distribution (WD) of a signal in the clockwise direction by angle $\alpha = a\pi/2$ in the time frequency plane as [13]

$$W_{F^a[f(x)]}(\mu, \mu_a) \equiv W_{f(x)}(\mu\cos\alpha - \mu_a \sin\alpha, \mu\sin\alpha + \mu_a\cos\alpha) \tag{2.16}$$

It is consistent with the operators of Table-2.1. The index additivity property also follows from the angle additivity of the rotation matrix.

The LCT $C^M[f(x)]$ of $f(x)$ is most conveniently defined as [79]

$$C^M[f(x)] = \int C^M(x, x_a) f(x) dx \tag{2.17}$$

where, $C^M(x, x') = A^M \exp[i\pi(\xi x^2 - 2\beta x x_a + \gamma {x_a}^2)]$ and $A^M = \sqrt{\beta} e^{-i\pi/4}$,

where, ξ, β and γ are real parameters independent of x and x_a and C^M is a linear canonical operator.

Comparing equations (2.1) and (2.17),

$$\xi = \gamma = \cot\alpha, \quad \text{and } \beta = \csc\alpha \tag{2.18}$$

As this definition used a unit magnitude complex constant, it is slightly weaker than other definitions of FrFT. This situation is not harmful because the complex constants of unit or non-unit magnitude commonly have no major consequences, but the discrepancy arises when it is seen in relation to commonly accepted definition of LCT and FrFT. Hence, the integral differing from the mathematical definitions by a complex constant is still being LCT or FrFT. This relationship between FrFT and the LCT with matrix M can be given as [79]

$$C^M = e^{-ia\pi/4} F^a \qquad \text{for } -2 \le a \le 2 \tag{2.19}$$

$$\text{or} \qquad C^M[f(x)] = e^{ia\pi/4} F^a[f(x)] \tag{2.20}$$

The equivalence set of parameters ξ, β and γ is given by (2.17). This allows obtaining (2.1) using (2.17). Alternatively, from definition of linear integral transform given by (2.1) and using parameters ξ, β and γ the corresponding matrix coefficients of LCT can be obtained as [79]

$$M = \begin{bmatrix} A & B \\ C & D \end{bmatrix} \equiv \begin{bmatrix} \gamma/\beta & 1/\beta \\ -\beta + \xi\gamma/\beta & \xi/\beta \end{bmatrix} = \begin{bmatrix} \xi/\beta & -1/\beta \\ \beta - \xi\gamma/\beta & \gamma/\beta \end{bmatrix}^{-1} \tag{2.21}$$

with determinant $AD - BC = 1$.

This is same as (2.15). It is sufficient to establish the equivalence of all these definitions. The direct relationship between fractional powers of FT definition and rotation in the time-frequency plane is given by

$$K^M(x, \mu; x_a, \mu_a) = \delta(x_a - \cos\alpha x + \sin\alpha\mu)\, \delta(\mu_a - \sin\alpha x - \cos\alpha\mu) \tag{2.22}$$

using the effect of linear system on the WD.

2.2.4 Transformation of Coordinate Multiplication and Differentiation Operators

Before defining the FrFT in terms of transformation of coordinate multiplication and differentiation operators the following properties of these operators in the time-frequency domains are recalled [79]

$$UF^0[f(t)] = tF^0[f(t)] \tag{2.23}$$

$$DF^0[f(t)] = \frac{1}{i2\pi}\frac{d}{dt}F^0[f(t)] \tag{2.24}$$

$$-UF^1[f(t)] = \frac{1}{i2\pi}\frac{d}{df}F^1[f(f)] \tag{2.25}$$

$$DF^1[f(f)] = fF^1[f(f)] \tag{2.26}$$

where, $f(t)$ corresponds to time domain function and $f(f)$ is frequency domain function. U is coordinate multiplication operator and D is differentiation operator.

The two operators U^a (a^{th} domain) and D^a (a^{th} domain) are defined as

$$\begin{bmatrix} U^a \\ D^a \end{bmatrix} \equiv \begin{bmatrix} \cos\alpha & \sin\alpha \\ -\sin\alpha & \cos\alpha \end{bmatrix} \begin{bmatrix} U \\ D \end{bmatrix} \tag{2.27}$$

such that $U^0 = U$, $U^1 = D$, $D^0 = D$ and $D^1 = -U$.

The fractional Fourier domain representation $F^a[f(x)]$ of a signal $f(x)$ such that it satisfies the properties [80]

$$U^a F^a[f(x)] = x_a F^a[f(x)] \tag{2.28}$$

$$D^a F^a[f(x)] = \frac{1}{i2\pi}\frac{d}{dx_a}F^a[f(x)] \tag{2.297}$$

which are generalizations of (2.23), (2.26) and (2.24), (2.25) respectively. The operator U^a corresponds to multiplication by the coordinate variable and the operator D^a corresponds to differentiation with respect to the coordinate variable in the a^{th} order fractional Fourier domain representation. The unitary transformation from the time domain representation $f(x)$ to the fractional Fourier domain representation $F^a[f(x)]$ is the FrFT operator. This definition can be used to provide a different perspective as shown below [79]

$$U\left[K^0(x,t)\right]^{-1} = t\left[K^0(x,t)\right]^{-1} \tag{2.29}$$

$$D\left[K^1(x,f)\right]^{-1} = f\left[K^1(x,f)\right]^{-1} \tag{2.30}$$

The inverse of kernel $\left[K^0(x,t)\right]^{-1} = \delta(t-x)$ of the identity operation *I*, which is a function of x, is the eigenfunctions of the coordinate multiplication operator U with eigenvalue *t*. This is given by (2.29) and the inverse of the kernel $K^1(f,x) = \exp(-i2\pi fx)$ of the FT operator F^1, which is a function of *f*, is the eigenfunctions of the differentiation operator D with eigenvalue f. The duals of these equations are given as [79]

$$-D\left[K^0(x,t)\right]^{-1} = \frac{1}{i2\pi}\frac{d}{dt}\left[K^0(x,t)\right]^{-1} \tag{2.31}$$

$$U\left[K^1(x,f)\right]^{-1} = \frac{1}{i2\pi}\frac{d}{df}\left[K^1(x,f)\right]^{-1} \tag{2.32}$$

The relationship between the identity operator and the coordinate multiplication operator is given by (2.29) and (2.30) gives the relation between FT operator and the differentiation operator. Similarly, the parity operator and the inverse Fourier operator is related to $-U$ and $-D$ respectively. The transformation from one representation to another representation is simply the

representation of the members of one basis set to another basis set, *viz.*, $K^0(x,t)$ to $K^1(x,f)$. The same is true for inverse kernel. The eigensignals of the operator U and D are the orthonormal basis set of impulses and harmonic basis sets. From the above discussion it is clear that there is a relation between the identity operator, the impulse basis, the time domain representation and the operator U. Like wise a relationship exists between the conventional FT operator, the harmonic basis, the frequency domain representation of the signal and the operator D. Using (2.27) it can be said that the a^{th} order FrFT operator F^a is related with D^a and U^a in the same way the conventional FT operator with D and U. This is given as [80]

$$U^a\left[K^0(x,x_a)\right]^{-1} = x'\left[K^0(x,x_a)\right]^{-1} \tag{2.33}$$

$$-D^a\left[K^a(x,x_a)\right]^{-1} = \frac{1}{i2\pi}\frac{d}{dx_a}\left[K(x,x_a)\right]^{-1} \tag{2.34}$$

which is the generalization of the (2.29), (2.30) and (2.31), (2.32), where $\left[K^a(x,x_a)\right]^{-1}$ is interpreted as a function of x. Also $F^a\left[f(x)\right]$ is related to $f(x)$ through the relation $f(x) = \int\left[K^a(x,x_a)\right]^{-1} f^a(x_a)dx_a$ or $f^a(x_a) = \int K^a(x_a,x)f(x)dx$ can be written using (2.28) in time domain as

$$U^a\int\left[K^a(x,x_a)\right]^{-1}F^a\left[f(x)\right]dx = \int\left[K^a(x,x_a)\right]^{-1}x_aF^a\left[f(x)\right]dx \tag{2.35}$$

From (2.32) it is clear that the LHS is nothing but the operator U^a applied to $f(x)$ and the RHS is simply the time domain representation of $x_aF^a\left[f(x)\right]$. (2.29) can also be rewritten in time domain as

$$D^a \int \left[K^a(x,x_a)\right]^{-1} F^a[f(x)]dx_a = \int \left[K^a(x,x_a)\right]^{-1} \frac{1}{i2\pi} \frac{dF^a[f(x)]}{dx_a} dx_a \qquad (2.36)$$

Integrating the RHS by parts and using the fact that as argument of finite energy signals approaches infinity the signal approaches zero, the following equation is obtained [80]

$$D^a \int \left[K^a(x,x_a)\right]^{-1} F^a[f(x_a)]dx_a = \int \frac{1}{i2\pi} \frac{\left[K^a(x,x_a)\right]^{-1}}{dx_a} F^a[f(x_a)]dx_a \qquad (2.37)$$

It is clear that (2.33) and (2.34) imply (2.35) and (2.37) and conversely (2.35) and (2.37) implies (2.33) and (2.34). Thus the equivalence of (2.27) with (2.33) and (2.34) is established. For proving its equivalence with the first definition i.e., of linear integral transform the (2.27) can be rewritten using (2.33) and (2.34) as

$$\left(\cos\alpha + \sin\alpha \frac{1}{i2\pi} \frac{d}{dx}\right)\left[K^a(x,x_a)\right]^{-1} = x_a\left[K^a(x,x_a)\right]^{-1} \qquad (2.38)$$

$$-\left(-\sin\alpha x + \cos\alpha \frac{1}{i2\pi} \frac{d}{dx}\right)\left[K^a(x,x_a)\right]^{-1} = \frac{1}{i2\pi} \frac{d}{dx_a}\left[K^a(x,x_a)\right]^{-1} \qquad (2.39)$$

where, $\left[K^a(x,x_a)\right]^{-1}$ is a function of x. The solution of the pair of the differential equation is

$$\left[K^a(x,x_a)\right]^{-1} = (\textbf{\textit{constant}})[-i\pi(x^2\cot\alpha - 2xx_a\csc\alpha + {x_a}^2\cot\alpha)]. \qquad (2.40)$$

The angle additivity of (2.27) translates to index additivity property of the kernel. The relationship with the definition of rotation in time-frequency plane is clear from (2.27) and it can be seen that (2.27) is a special case of the coordinate multiplication and differentiation operator of the LCT given as [80]

$$\begin{bmatrix} U^M \\ D^M \end{bmatrix} \equiv \begin{bmatrix} A & B \\ C & D \end{bmatrix}\begin{bmatrix} U \\ D \end{bmatrix} \qquad (2.41)$$

By using above property of LCT the operator U^a and D^a can be written as

$$U^a = F^{-a} U F^a \tag{2.42}$$

$$D^a = F^{-a} D F^a \tag{2.43}$$

2.2.5 Differential Equation

In this definition the FrFT, $f^a(x_a)$ of a function $f(x)$ is defined as the solution of a quantum mechanics harmonic oscillator differential equation or the equation governing optical propagation in the graded index medium, with $F^0[f(x)]$ as the initial condition. The solution of this equation is well known and some sources of the solution have written it in the form of an integral transform whose kernel is sometimes referred to as harmonic Green's oscillator [81]. Now considering the differential equation

$$\left[-\frac{1}{4\pi}\frac{\partial^2}{\partial x^2} + \pi x^2 - \frac{1}{2}\right] F^a[f(x)] = i\frac{2}{\pi}\frac{\partial F^a[f(x)]}{\partial a} \tag{2.44}$$

with the initial condition $F^0[f(x)] = f(x)$. The solution $F^a[f(x)]$ of (2.44) is the a^{th} order FrFT of $f(x)$. By direct substitution the solution of this differential equation is

$$F^a[f(x)] = \int K^a(x, x_a) F^0[f(x)]dx \tag{2.45}$$

with $K^a(x, x_a)$ given by (2.1). Namias solved (2.44) in two steps by substituting (2.45) in (2.44) and obtaining the differential equation [4]

$$\left[-\frac{1}{4\pi}\frac{\partial^2}{\partial x^2} + \pi x^2 - \frac{1}{2}\right] K^a(x, x_a) = i\frac{2}{\pi}\frac{\partial K^a(x, x_a)}{\partial a} \tag{2.46}$$

with initial condition $K^0(x, x_a) = \delta(x - x_a)$. The kernel obtained by Namias is same as in equation (2.1) and this satisfies the equivalence of the definitions. Alternatively, the eigensolutions of the (2.44) is first sought and then the arbitrary solutions as the linear superposition of these eigensolutions are constructed. Substituting the eigensolution form $F^a[f(x)] = \lambda_a F^a[f(x)]$ in (2.44) gives

$$\frac{d^2F^0[f(x)]}{dx^2} + 4\pi^2\left(\frac{1}{2\pi} + \frac{i2}{\pi^2\lambda_a}\frac{d\lambda_a}{da} - x^2\right)F^0[f(x)] = 0 \qquad (2.47)$$

Now comparing with

$$\frac{d^2f(x)}{dx^2} + 4\pi^2\left(\frac{2n+1}{2\pi} - x^2\right)f(x) = 0 \qquad (2.48)$$

which is having Hermite-Gaussian functions as the solution, it is clear that (2.48) is having Hermite-Gaussian functions as its solutions provided [11]

$$\frac{2l+1}{2\pi} = \frac{1}{2\pi} + \frac{i2}{\pi^2\lambda_a}\frac{d\lambda_a}{da} \qquad (2.49)$$

which gives

$$\frac{d\lambda_a}{da} = -il\left(\frac{\pi}{2}\right)\lambda_a \qquad (2.50)$$

yielding

$$\lambda_a = e^{-ial\pi/2} \qquad (2.51)$$

as the eigenvalue related with the l^{th} Hermite-Gaussian functions. This demonstrates the equivalence with definition of fractional powers of the FT. If the initial condition $F^0[f(x)]$ is

$\psi_l(x)$, the solution $F^a[f(x)]$ is $\exp(-ial\pi/2)\psi_l(x)$, which can be expanded in terms of Hermite-Gaussian functions as

$$F^0[f(x)] = \sum_{l=0}^{\infty} C_l \psi_l(x) \tag{2.52}$$

where $C_l = \int \psi_l(x) F^0[f(x)] dx$

As (2.44) is linear, the corresponding solution to the initial condition in (2.52) is obtained as

$$F^a[f(x)] = \sum_{l=0}^{\infty} C_l e^{-ial\pi/2} \psi_l(x) \tag{2.53}$$

which can be written as

$$F^a[f(x)] = \int K^a(x, x_a) F^0[f(x)] dx \tag{2.54}$$

where $K^a(x, x_a) = \sum_{l=0}^{\infty} e^{-ial\pi/2} \psi_l(x) \psi_l(x_a)$ as in (2.10).

Now considering the differential equation of the form

$$\mathsf{H} F^a[f(x)] = i \frac{\partial F^a[f(x)]}{\partial(a\pi/2)} \tag{2.55}$$

where, H is a quadratic Hermitian operator in U and D. Since it is known that the Hermitian conjugate of DU is UD and vice versa, such that an operator may only contain terms proportional to U^2, D^2 and $UD + DU$. The solution of this equation is given as [79]

$$F^a[f(x)] = e^{-(i\pi/2)H} F^0[f(x)] \tag{2.56}$$

where $F^0[f(x)]$ is the initial or boundary condition. Specializing this equation to $\mathsf{H} = \pi(U^2 + D^2)$, the following equation is obtained

$$\pi(U^2 + D^2)F^a[f(x)] = i\frac{\partial F^a[f(x)]}{\partial(a\pi/2)} \tag{2.57}$$

To find the relation between (2.57) and (2.44), the effect of $U^2 + D^2$ on $F^a[f(x)]$ is to be determined first. If $F^a[f(x)]$represents different functions of x for different values of *a* then using $UF^a[f(x)] = xF^a[f(x)]$and $DF^a[f(x)] = (i2\pi)^{-1}\partial F^a[f(x)]/\partial x$ gives [11]

$$\left[-\frac{1}{4\pi}\frac{\partial^2}{\partial x^2} + \pi x^2\right]F^a[f(x)] = i\frac{2}{\pi}\frac{\partial F^a[f(x)]}{\partial a} \tag{2.58}$$

The result in (2.58) relates the present definition to that given in section 2.2.4 and indirectly to definition of rotation of time-frequency plane.

2.2.6 Hyperdifferential Operator

The FrFT can be defined in the hyper differential form by using a hyper differential operator as

$$F^a = \exp(-i(a\pi/2)\mathsf{H}) \tag{2.59}$$

where, $\mathsf{H} = \pi(D_2 + U_2) - 0.5$.

To give the equivalence of this definition with that of differential equation form the (2.59) can be written in time domain as [4]

$$F^a[f(x)] = \exp\left[-i\left(\frac{a\pi}{2}\right)\left(-\frac{1}{4\pi}\frac{d^2}{dx^2} + \pi x^2 - \frac{1}{2}\right)\right]f(x) \tag{2.60}$$

From (2.54) it is clear that this is closely related to that of differential equation form. Also the solution of the differential equation $\mathsf{H}F^a[f(x)] = i(2/\pi)\partial/\partial a F^a[f(x)]$ is given by

$F^a[f(x)] = \exp(-i(a\pi/2)\mathsf{H})F^0[f(x)]$. Where, $F^0[f(x)]$ serves as the initial or boundary condition. It can be seen that the above definition is simply the solution of the differential equation (2.44) expressed in hyper differential form.

The equivalence with the definition of fractional powers of the FT, which is based on the eigenvalue equation [4] is given by

$$F^a[\psi_l(x)] = e^{-ial\pi/2}\psi_l(x) = e^{-i\alpha l}\psi_l(x) \tag{2.61}$$

where, $\psi_l(x)$ are the Hermite-Gaussian functions satisfying the differential equation

$$\left[\frac{d^2}{dx^2} + 4\pi^2\left(\frac{2l+1}{2\pi} - x^2\right)\right]\psi_l(x) = 0 \tag{2.62}$$

Now from (2.61) and (2.62) a hyperdifferential representation of F^a in the form of $\exp(-i\alpha\mathsf{H})$ can be calculated by differentiating with respect to α as

$$\exp(-i\alpha\mathsf{H})\psi_l(x) = e^{-i\alpha l}\psi_l(x) \tag{2.63}$$

setting $\alpha = 0$ the following equation is obtained

$$\mathsf{H}\psi_l(x) = l\psi_l(x), \tag{2.64}$$

and comparison with (2.62) leads to

$$\mathsf{H}\psi_l(x) = \left(-\frac{1}{4\pi}\frac{d^2}{dx^2} + \pi x^2 - \frac{1}{2}\right)\psi_l(x). \tag{2.65}$$

By expanding arbitrary $f(x)$ in terms of $\psi_l(x)$ and by virtue of the linearity of *H*, the (2.65) becomes

$$\mathsf{H}f(x) = \left(-\frac{1}{4\pi}\frac{d^2}{dx^2} + \pi x^2 - \frac{1}{2}\right)f(x). \tag{2.66}$$

This can be written in abstract operator form as

$$\mathsf{H} = \pi\left(D^2 + U^2\right) - \frac{1}{2} \tag{2.67}$$

which precisely corresponds to the present definition and also equivalent to the definition given in section 2.2.2. To establish the equivalence of the present definition to that in section 2.2.4 the hyperdifferential form of F^a is used in (2.42) and (2.42) to obtain expressions for U^a and D^a as follows [3]:

$$F^a = e^{-i\alpha\mathsf{H}} = e^{-i\alpha\left[\pi\left(U^2+D^2\right)-1/2\right]} \tag{2.68}$$

$$= e^{-i\pi(\csc\alpha-\cot\alpha)U^2} e^{-i\pi(\sin\alpha)D^2} e^{-i\pi(\csc\alpha-\cot\alpha)U^2} e^{i\alpha/2} \quad .$$

The (2.68) is the identity which corresponds to the decomposition of the FrFT into a chirp multiplication followed by a chirp convolution followed by another chirp multiplication. Substituting this decomposition in (2.42) and using the commutation relations $[U, \Gamma(U)] = 0$ and $[U, \Gamma(D)] = (i/2\pi)\Gamma'(D)$ where $\Gamma(z)$ is a complex variable whose polynomial series is defined as $\Gamma(z) = \sum_{n=0}^{\infty} \Gamma_n z^n$, and moving U towards the left, gives [3]

$$U^a = U + \sin\alpha e^{-i\pi(\csc\alpha-\cot\alpha)U^2} D e^{-i\pi(\csc\alpha-\cot\alpha)U^2} \tag{2.69}$$

Now using $[D, \Gamma(U)] = (-i/2\pi)\Gamma'(D)$ to move D towards the left

$$U^a = U + \sin\alpha\left[D - (\csc\alpha - \cot\alpha)U\right] = \cos\alpha U + \sin\alpha D \tag{2.70}$$

as in (2.27). Substituting the dual of (2.68) (in which the roles of U and D are exchanged) in (2.42), it is possible to show that

$$D^a = -\sin\alpha U + \cos\alpha D \tag{2.71}$$

as in (2.27). Thus it is shown that the hyperdifferential form of F^a implies (2.27) which constitutes the definition of transformation of coordinate multiplication and differentiation operators. Since the (2.27) shows that the coordinate multiplication and differentiation operators corresponding to different values of a are related by the rotation matrix, this derivation also relates the present definition with that of section 2.1.3. The operators U and D are replaced by classical variables time or space variable *t* and frequency variable *f*, respectively. In such operators context, (2.27) serves as the complete expression of rotation in time-frequency or space-frequency plane, corresponding to (2.16) written in terms of WD $W_{F^1[f(x)]}(t, f)$. The effect of Hamiltonian $\mathsf{H} = \pi\left(D^2 + U^2\right) - 1/2$ is to rotate the WD. It can be said that the operation represented by the hyperdifferential form (all differential equation) associated with this Hamiltonian [3], corresponding to rotation in time-frequency or space-frequency plane, is closely related to the fact that this Hamiltonian is rotationally invariant. As a result of (2.27), the rotational invariance simply means

$$\mathsf{H}^a = \pi\left(\left[D^a\right]^2 + \left[U^a\right]^2\right) - 1/2 = \pi\left(D^2 + U^2\right) - 1/2 = \mathsf{H} \qquad (2.72)$$

The index additive property and the special case $a = 0$ follows from the exponential form $exp(-i\alpha H)$. The special case $a = 1$, which is, $F^1 = \exp\left[-i(\pi/2)H\right]$ is nothing but the hyperdifferential form of conventional FT. The hyperdifferential form is very useful when very small order a is considered. When a is infinitesimal, the operator $F^a = \exp\left[-i(\pi a/2)\mathsf{H}\right]$ is called an infinitesimal operator. Such operators are expressed as a first order expansion of the form $F^a = I + \left[-i(\pi\, a/2)\mathsf{H}\right]$. This implies

$$F^a\left[f(x_a)\right] - f(x) = i(a\pi/2)\mathsf{H} f(x) = i\left(\frac{a\pi}{2}\right)\left(-\frac{1}{4\pi}\frac{d^2}{dx^2} + \pi x^2 - \frac{1}{2}\right) f(x) \qquad (2.73)$$

so that the change in wave amplitude without integration can be determined. The hyper differential form of FrFT is also discussed by Mustard [5], [7].

2.2.7 Discussions

The FrFT operator $F^{a}[f(x)]$ is

1. linear
2. verifies FT condition $F^{1} = F$
3. has additive property $F^{a+b} = F^{a} F^{b}$ for every choice of *a* and *b*.

Given the widespread use of conventional FT in science and engineering, it is important to recognize this integral transform as the fractional power of FT. Indeed, it has been this recognition, which has inspired most of the many recent applications replacing the ordinary FT with FrFT (which is more general and includes FT as a special case) adding an additional degree of freedom to the problem, represented by the fraction or order parameter *a*. This in turn may allow either a more general formulation of the problem or improvement based on possibility of optimizing over *a* (as in optimal Wiener filter resulting in smaller mean square error at practically no additional cost) [59].

2.3 PROPERTIES OF FRFT

In this section, some important properties of FrFT are discussed. The properties of FrFT are useful not only in deriving the direct and inverse transform of many time varying functions but also in obtaining several valuable results in signal processing. The properties are sumarised in Table-2.2, Table-2.3 and Table-2.4. The FrFT of some simple functions are listed in Table-2.5. The properties listed in Table-2.1 are the most basic one. The mathematical proofs of these properties have been reported [71]. Here these properties are verified with simulation process and illustrated graphically

which substantiate the mathematical conclusions. The functions used to verify the established properties of FrFT are unique and taken for the first time as literature reveals.

2.3.1 Illustration of Basic FrFT Properties

The FrFT is evidently linear but not shift invariant. First property of Table-2.2 states that when a is equal to an integer j, the a^{th} order FrFT is equivalent to the j^{th} integer power of the ordinary FT. It also follows that $F^2 = P$ (the parity operator), $F^3 = F^{-1} = (F)^{-1}$ (the inverse transform operator), $F^4 = F^0 = I$ (the identity operator), and $F^j = F^{j \bmod 4}$. When a is equal to $4j+1$, the FrFT kernel becomes FT kernel and when $a = 4j+3$, the FrFT kernel becomes inverse FT kernel. When $a = 4j$, the kernel reduces to $\delta(x - x_a)$ and when $a = 4j \pm 2$, then the kernel becomes $\delta(x + x_a)$. Third property associates positive orders with forward transforms and negative orders with inverse transforms. In terms of kernel this property can be stated as $\left[K^a(x, x_a)\right]^{-1} = K^{-a}(x, x_a)$. Property 4 is stated as $K^{-a}(x, x_a) = \left[K^a(x_a, x)\right]^*$, which when combined with the previous property implies $(F^a)^{\mathrm{H}} = F^{-a}$. Property 5 is expressed in terms of the kernels as $K^{a2+a1}(x, x_{a1}) = \int K^{a2}(x, x_{a2}) K^{a1}(x_{a2}, x_{a1}) dx_{a2}$. Property 6 follows from property 5. Property 7 is not special to FrFT and is valid for all LCT. Property 8 has been discussed in detail in section 2.2.2. It simply states that the eigenfunctions of the FrFT are Hermite-Gaussian functions. Property 9 is also discussed in section 2.2.3 and it states that the WD of the FrFT of a function is a rotated version of the WD of the original function. Last property describes the Parseval theorem. Energy or norm conservation $\left(En[f^a(x_a)] = \left\| f^a(x') \right\| = \left\| f(x) \right\|\right)$ is a special case. It is noted that a slightly more general way of writing this property

$\left\langle F^{a1}[f(x)], F^{a2}[g(x)] \right\rangle = \left\langle F^{a3}[f(x)], F^{a4}[g(x)] \right\rangle$ when $a_1 - a_2 = a_3 - a_4$ which is seen to be true by noting that $F^{a3}[f(x)]$ is the $(a_3 - a_1)^{th}$ transform of $F^{a1}[f(x)]$ and $F^{a4}[g(x)]$ is the $(a_4 - a_2)^{th}$ transform of $F^{a2}[g(x)]$.

For verification of the properties of FrFT a simulation study has been carried out. The Riemann function is used to verify the properties of FrFT. The function is expressed as follows -

$$f(x) = \frac{\sin\left(\frac{\pi x}{\iota}\right)}{\frac{\pi x}{\iota}} \quad |x| \le \iota \tag{2.74}$$

and is shown in Figure 2.1

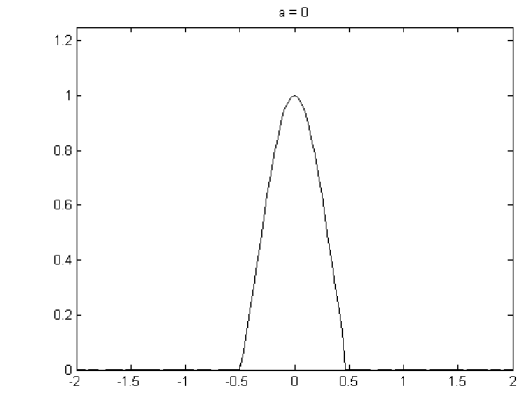

Figure-2.1: Riemann function in the range from $-\iota$ to ι for $\iota = 0.5$.

Table-2.2: Properties of the FrFT, part I.

1.	Integer orders	$F^{j} = (F)^{j}$
2.	Inverse	$\left(F^{a}\right)^{-1} = F^{-a}$
3.	Unitary	$\left(F^{a}\right)^{-1} = \left(F^{a}\right)^{H}$
4.	Index additivity	$F^{a2}F^{a1} = F^{a2+a1}$
5.	Commutativity	$F^{a2}F^{a1} = F^{a1}F^{a2}$
6.	Associativity	$F^{a3}\left(F^{a2}F^{a1}\right) = \left(F^{a3}F^{a2}\right)F^{a1}$
7.	Linearity	$F^{a}\left[\sum_{j}\alpha_{j} f_{j}(x)\right] = \sum_{j}\alpha_{j}\left[F^{a} f_{j}(x)\right]$
8.	Eigenfunctions	$F^{a}[\psi_{l}(x)] = \exp(-ial\pi/2)\psi_{l}(x)$
9.	Wigner distributions	$W_{F^{a}[f(x)]}(x,x') = W_{f(x)}(x\cos\alpha - x'\sin\alpha, x\sin\alpha + x'\cos\alpha)$
10.	Parseval	$\langle f(x), g(x)\rangle = \langle f^{a}(x), g^{a}(x)\rangle$

α_{j} are arbitrary complex constraints and j is an arbitrary integer.

The first property of Table-2.2 for integer order is illustrated by taking the FrFT of the Riemann function in the integer domains i.e., a = 0,1,2,3 and 4. Figure-2.2 shows the illustration of this property.

Because the Riemann function is an even function hence integer property is not clearly evident from the plots shown in Figure-2.2. In order to have clarity, the function is modified in such a way so that the property can be understood in a better way. After modifying the Reimann function the FrFT of the integer order is illustrated in Figure-2.3 which clearly shows that at a = 0 and a = 4 the function the same and at a = 1 and a = 3 the result is the FT and inverse FT.

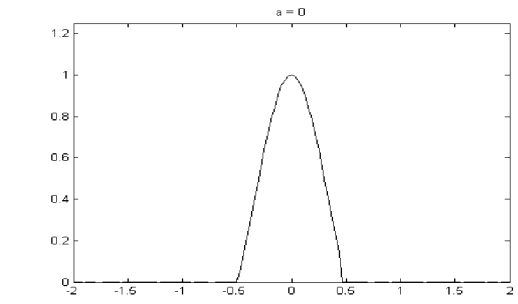

(a) $F^0[f(x)]$

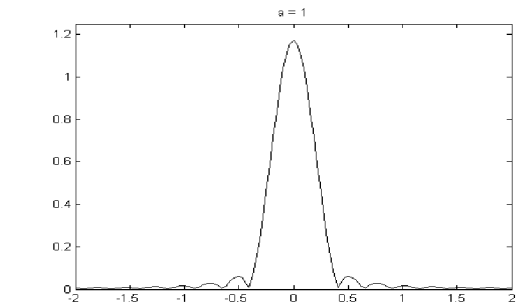

(b) $F^1[f(x)]$

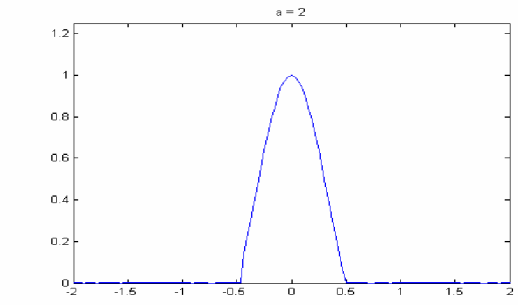

(c) $F^2[f(x)]$

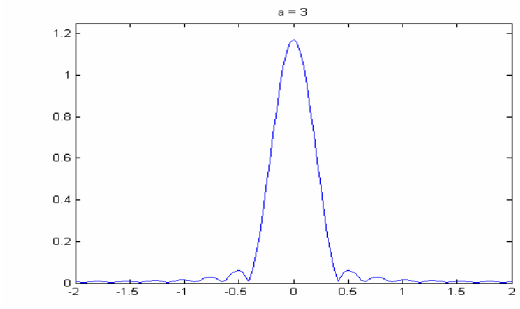

(d) $F^3[f(x)]$

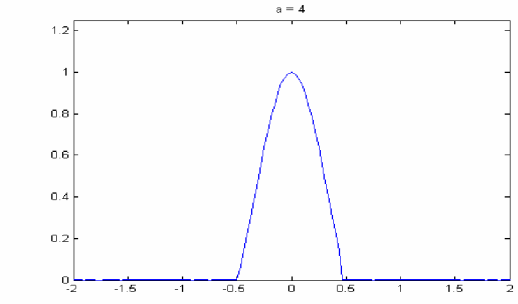

(e) $F^4[f(x)]$

Figure-2.2: Illustration of integer property using Riemann function.

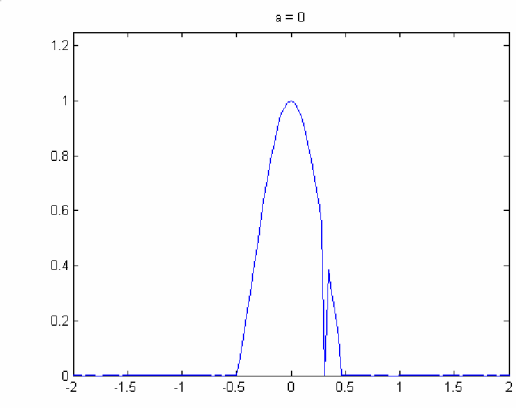

(a) $F^0[f(x)]$

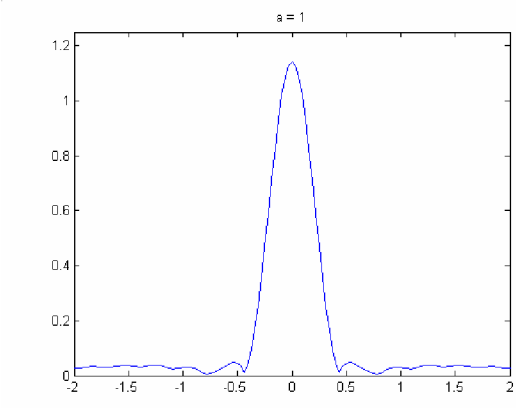

(b) $F^1[f(x)]$

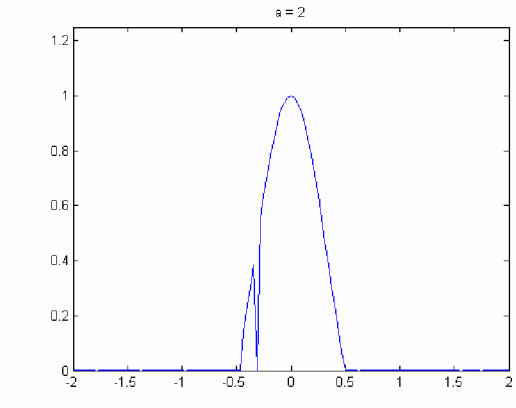

(c) $F^2[f(x)]$

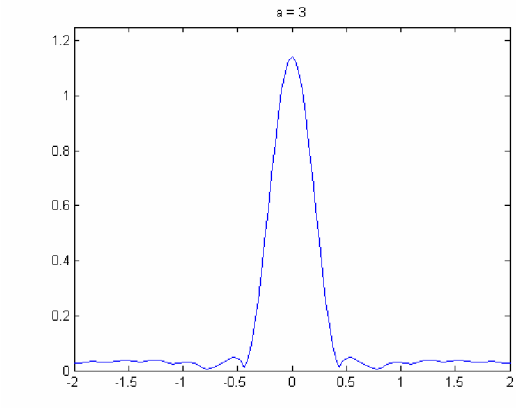

(d) $F^3[f(x)]$

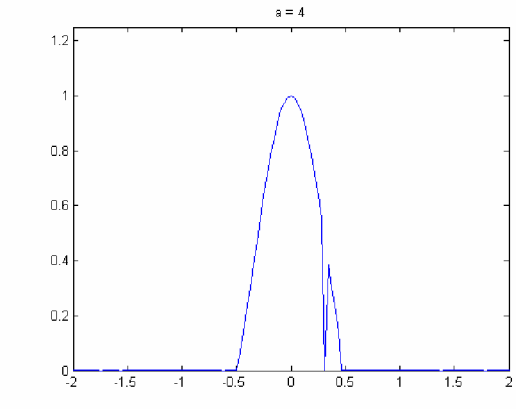

(e) $F^4[f(x)]$

Figure-2.3: Illustration of index property by modifying Riemann function.

The inverse property is illustrated in Figure-2.4. First the FrFT of the Riemann function is taken in 0.7^{th} domain and then its inverse is taken, which is as shown in Figure-2.4(a). In Figure-2.4(b) the FrFT of the Riemann function in -0.7^{th} domain is shown. It can be seen from these figures that the $\left(F^{0.7}\right)^{-1} = F^{-0.7}$.

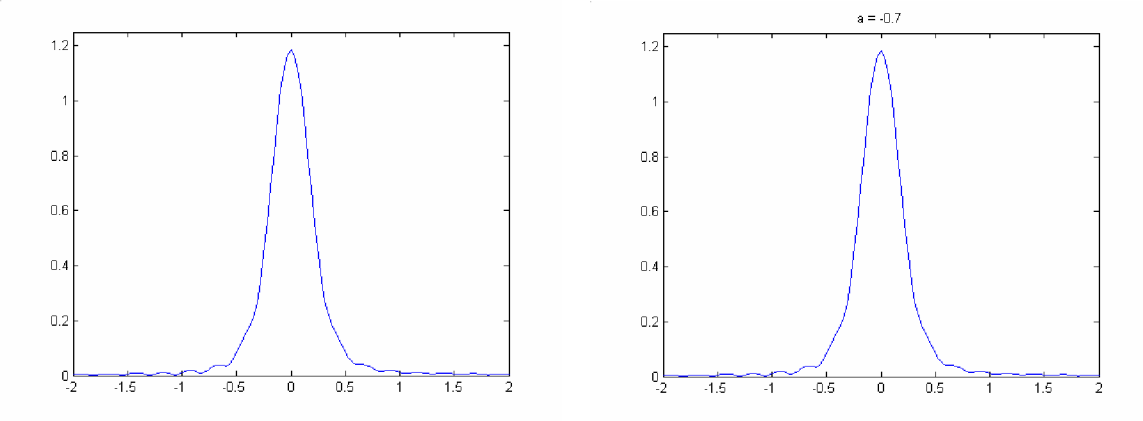

(a) $[F^{0.7}[f(x)]]^{-1}$ (b) $F^{-0.7}[f(x)]$

Figure-2.4: Illustration of inverse property.

To prove the index additivity the FrFT of the function is taken in 0.2^{th} domain (shown in Figure-2.5(a)) and then the FrFT of resultant function is taken in 0.6^{th} domain (shown in Figure-2.5(b)). The FrFT of the Riemann function is taken in 0.8^{th} domain which is shown in Figure 2.5(c). It is clear from these figure that Figure-2.5(b) is equal to Figure-2.5(c), which proves the index additivity property.

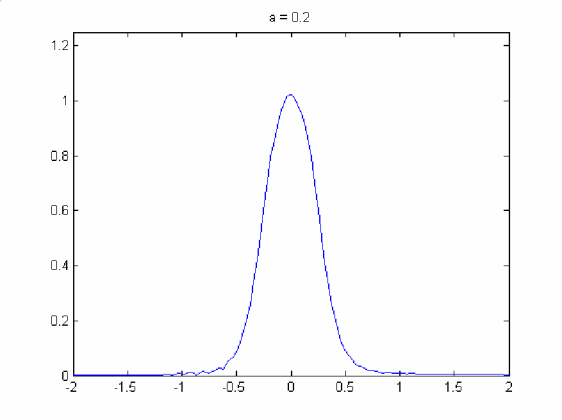

(a) $F^{0.2}[f(x)]$

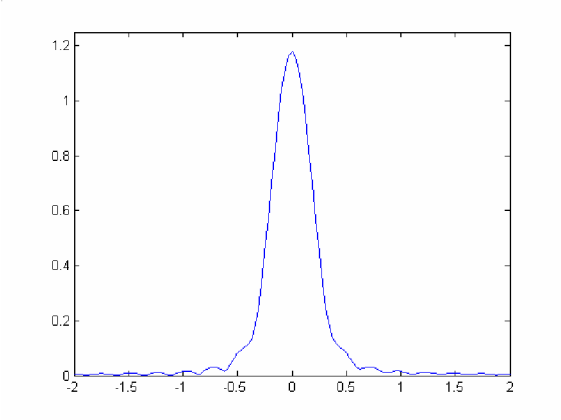

(b) $F^{0.6}[F^{0.2}[f(x)]]$

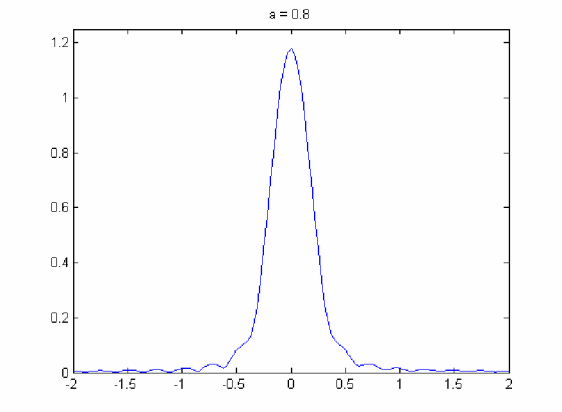

(c) $F^{0.8}[f(x)]$

Figure-2.5: Illustration of index additivity property.

The commutative property has been illustrated by taking FrFT of function with a = 0.4 (Figure-2.6(a)) and then with a = 0.5 (Figure-2.6(b)). This sequence of transform is reversed i.e., first FrFT is taken with a = 0.5 (Figure-2.6(c)) and then with a = 0.4 domain and this has also been established that FrFT of a function with a = 0.9 (Figure-2.6(e)), is equal to Figure-2.6(b) and Figure-2.6(d).

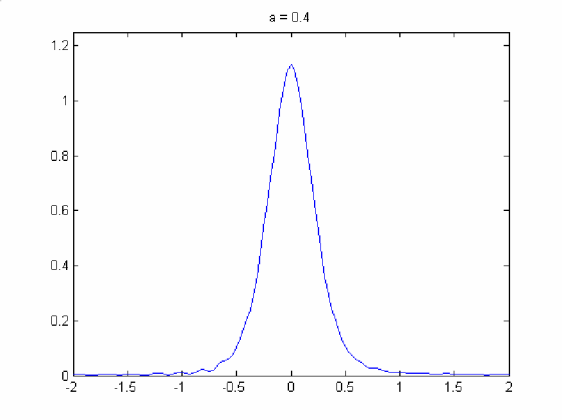

(a) $F^{0.4}[f(x)]$

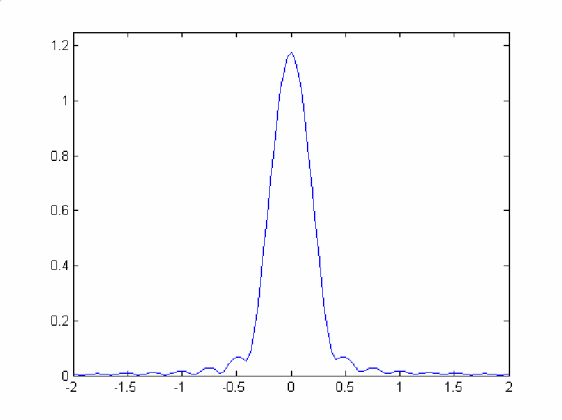

(b) $F^{0.5}[F^{0.4}[f(x)]]$

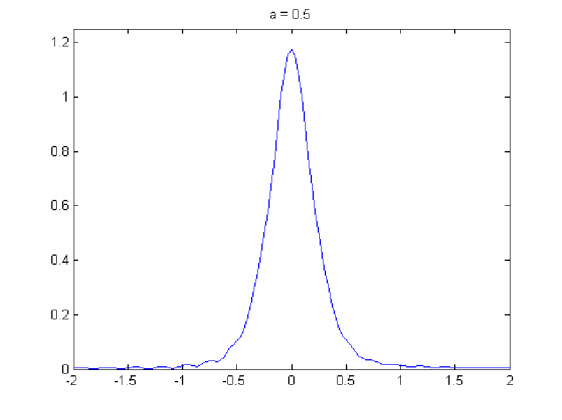

(c) $F^{0.5}[f(x)]$

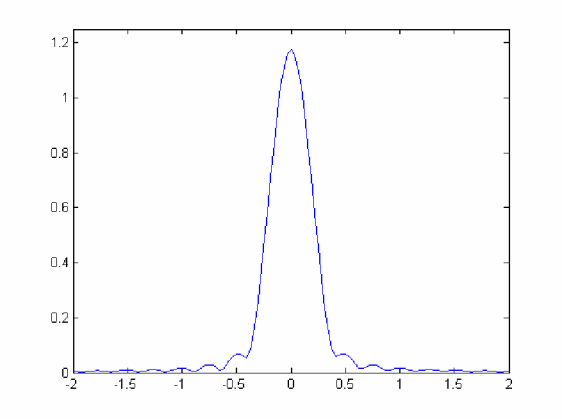

(d) $F^{0.4}[F^{0.5}[f(x)]]$

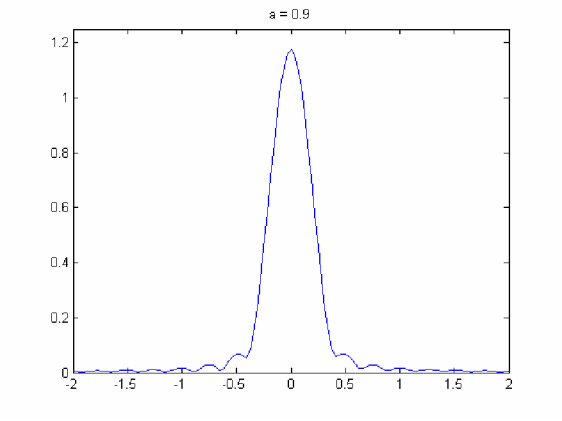

(e) $F^{0.9}[f(x)]$

Figure-2.6: Illustration of commutativity property.

For associativity the domains are taken viz 0.15, 0.37 and 0.41 and results are shown in Figure-2.7.

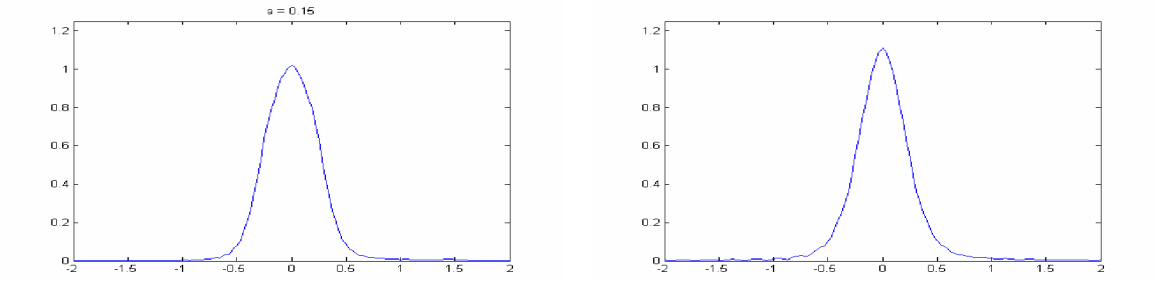

(a) $F^{0.15}[f(x)]$ (b) $F^{0.37}[F^{0.15}[f(x)]]$

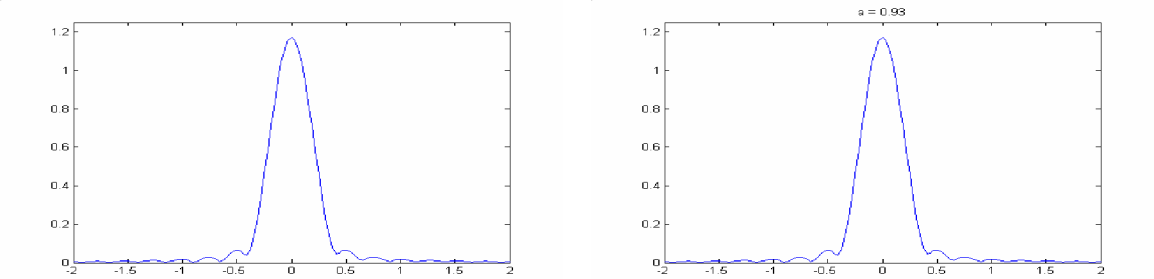

(c) $F^{0.41}[F^{0.37}[F^{0.15}[f(x)]]]$ (d) $F^{0.93}[f(x)]$

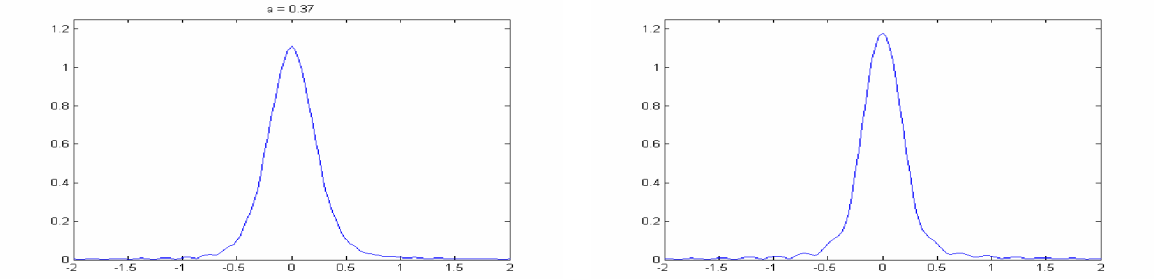

(e) $F^{0.37}[f(x)]$ (f) $F^{0.41}[F^{0.37}[f(x)]]$

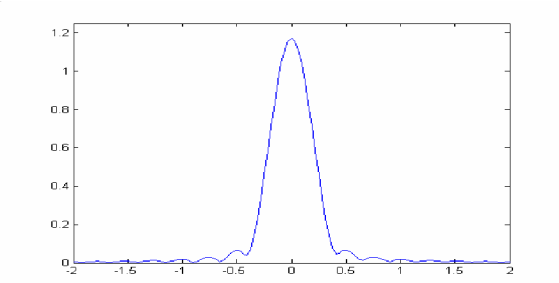

(g) $F^{0.15}[F^{0.41}[F^{0.37}[f(x)]]]$

Figure-2.7: Illustration of associativity property.

The FrFT of the Riemann function is calculated with a = 0.15 (Figure-2.7(a)), then again transformed with a = 0.37 (Figure-2.7(b)). The FrFT of this resultant function is then taken with a = 0.41 (Figure-2.7(c)). The Figure-2.7(d) shows the FrFT of the Riemann function with a = 0.93 and is same as Figure-2.7(c).The Figure-2.7(e) shows the FrFT of Riemann function with a = 0.37, Figure-2.7(f) shows the FrFT of Figure-2.7(e) and Figure-2.7(g) shows the FrFT of the Figure-2.7(f). The Figure-2.7(c), Figure-2.7(d) and Figure-2.7(g) are similar which proves the commutativity property.

To prove linearity property, Hanning function has been taken as second function alongwith Riemann function. The Hanning function is described as

$$g(x) = \cos^2\left(\frac{\pi x}{2\iota}\right) \quad |x| \le \iota \tag{2.74a}$$

Firstly the FrFT of expression $F^{0.3}[2\,g(x) + 3\,f(x)]$ is calculated and shown in Figure-2.8(a). Subsequently the FrFT with a = 0.3 is evaluated of $2\,g(x)$ and $3\,f(x)$ separately which is shown in Figure-2.8(b) and Figure-2.8(c) and then these two FrFT's are added together as shown in Figure-2.8(d). Figure 2.8(a) and Figure-2.8(d) are similar which in itself proves the linearity property.

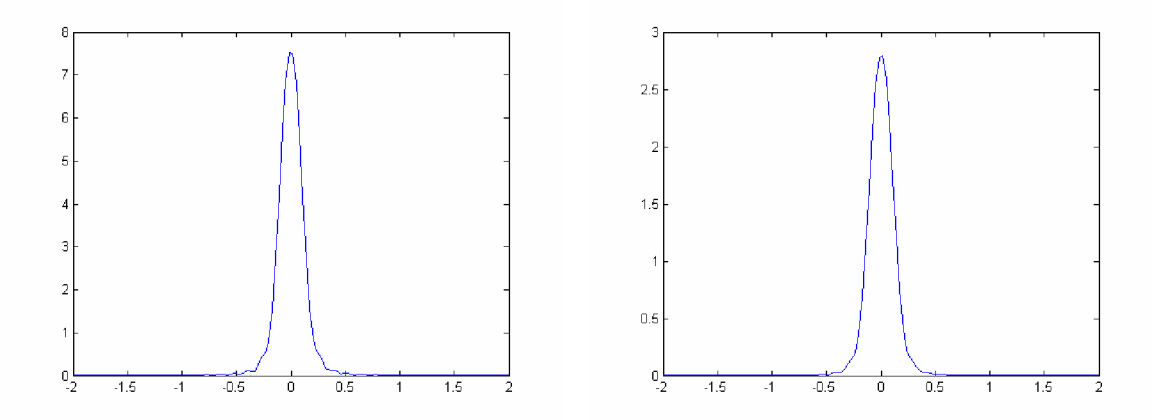

(a) $F^{0.3}[2g(x)+3f(x)]$ (b) $F^{0.3}[2g(x)]$

(c) $F^{0.3}[3f(x)]$ (d) $F^{0.3}[2g(x)]+F^{0.3}[3f(x)]$

Figure-2.8: Illustration of linearity property

The property of WD and Parsevals relation has been established by taking WD of the Riemann function in various domains as shown in Figure 2.9. This property can be further illustrated using a cosine function and is shown in Figure 2.10. It is clear from Figure 2.9 and 2.10 that the distribution rotates with an angle $\alpha = a\pi/2$ and the total energy remains the same.

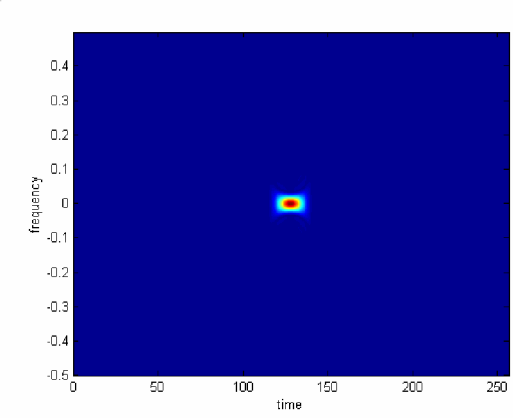

(a) WD in a = 0 domain

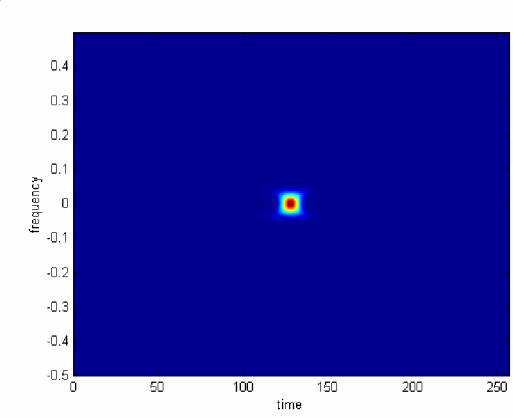

(b) WD in a = 1 domain

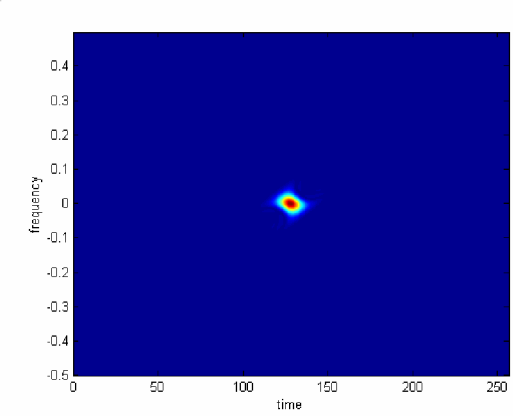

(c) WD in a = 0.5 domain

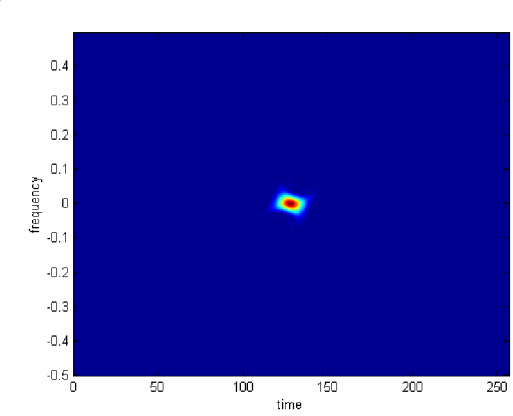

(d) WD in a = 0.25 domain

Figure-2.9: Illustration of WD and Parseval relation property using Riemann function.

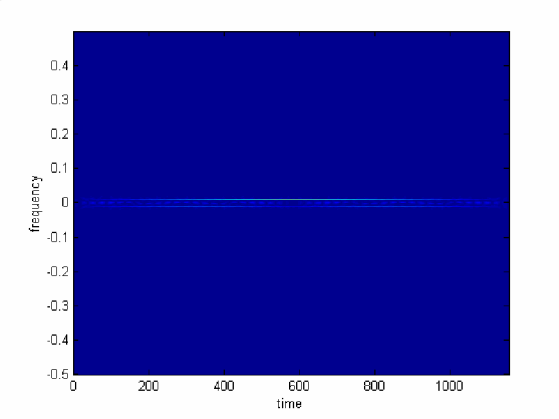

(a) WD in a = 0 domain

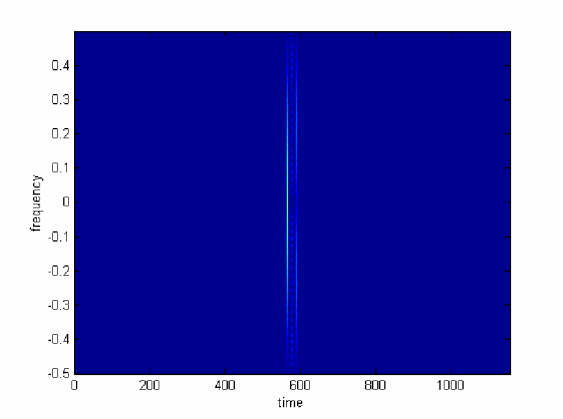

(b) WD in a = 1 domain

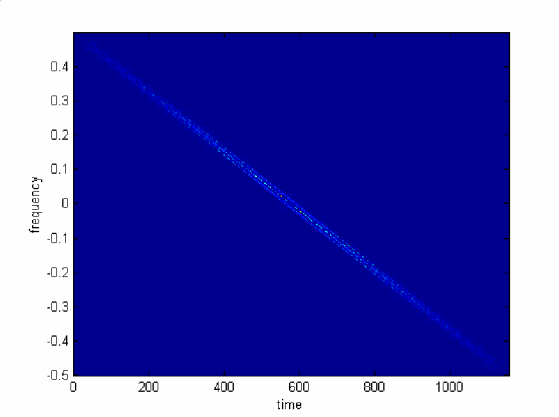

(c) WD in a = 0.5 domain

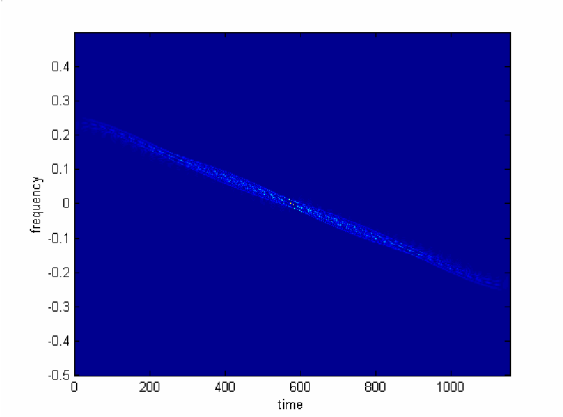

(d) WD in a = 0.25 domain

Figure-2.10: Illustration of WD and Parseval relation property using cosine function.

Table-2.3: Properties of the FrFT, part II.

	$f(x)$	$f^{a}(x_a)$
1.	$f(-x)$	$f^{a}(-x_a)$
2.	$\lvert M\rvert^{-1} f(x/M)$	$\sqrt{\frac{1-i\cot\alpha}{1-iM^2\cot\alpha}}\exp\left[i\pi x_a{}^2\cot\alpha\left(1-\frac{\cos^2\alpha'}{\cos^2\alpha}\right)\right]f^{a}\left(\frac{Mx_a\sin\alpha'}{\sin\alpha}\right)$
3.	$f(x-\xi)$	$\exp(i\pi\xi^2\sin\alpha\cos\alpha)\exp(-i2\pi\xi\sin\alpha)\,f^{a}(x_a-\xi\cos\alpha)$
4.	$\exp(i2\pi\xi x)f(x)$	$\exp(-i\pi\xi^2\sin\alpha\cos\alpha)\exp(i2\pi\xi\sin\alpha)\,f^{a}(x_a-\xi\sin\alpha)$
5.	$x^n f(x)$	$\left[\cos\alpha x_a-\sin\alpha(i2\pi)^{-1}d/dx_a\right]^n f^{a}(x_a)$
6.	$\left[(i2\pi)^{-1}d/dx\right]^n f(x)$	$\left[\sin\alpha x_a+\cos\alpha(i2\pi)^{-1}d/dx_a\right]^n f^{a}(x_a)$
7.	$f(x)/x$	$-i\csc\alpha\exp(i\pi x_a{}^2\cot\alpha)\int_{-\infty}^{2\pi x} f^{a}(x_a)\exp(-i\pi x_a{}^2\cot\alpha)dx_a$
8.	$\int_{\xi}^{x} f(x_a)dx_a$	$\sec\alpha\exp(i\pi x_a{}^2\tan\alpha)\int_{\xi}^{\chi} f^{a}(x_a)\exp(-i\pi x_a{}^2\tan\alpha)dx_a$
9.	$f^{*}(x)$	$\left[f^{-a}(x_a)\right]^{*}$
10	$f^{*}(-x)$	$\left[f^{-a}(-x_a)\right]^{*}$
11	$[f(x)+f(-x)]/2$	$\left[f^{a}(x_a)+f^{a}(-x_a)\right]/2$
12	$[f(x)-f(-x)]/2$	$\left[f^{a}(x_a)-f^{a}(-x_a)\right]/2$

Table-2.4: Important properties of FrFT.

Sr. No.	Properties	Calculus
1	Multiplication Rule	$F^{a}[g(x)f(x)] = g\left(x\cos\alpha + \frac{1}{i}\sin\alpha\,\frac{d}{dx}\right)F^{a}[f(x)]$
2	***The Division Rule***	$F^{a}(f(x)/x) = (i/\sin\alpha)\exp\left(-\frac{ix^2}{2}\cot\alpha\right)\int_{-\infty}^{x}\exp\left(+\frac{ix^2}{2}\cot\alpha\right)F^{a}[f(x)]dx$
3	Mixed Product Rule	$F^{a}[f(x)]\left(x\frac{d}{dx}\right) = -(\sin\alpha + ix^2\cos\alpha)\sin\alpha.F^{a}[f(x)] + x\cos 2\alpha\frac{d}{dx}F^{a}[f(x)] - \frac{1}{2}\sin 2\alpha\frac{d^2}{dx^2}F^{a}[f(x)]$
4	Differentiation Rule	$F^{a}\left(\frac{df(x)}{dx}\right) = \left(-ix\sin\alpha + \cos\alpha\,\frac{d}{dx}\right)F^{a}[f(x)]$ and $F^{a}\frac{d^m}{dx^m} = \left(-ix\sin\alpha + \cos\alpha\,\frac{d}{dx}\right)^m F^{a}$
5	***Integration Rule***	$F^{a}\left(\int_a^x f(x)dx\right) = \sec x\exp\left(-\frac{ix^2}{2}\tan\alpha\right)\int_a^x\exp\left(+\frac{ix^2}{2}\tan\alpha\right)F^{a}[f(x)]dx.$
6	***Shift Rule***	$F^{a}[f(x+k)] = \exp\left[-ik\sin\alpha\left(x+\frac{k}{2}\cos\alpha\right)\right]F^{a}[f(x)]_{[x+k\cos\alpha]},$
7	***Similarity Rule***	$F^{a}[f-x] = F^{[(a\pi/2)-\pi]}f(x)$
8.	***Convolution Rule***	$f(x)*^{a}g(x) = \exp(-ibx^2)\int_{-\infty}^{\infty}f(\tau)e^{ibx^2}g(x-\tau)e^{ib(x-\tau)^2}d\tau$ where $b = 0.5\cot(0.5\pi a)$ and $*^{a}$ denotes convolution in a^{th} domain

Table-2.5:The FrFT of Simple Functions.

Sr. No.	Function $f(x)$	Fractional Fourier transform $F^a[f(x)]$
1.	$\exp(-x^2/2)$	$\exp(-x_a{}^2/2)$
2.	$H_n(x)\exp(-x^2/2)$	$H_n(x)\exp(-x_a{}^2/2)$
3.	$\exp(-x^2/2+ax)$	$\exp\left(-\frac{x_a{}^2}{2}-\frac{ia^2}{2}e^{i\alpha}\sin\alpha+ax_a e^{i\alpha}\right)$
4.	$\delta(x)$	$\frac{\exp(i\pi/4-i\alpha/2)}{\sqrt{2\pi\sin\alpha}}\exp\left(\left[-\frac{ix_a{}^2}{2}\cot\alpha\right]\right)$
5.	$\delta(x-a)$	$\frac{\exp(i\pi/4-i\alpha/2)}{\sqrt{2\pi\sin\alpha}}\exp\left[-\frac{i}{2}\cot\alpha(x_a{}^2+a^2)+iax_a\cos ec\alpha\right]$
6.	1	$\frac{e^{-i\alpha/2}}{\sqrt{\cos\alpha}}\exp\left[+\frac{ix_a{}^2}{2}\tan\alpha\right]$
7.	e^{ikx}	$\frac{e^{-i\alpha/2}}{\sqrt{\cos\alpha}}\exp\left[\frac{i}{2}\tan\alpha(k^2+x_a{}^2)+ikx_a\sec\alpha\right]$

Table 2.6 illustrates FrFT Fourier transform of some common functions in a^{th} domains.

Table-2.6: The FrFT of Simple Functions.

Sr. No.	Function in $a = 0$ domain	Function in a domain
1	$\sin(x)$	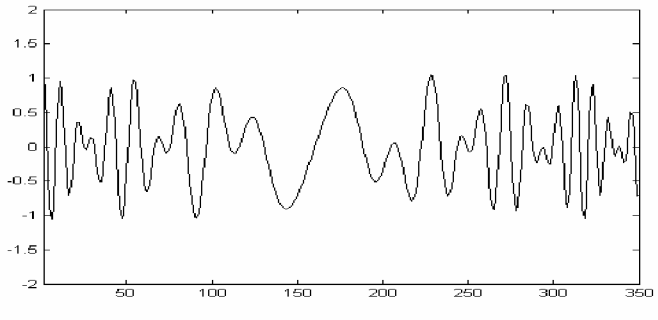 real part of $\sin(x)$ at $a = 0.3$ 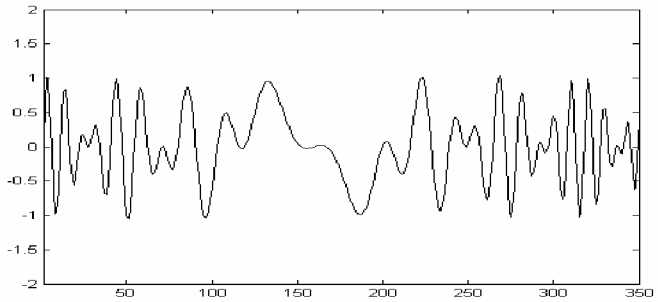 imaginary part of $\sin(x)$ at $a = 0.3$
2	$\cos(x)$	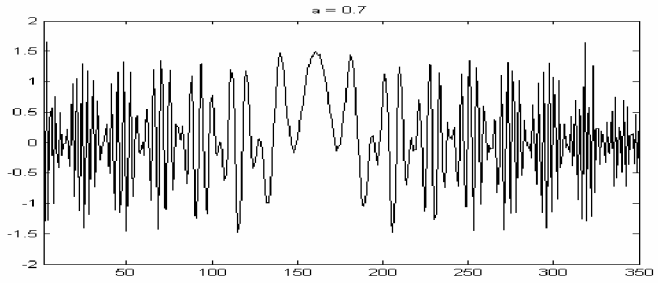 real part of $\cos(x)$ at $a = 0.7$ 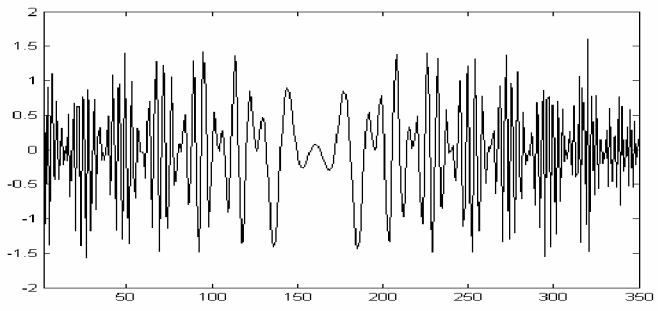 imaginary part of $\cos(x)$ at $a = 0.7$

Sr. No.	Function in $a = 0$ domain	Function in a domain
3	$\exp(ix)$	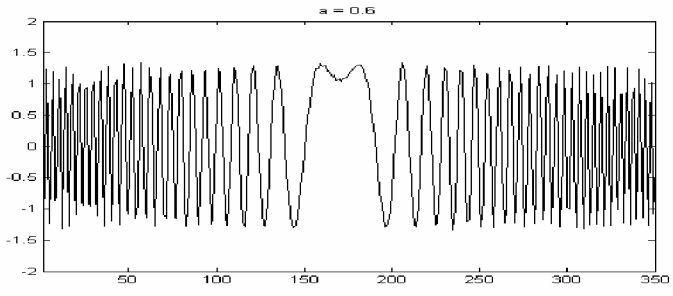 real part of $\exp(ix)$ at $a = 0.6$ 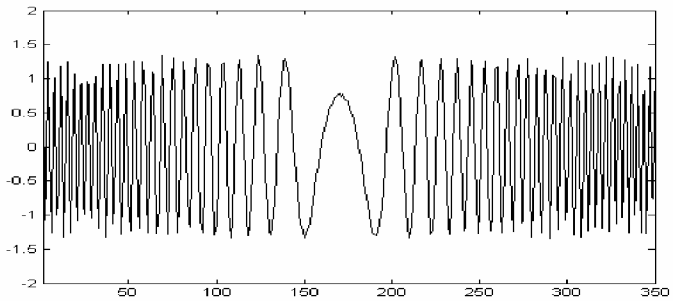 imaginary part of $\exp(ix)$ at $a = 0.6$
4	$\exp(-ix^2)$	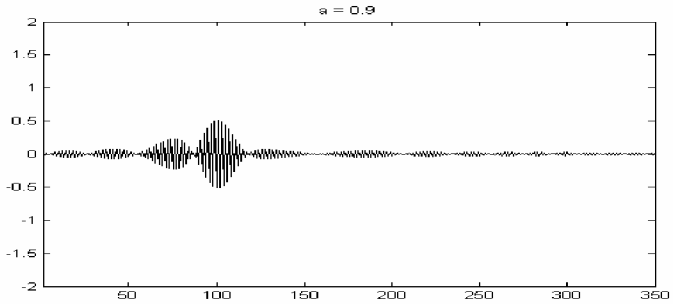 real part of $\exp(-ix^2)$ at $a = 0.9$ 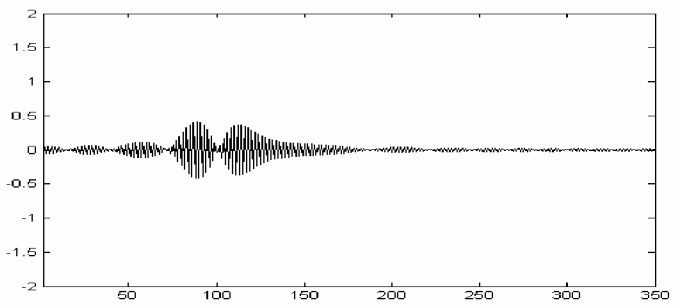 imaginary part of $\exp(-ix^2)$ at $a = 0.9$

Sr. No.	Function in $a = 0$ domain	Function in a domain
5	$\delta(x)$	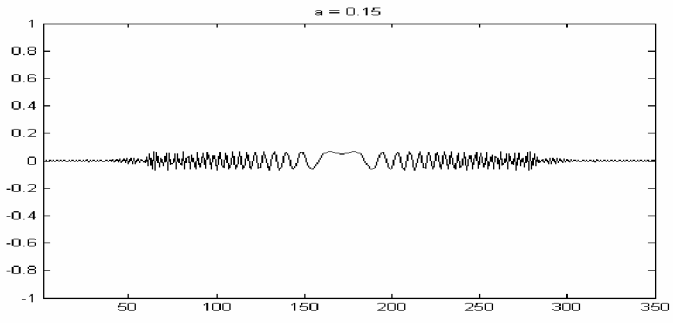 real part of $\delta(x)$ at $a = 0.15$ 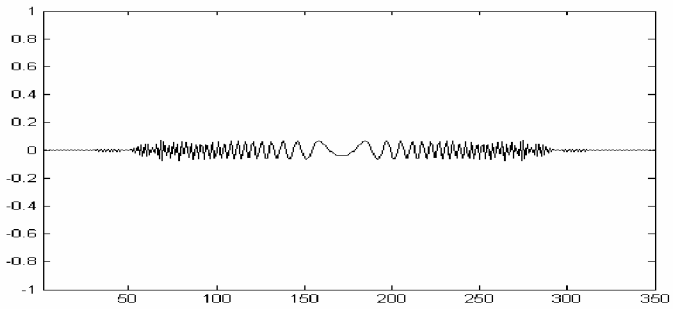 imaginary part of $\delta(x)$ at $a = 0.15$

2.4 FRACTIONAL SINE AND COSINE TRANSFORM

Recently fractional sine and cosine transforms have been derived by the researchers [82]. The fractional sine / cosine transforms are derived by taking the imaginary / real parts of the FrFT kernel. The real part of FrFT kernel is chosen as the kernel for FrCT as in case of cosine transform (CT) where real part of FT is chosen as CT kernel and the imaginary part of the FrFT kernel is chosen as fractional sine transform (FrST).

$$F_S^a[f(x)] = \int_{-\infty}^{\infty} \mathrm{Im}[K^a(x, x_a)] f(x) dx \tag{2.75}$$

$$F_C^a[f(x)] = \int_{-\infty}^{\infty} \mathrm{Re}[K^a(x, x_a)] f(x) dx \tag{2.76}$$

These fractional sine / cosine transform have the advantages that the transform results are real for real input but they do not demonstrate the additivity property and inverse transform property [82].

2.5 TWO DIMENSIONAL FrFT

The one-dimensional FrFT is useful in the processing one-dimensional signals such as speech waveforms. For analysis of two-dimensional signals such as images, a two-dimensional version of the FrFT is required. The general expression of the two-dimensional FrFT is given in [36], [37], [82].

$$F^{a}[q(x,v)] = F^{a_x a_v}[f(x,v)]$$

$$= \iint K^{a_x a_v}(x,v;x_{ax},v_{av}) f(x_{ax},v_{av}) dx_{ax} dx_{av} \qquad (2.77)$$

where, $K^{a_x a_v}(x,v;x_{ax},v_{av}) = K^{a_x}(x,x_{ax}) K^{a_x}(v,v_{av})$

where, $q = u\hat{u} + v\hat{v}$ and $a = a_u\ \hat{u} + a_v\ \hat{v}$, where $\hat{u}$ and $\hat{v}$ are unit vectors in the u and v directions.

The effect of a one-dimensional FrFT on a two-dimensional function is interpreted by treating the other dimension as a parameter. One-dimensional transform can be represented in two dimensions as

$$F^{a} = F^{a_x \vec{x}} F^{a_{x'} \vec{x}'} = F^{a_{x'} \vec{x}'} F^{a_x \vec{x}}. \qquad (2.78)$$

2.6 SUMMARY

The available definitions of FrFT are studied and implemented. The simulation studies for the determination of FrFT of any given function confirms the theoretical results. The simulation

studies have been carried out with Mathematica (version 4.2) package. It has also been observed that all the definitions of FrFT are giving the same transformed function in a particular domain. It has also emerged during this course of study that linear integral transform definition of FrFT is the best candidate for calculation of FrFT. To further strengthen the know how the properties of FrFT are also verified by using Riemann and Hanning function. In the available literature the rectangular and triangular window functions were used by most of the authors to demonstrate their respective FrFT. In this study the listed properties are verified by using Riemann function for the first time and their proofs are given with graphical illustrations (with the help of simulation process). This can be considered as contribution to the available literature in this area of FrFT.

The studies performed during this investigation and reported in the chapter are good enough for consolidation of background. The next chapter deals with the discrete version of FrFT.

CHAPTER 3

DISCRETE FRACTIONAL FOURIER TRANSFORM

3.1 INTRODUCION

The definitions of FrFT and its properties are reviewed in the previous chapter. Due to the computational complexity involved in the continuous domain a discrete version of FrFT is required which can be calculated in an efficient and faster way. In contrast, to the case of DFT where it has one basic definition and lot of algorithms available for its fast computation, FrFT has many definitions in discrete domain.

The work on DFrFT was first reported in 1995 by Santhanam and McClellan [30]. Thereafter within a short span of time many definitions of DFrFT came into existence and these definitions are classified according to the methodology used for calculations in 2000 by Pie *et al.* [24]. The comparison of various DFrFT definitions with continuous FrFT has been done by various authors[23], [33]-[35]. Different parameters have been used for the performance evaluation of various classes of DFrFT's.

The basic problem for the signal processing community is the exactness of DFrFT that can be used for signal processing applications with least possible error and has the fastest evaluation.

In this chapter various classes of DFrFT are introduced along with a review. The performance of available DFrFT at $a = 1$ is also compared with FFT in order to further consolidate the work on

DFrFT and its usage in signal processing applications. Also DFrFT has been used as a tool to carry out the analysis of window functions in fractional domain, that are having significant utility in signal processing applications.

3.2 DFrFT CLASSES

Various definitions of DFrFT are available in literature but none of them obeys all the properties of the FrFT. Pie *et al*. [24] classified these definitions and are given as -

3.2.1. Direct Form of DFrFT

The simplest way to derive the DFrFT is sampling the continuous FrFT and computing it directly. But when the continuous FrFT is sampled directly, the resultant discrete transform looses many important properties such as unitary, reversibility, additivity and closed form expression. Therefore, its domain is confined.

3.2.2. Improved Sampling DFrFT

In this class of DFrFT, the continuous FrFT is properly sampled and it is observed that the resultant DFrFT has the similar transform results as the continuous FrFT. Although, in this case, the DFrFT can work very similar to the continuous case with fast computation, but the transform kernel is not orthogonal and additive. The major constraint in this class is that it is applicable to only a set of signals [29].

The FrFT given in (2.1) cannot be evaluated analytically and therefore, numerical integration is used to evaluate the integration. Due to the rapid oscillations of the kernel, the quadratic exponentials requires a very large number of samples if conventional methods are to be employed. In particular when a is very close to 0 or ± 2, the problem is very severe. This difficulty can be overcome by assuming that the function and its FT both are confined to a finite interval. The integral is directly evaluated when $a \in [0.5,1.5]$ or $a \in [2.5,3.5]$ and when $a \in (-0.5,1.5)$ or $a \in (1.5,2.5)$ the property $F^a = F^1 F^{a-1}$ is used. From this it is clear that in later case, the $(a-1)^{th}$ transform can be evaluated directly [29].

The FrFT given in (2.1) can also be evaluated by using the spectral decomposition of the kernel [72], [10]-[12]. This is equivalent to first expanding the function $f(x)$ as $\sum_{n=0}^{\infty} c_n \psi_n(x)$, multiplying the expansion coefficients c_n, respectively, with $e^{-ian\pi/2}$, and summing the components.

Although both ways of evaluating the DFrFT may be expected to give accurate results, but they are not considered since they take $O(N^2)$ time. It is already discussed that the FrFT is a member of a more general class of transformations called LCT or quadratic-phase transforms [37]. Members of this class of transformations can be broken down into a succession of simpler operations, such as chirp multiplication, chirp convolution, scaling and ordinary Fourier transformation. For the fast computation of the transform there are various ways of decomposing this class of integrals. One of these algorithm is discussed in detail.

In this algorithm, the fractional transform is broken down into a chirp multiplication followed by chirp convolution followed by another chirp multiplication [29]. In this approach, it is assumed that $a \in [-1,1]$. The equation (2.1) can be manipulated as

$$F^{a}[f(x)] = \exp[-i\pi x^2 \tan(\phi/2)]g'(x), \quad (3.1)$$

$$g'(x) = A_{\phi}\int_{-\infty}^{\infty} \exp[-i\pi\beta(x-x_a)^2]g(x)dx, \quad (3.2)$$

$$g(x) = \exp[-i\pi x^2 \tan(\phi/2)]f(x) \quad (3.3)$$

where $g(x)$ and $g'(x)$ represent intermediate results, and $\beta = \csc\phi$.

In the first step the signal $f(x)$ is multiplied by a chirp function. In second step the function $g(x)$, having bandwidth and time-bandwidth product as large as twice that of $f(x)$, is convolved with the chirp function as given by (3.2). Then it is again multiplied by a chirp function in (3.3).

It is well known that a function and its FT cannot be both compact. However, in practice finite time interval and finite bandwidth is considered. This discrepancy between the mathematical idealization and the real world is usually not a problem for the signals of large time-bandwidth product. It can be assumed that the time domain signal is approximately confined to $[-\Delta t/2, \Delta t/2]$ and its frequency domain representation is confined to interval $[-\Delta f/2, \Delta f/2]$. In other words it can be stated that large percentage of the signal energy is confined to these intervals. The time-bandwidth product is defined as $N = \Delta t \Delta f$. A scaling parameter s with dimensions of time is used to scale the coordinates as $x = t/s$ and $\nu = fs$. The time and frequency domain representations will be confined to intervals $\Delta t/s$ and Δfs. The scaling parameter can be

chosen $s = \sqrt{\Delta t / \Delta f}$, so that the lengths of both the intervals are equal to a dimensionless quantity $\Delta x = \sqrt{\Delta f \Delta t}$. In these newly defined coordinates the function can be represented in both domains with $N = \Delta x^2$ samples spaced $\Delta x^{-1} = 1/\sqrt{N}$ apart. After this dimensional normalization, the coordinates appearing in the definition of FrFT becomes dimensionless. Thus, the representation of signal in all domains is assumed to be confined to an interval of length Δx around the origin, which is equivalent to assuming that the WD is confined within a circle of diameter Δx. Now, when the time domain representation of the signal $f(x)$ is multiplied by a chirp function $\exp\left[-i\pi x^2 \tan(\phi/2)\right]$, where $-\pi/2 \le \phi \le \pi/2$, the effect will be to shear the WD in ν direction. The instantaneous frequency of this chirp is $\tan(\phi/2)x$. If this chirp is confined to the interval $[-\Delta x/2, \Delta x/2]$, the largest instantaneous frequency will be $\left|\tan(\phi/2)\right|\Delta x/2$. If this is taken approximately equal to the bandwidth of the chirp, then the double-sided bandwidth of chirp is $\left|\tan(\phi/2)\right|\Delta x$. Multiplying the function $f(x)$ with chirp will result in the convolution of their FT, which results in an over all double-sided bandwidth of $[1+\left|\tan(\phi/2)\right|]\Delta x$. Thus the samples of $g(x)$ are required at intervals of $1/2\Delta x$, if the samples of $f(x)$ are spaced at $1/\Delta x$. Hence the samples of $f(x)$ are interpolated before multiplication with the chirp to obtain the desired samples of $g(x)$ [29].

To perform the convolution, the chirp function can be replaced by its band limited version without any effect as:

$$g'(x) = A_\phi \int_{-\infty}^{\infty} \exp\left[-i\pi\beta(x - x_a)^2\right] g(x_a)\,dx_a = A_\phi \int_{-\infty}^{\infty} h(x - x_a)^2 g(x_a)\,dx_a \qquad (3.4)$$

where, $h(x) = \exp \int_{-\Delta x}^{\Delta x} H(v) \exp(i2\pi v x)\,dv$ (3.5)

and $H(v) = \frac{1}{\sqrt{\beta}} e^{i\pi/4} \exp(-i\pi v^2/\beta)$ (3.6)

is the FT of $\exp(i\pi\beta x^2)$. It is possible to express $h(x)$ explicitly in terms of the Fresnel integral [29] as:

$$F(z) = \int_0^{\pi} \exp(\pi z^2/2)\, dz \tag{3.7}$$

Now, (3.2) can be sampled, giving

$$g'\left(\frac{m}{2\Delta x}\right) = \sum_{n=-N}^{N} h\left(\frac{m-n}{2\Delta x}\right) g\left(\frac{n}{2\Delta x}\right). \tag{3.8}$$

This convolution can be evaluated using FFT. Then after multiplying with second chirp $\exp\left[-i\pi x^2 \tan(\phi/2)\right]$ the samples of $f^a(x')$ spaced at $1/2\Delta x$. Since all the transforms of $f(x)$ are assumed to be band limited to the interval $\left[-\Delta x/2, \Delta x/2\right]$, to obtain samples of $f^a(x')$ spaced at $1/\Delta x$, these samples are decimated by a factor of 2.

Thus, the procedure starts with N samples placed at $1/\Delta x$, which uniquely characterize the function $f(x)$, and returns the same for $f^a(x')$. Let $\mathbf{f}$ and $\mathbf{f}^a$ denote column vectors with N elements containing the samples of $f(x)$ and $f^a(x_a)$, the overall procedure can be represented as

$$\mathbf{f}^a = F_I^a \mathbf{f}, \tag{3.9}$$

$$F_I^a = \mathbf{D} \quad H_{lp} \quad \mathbf{J} \tag{3.10}$$

where, **D** and **J** are matrices representing the decimation and interpolation operations [29]. is a diagonal matrix that corresponds to chirp multiplication, and H_{lp} corresponds to the convolution operation. It can be noted from here that F_I^a allows obtaining the samples of the a^{th} transform in terms of the original function, which is the basic requirement for a definition of the DFrFT matrix.

The above algorithm works in the interval from $-1 \le a \le 1$. If a lies outside this interval, the properties $F^4[f(x)] = f(x)$ and $F^2[f(x)] = f(-x)$ can be used to easily obtain the desired transform.

3.2.3 Linear Combination DFrFT

This DFrFT is derived by using the linear combination of identity operator, DFT, time inverse operation and IDFT. In this case, the transform matrix is orthogonal and the additivity property along with the reversibility property is satisfied. However the main problem is that the transform results do not match to the continuous FrFT [24], [30].This DFrFT can be interpreted as a rotation in time-frequency plane and is also referred to as discrete rotational FT or discrete angular FT with α as the angle or rotation parameter.

The discrete version of the angular FT which is an angular generalization of the DFT is discussed in this section. The DFT operator W is defined as $N \times N$ matrix as

$$W_{nk} = \frac{1}{\sqrt{N}} \exp\left(-j \frac{2\pi}{N} nk \right). \tag{3.11}$$

The operator W is a unitary operator with a set of N eigenvectors and four distinct eigenvalues $[1, -1, j, -j]$. The discrete version of the angular FT is obtained by an angular generalization of these eigenvalues to a continuous angular parameter by using fractional powers of eigenvalues.

Successive applications of the Fourier transformation F on $f(x)$ yields

$$F^2[f(x)] = f(-x), \qquad F^3[f(x)] = f^a(-x_a), \qquad F^4[f(x)] = f(x) \tag{3.12}$$

In a similar fashion, the DFT operator defined in (3.11) when applied to $x(n)$ yields

$$W^2[f(n)] = x[((-n))_N], \qquad W^3[f(n)] = X[((-k))_N], \qquad W^4[f(n)] = f(n) \qquad (3.13)$$

These equations lead to interpret the continuous time FT as a 90° rotation operator in the (x, x_a) plane and the DFT as a 90° rotation operator in the (n, k) space. Application of the operator twice is a reflection or a 180° rotation; thrice is a reflection of the transform or a 270° rotation; and four times corresponds to the identity operation or a 360° rotation. The discrete version of this angular FT defined in equation (2.1) by replacing x with n and x_a by k does not produce a discrete rotational operator because a discrete (n, k) grid does not permit transformations with non-integer entries instead, the discrete rotational Fourier transform (DRFT) is defined as [30]

$$A^{\alpha}(f) = W^{\frac{2\alpha}{\pi}}(f) \qquad (3.14)$$

The evaluation of this operator for $\alpha = 0, 2\pi$ gives

$$A^{2\pi} = W^4 = I = W^0 = A^0 \qquad (3.15)$$

and for $\alpha = \frac{\pi}{2}$, it becomes

$$A^{\pi/2} = W^1 = W \qquad (3.16)$$

which is the DFT operator.

For $\alpha = \pi$ a cyclic flip matrix is obtained which is given as

$$A^{\pi} = W^2 \qquad (3.17)$$

The equations (3.14) to (3.17) provide the motivation to interpret the operator A^{α} as a rotation through α in (n, k) plane. A Taylor series expansion of the matrix operator A^{α} followed

by application of the Cayley-Hamilton theorem, which states that every matrix satisfies its characteristic equation, suggests that [30]

$$A^{\alpha} = a_0(\alpha)I + a_1(\alpha)W + a_2(\alpha)W^2 + a_3(\alpha)W^3 \tag{3.18}$$

where the coefficients $a_i(\alpha)$ are obtained on regrouping of terms containing I, W, W^2 and W^3 from the Taylor series expansion. This equation gives an interesting interpretation of subspace mixing, where the coefficients $a_0(\alpha), a_1(\alpha), a_2(\alpha)$ and $a_3(\alpha)$ generate an angular mixture of the basis matrices I, W, W^2 and W^3 [30].

The operator W defined in (3.11) is a unitary operator and consequently has a set of N orthonormal eigenvectors v_i [30]. The operator W has an eigen-decomposition given by

$$W = \sum_i \lambda_i \overset{\circ}{v}_i \overset{\circ}{v}_i^H = \sum_{i \in N_1} \overset{\circ}{v}_i \overset{\circ}{v}_i^H - \sum_{i \in N_2} \overset{\circ}{v}_i \overset{\circ}{v}_i^H + j\left(\sum_{i \in N_3} \overset{\circ}{v}_i \overset{\circ}{v}_i^H - \sum_{i \in N_4} \overset{\circ}{v}_i \overset{\circ}{v}_i^H \right) \tag{3.19}$$

where N_1 is the set of indices for eigenvectors belonging to $\lambda = 1, N_2$ for $\lambda = -1$ and so on. A^{α}, being a matrix function of W is also unitary and has an eigen-decomposition defined by taking a fractional power of the eigenvalues $(\lambda_i)^{\frac{2\alpha}{\pi}}$.

$$\begin{aligned} A^{\alpha} = & \sum_{i \in N_1} \exp(j4k_1\alpha) \overset{\circ}{v}_i \overset{\circ}{v}_i^H + \sum_{i \in N_2} \exp(j(4k_2+2)\alpha) \overset{\circ}{v}_i \overset{\circ}{v}_i^H \\ & + \sum_{i \in N_3} \exp(j(4k_3+1)\alpha) \overset{\circ}{v}_i \overset{\circ}{v}_i^H + \sum_{i \in N_4} \exp(j(4k_4-1)\alpha) \overset{\circ}{v}_i \overset{\circ}{v}_i^H \end{aligned} \tag{3.20}$$

where k_1, k_2, k_3 and k_4 are integers. Because of the ambiguity present in the fractional power operation, the operator A^{α} defined by (3.14) is not unique. The branch cut $k_1 = 0, k_2 = 0, k_3 = 0$ and $k_4 = 0$ is imposed to make the operation unique. A specific ordering on the eigenvalues of $W, \lambda_1 = 1, \lambda_2 = -1, \lambda_3 = j$ and $\lambda_4 = -j$ is also imposed to make the solution unique.

Computation of the transform directly for an angle α requires an eigen-decomposition on the operator W to be performed and the new operator A^{α} be computed. This would be an impractical to do for large orders. Instead, the matrices I, W, W^2 and W^3 are generated for a given dimension N (where W^2 is the circular flip matrix and W^3 is a circularly flipped version of W). The transform and its inverse $A^{-\alpha}$ are then computed through the subspace projection equations.

$$A^{\alpha} = a_0(\alpha)I + a_1(\alpha)W + a_2(\alpha)W^2 + a_3(\alpha)W^3 \tag{3.21}$$

$$A^{-\alpha} = a_0^*(\alpha)I + a_3^*(\alpha)W + a_2^*(\alpha)W^2 + a_1^*(\alpha)W^3 \tag{3.22}$$

where the coefficients $a_0(\alpha), a_1(\alpha), a_2(\alpha)$ and $a_3(\alpha)$ in the expansion are given by [30]

$$a_0(\alpha) = \frac{1}{2}\left(1 + e^{j\alpha}\right)\cos\alpha ,$$

$$a_1(\alpha) = \frac{1}{2}\left(1 - e^{-j\alpha}\right)\sin\alpha ,$$

$$a_2(\alpha) = \frac{1}{2}\left(e^{j\alpha} - 1\right)\cos\alpha \quad \text{and}$$

$$a_3(\alpha) = \frac{1}{2}\left(-1 - je^{j\alpha}\right)\sin\alpha \tag{3.23}$$

The DFrFT of a signal $f(n)$ can also be written as

$$F^a[f(n)] = \sum_{n=0}^{N-1} K^a(n,k) f(n) \tag{3.24}$$

where the kernel of the transformation corresponding to the operator A^{α} is given by

$$\begin{aligned} K^a(n,k) = {} & a_0(\alpha)\delta(n-k) + \frac{a_1(\alpha)}{\sqrt{N}}\exp\left(-j\frac{2\pi}{N}nk\right) \\ & + a_2(\alpha)\delta[((n+k))_N] + \frac{a_3(\alpha)}{\sqrt{N}}\exp\left(j\frac{2\pi}{N}nk\right) \end{aligned} \tag{3.25}$$

The signal is recovered through the IDFrFT relation

$$f(n) = \sum_{k=0}^{N-1} K^{-a}(n,k) f^{a}(k) \tag{3.26}$$

3.2.4 Group Theory DFrFT

The concept of group theory is used in deriving this definition of DFrFT as multiplication of DFT and periodic chirps. The DFrFT determined by this process satisfies the rotational property of WD, the additivity property and the reversibility property of FrFT. However, this type of DFrFT can be derived only when the fractional order of the DFrFT equals some specified angles and when the number of points *N* is not prime [24], [31].

The concept of rotations in continuous time, continuous frequency is extended to discrete time, discrete frequency as it applies to the WD. As in the continuous domain, discrete rotations are defined to be elements of the special orthogonal group over the appropriate (discrete) field. Use of this definition ensures that discrete rotations will share many of the same mathematical properties as continuous ones. This algorithm provides a further connection between the DFT and the discrete WD based on group theory.

The WD satisfies many desirable properties and one of them is the property of maximal covariance. This property results from the relationship between the WD and the Weyl correspondence [31]. Applying a change of coordinates to WD of a signal is identical to computing the WD of that signal after an appropriate combination of dilations, shearings, and rotations has been applied to it. These concepts are completely straightforward for the continuous WD. In particular, the concept of applying a rotation to a continuous time-frequency distribution is easily understood. To rotate a distribution by an angle θ, simply apply the matrix $R(\theta)$, given by

$$R(\theta)=\begin{bmatrix}\cos\theta & \sin\theta\\ -\sin\theta & \cos\theta\end{bmatrix} \tag{3.27}$$

to the coordinates of the WD. In the time domain, this is equivalent to applying the appropriate FrFT. The case of $\theta=-\frac{\pi}{2}$ is particularly significant, as this corresponds in the time domain to a FT. Poletti [83] gave a time-frequency interpretation of how this rotation would be decomposed into a series of chirps in the context of ambiguity function.

For the case of discrete-time discrete-frequency time-frequency distributions, rotations are more difficult to understand because the time-frequency plane is periodic and has finitely many points. Until recently, there was not a formulation of the WD in the signal processing literature that could be related to the discrete Weyl correspondence. In [84] a discrete-time, discrete-frequency WD is derived that does satisfy the Weyl correspondence for this discrete domain. Since it is clear that the discrete-time, discrete-frequency domain is different from the continuous-time, continuous-frequency domain [84], it is not surprising that the interpretation of rotations is different as well. The concept of rotations is generalized to discrete-time, discrete-frequency using an algebraic construction.

In [85], the discrete-time, discrete-frequency WD was shown to satisfy the property of co-variance made possible by its relationship with the Weyl correspondence. Specifically, the application of a symplectic transformation, A, to a WD, $W_{f(x)g(x)}$, is equivalent to first applying a unitary transformation dependent on A,$U(A)$, to both $f(x)$ and $g(y)$, and then computing their WD, i.e.

$$W_{s(x)g(x)}[A(t,f)]=W_{U(A)[f(x)]\ U(A)[g(x)]}(t,f) \tag{3.28}$$

In other words, if a linear transformation with unit norm is applied to a WD in the time-frequency plane, there is a corresponding transformation of the signals that yields the same WD.

While there are three fundamentals types of symplectic transformations (dilation / compression, shearing, and rotations), the focus here is on rotations. The only rotation explored in [85] the symplectic transformation A^{γ} corresponding to rotation counterclockwise by 90 degrees and given by

$$A^{\gamma} = \begin{bmatrix} 0 & 1 \\ -1 & 0 \end{bmatrix} \tag{3.29}$$

And the corresponding unitary transformation $U(A^{\gamma})$ for a signal of length N $f(n)$ such that (3.28) is satisfied and is given by

$$U(A^{\gamma})[f(n)] = j^{1/2} \sum_{k=0}^{N-1} e^{\frac{j2\pi nk}{N}} F^{1}[f(n)] = j^{1/2} \sum_{k=0}^{N-1} e^{\frac{j2\pi nk}{N}} F(k) \tag{3.30}$$

where, $F(k)$ is the DFT of $f(n)$. $U(A^{\gamma})$ is proportional to the inverse DFT. It is clear that application of the symplectic transformation A^{γ} does result in a rotation by 90 degrees.

In the continuous time-frequency plane, a rotation by θ is given by the matrix in (3.27). The set of such rotation matrices in two dimensions comprise an algebraic group called the special orthogonal group of dimension 2 over the real numbers, or $SO(2, R)$. The elements $R(\theta)$ of $SO(2, R)$ should satisfy the following properties, [78]:

1. Zero rotation: $R(0) = I$
2. Consistency with Fourier transform: $R\left(-\frac{\pi}{2}\right) = F^{1}$
3. Additivity of rotations: $R(\alpha)R(\beta) = R(\alpha + \beta)$

In discrete-time, discrete-frequency for a p length signal (p prime), let a rotation matrix be any element in the analogous group of matrices, the special orthogonal group of dimension 2 over the integers modulo p, $SO(2, Z/p)$. Then every element R_p of $SO(2, Z/p)$ has the form [31],

$$R_p(a,b) = \begin{bmatrix} a & b \\ -b & a \end{bmatrix} \tag{3.31}$$

where, a and b are elements of the integers $\mathrm{mod}(p, Z/p)$, and the determinant of $R_p(a,b)$ is equal to 1, i.e.

$$a^2 + b^2 = 1 \bmod p \tag{3.32}$$

Such matrices have a similar form to that given in (3.27). Furthermore, since the identity matrix and $A^{-\gamma}$ are both elements of $SO(2, Z/p)$, this definition satisfies the first two properties [78]. The third property is satisfied by the fact that $SO(2, Z/p)$ has a generator [31], and so every element can be expressed as a power of the generator (multiplication of elements is accomplished by the addition of exponents).

Another consequence is that there are only finitely many rotations possible for any given p. To obtain the exact number for $p > 2$ ($p = 2$ is a trivial case), first expressing p as $p = 4l \pm 1$. Then, the number of possible rotations, i.e. number of elements of $SO(2, Z/p)$ is given by [31],

$$\text{Number of rotations} = \begin{cases} p-1 & if\ p = 4l+1 \\ p+1 & if\ p = 4l-1 \end{cases} \tag{3.33}$$

These rotations can be computed directly in the time-domain, by expressing a rotation matrix as a product of shearing and 90 degree rotation matrices, and then applying the corresponding sequence of time domain transformation, i.e. the product

$$\begin{bmatrix} 1 & 0 \\ \alpha & 1 \end{bmatrix} A^{-\gamma} \begin{bmatrix} 1 & 0 \\ -b & 1 \end{bmatrix} A^{\gamma} \begin{bmatrix} 1 & 0 \\ \alpha & 1 \end{bmatrix} = \begin{bmatrix} a & b \\ -b & a \end{bmatrix} \tag{3.34}$$

has the corresponding time domain operator

$$e^{\frac{j2\pi(2^{-1}\alpha n^2)p}{p}} F e^{\frac{j2\pi(2^{-1}(-b)n^2)p}{p}} F^{-1} e^{\frac{j2\pi(2^{-1}\alpha n^2)p}{p}} \tag{3.35}$$

where, $\alpha = (a-1)b^{-1}$, F refers to the DFT, and $(.)_p$ refers to arithmetic modulo p.

It is possible, albeit more complicated, to generalize the results here to non-prime lengths. Such complications arise from the fact that Z/n is harder to characterize when n is not prime. Based on the discussion presented here, there is some justification to consider (3.35) as a definition for the DFrFT. This differs from definitions given in [29], [30]. Due to the difficulties in interpreting some of the rotations obtained from (3.35), it would be premature to make any further claims about its relationship to the DFrFT. This analysis provides insight into why it is difficult to suitably define this transform.

3.2.5 Impulse Train DFrFT

This DFrFT can be viewed as a special case of continuous FrFT in which the input function is a periodic equally spaced impulse train. If in a period Δ_o, the number of impulses are N, then N should be equal to Δ_o^2. This DFrFT is a special case of FrFT, which satisfies many properties of the FrFT and has fast computational algorithms. However, this type of DFrFT has many constraints and cannot be defined for all fractions [24], [86].

Let, $f(x)$ be a sampled periodic signal with a period Δ_0:

$$f(x) = \sum_{k=-N/2}^{N/2-1} f\left(k\frac{\Delta_0}{N}\right)\sum_{n=-\infty}^{\infty} f\left(k\frac{\Delta_0}{N}\right)\delta\left(x-\left(n+\frac{k}{N}\right)\Delta_0\right) \tag{3.36}$$

where, N are the number of samples in a period is taken to be even. For order a the FrFT of $f(x)$ can be obtained by using (3.36), giving [86]

$$F^a[f(x)] = \int_{-\infty}^{\infty} K^a(x,x')f(x)dx = \sum_{k=-N/2}^{N/2-1} f\left(k\frac{\Delta_0}{N}\right)\sum_{n=-\infty}^{\infty} K^a\left(x,\left(n+\frac{k}{N}\right)\Delta_0\right) \tag{3.37}$$

For the transformed function in (3.37) to be periodic with a period Δ_α, $F^a[f(x)]$ should be equal to $F^a[f(x+l\Delta_\alpha)]$ for all x and l. By little algebraic manipulation the periodicity is satisfied if and only if

$$\Delta_\alpha \cos\phi = p\Delta_0 \tag{3.38}$$

$$\Delta_\alpha \sin\phi = q\frac{N}{\Delta_0} \tag{3.39}$$

where, for integers p and q such that pqN is even, which is satisfied since N is even. The ratio of (3.39) and (3.38) gives the condition on the transformation order:

$$\tan\phi = \frac{q}{p}\frac{N}{\Delta_0^2} \tag{3.40}$$

which implies that the $F^a[f(x)]$ is periodic for only a set of orders which satisfies (3.40) and hence have a cardinality equal to the rational numbers. Since the set of rationals are dense in the set of real numbers, this set of orders also forms a dense set in the set of all possible orders. The conditions in (3.38) and (3.39) can be easily interpreted by the identification of $\frac{N}{\Delta_0}$ as the period of $f(x)$ in the FT domain [87]. The first condition in (3.38) implies that the projection of the period on the transform domain of order a onto the original domain should be a multiple of the period in the original domain. Likewise, the second condition in (3.38) implies that the projection of the period on the transform domain of order a onto the FT domain. By choosing $N = \Delta_0^2$, the periods in the original and the FT domain can be made equal to each other, resulting in a square tiling pattern in the time-frequency domain [29]. In this case, the condition becomes:

$$\Delta_\alpha \cos\phi = p\Delta_0 \tag{3.41}$$

$$\Delta_\alpha \sin\phi = q\Delta_0 \tag{3.42}$$

which are satisfied by $\tan\phi = q/p$ and $\Delta_\alpha = \sqrt{p^2+q^2}\Delta_0$. It is assumed that ϕ satisfies these conditions. By using the shift property of the FrFT, (3.37) can be written as [86]:

$$F^a[f(x)] = \sum_{k=-N/2}^{N/2-1} f\left(k\frac{\Delta_0}{N}\right)\exp(B)\sum_{n=-\infty}^{\infty} K^a\left(x-\left(\frac{k}{N}\right)\Delta_0\cos\phi, n\Delta_0\right) \tag{3.43}$$

where, $B = j\pi\left(\sin\phi\cos\phi\left(k\frac{\Delta_0}{N}\right)^2 - 2\sin\phi x\frac{k\Delta_0}{N}\right)$.

The inner summation in (3.43) is the shifted fractional Fourier transformation of a uniform impulse train with period Δ_0, which is denoted by $\bar{\delta}^a[f(x)]$:

$$\bar{\delta}^a[f(x)] = \int_{-\infty}^{\infty} K^a(x,x_a)\sum_{n=-\infty}^{\infty}\delta(x-n\Delta_0) \tag{3.44}$$

By using the relation between the projections of the WD and the magnitude square of the FrFT, it can be shown that $\bar{\delta}^a[f(x)]$is also a uniform impulse train with a quadratic phase term:

$$\bar{\delta}^a[f(x)] = A_\phi\sqrt{\frac{2r^2}{pqN}}\sum_{n=-\infty}^{\infty}\exp\left(j\pi\cot\phi x^2\right)\delta\left(x-\frac{nr}{\Delta_\alpha}\right) \tag{3.45}$$

where, r is the greatest common divisor of q and N. If q and N are relatively prime, then the following transform relation can be obtained using (3.43) [86]-

$$F^a[f(x)] = \sqrt{\frac{2r^2}{pqN}}A_\phi\sum_{k=-N/2}^{N/2-1} f\left(\frac{k\Delta_0}{N}\right)\exp(Z)\sum_{n=-\infty}^{\infty}\delta\left(x-\frac{n}{\Delta_\alpha}\right) \tag{3.46}$$

where, $Z = j\pi\left(x^2\cot\phi - 2x\frac{k\Delta_0}{N}\csc\phi + \left(\frac{k\Delta_0}{N}\right)^2\cot\phi\right)$.

To get (3.46) the fact that $\left(\frac{k}{N}\right)\Delta_0\cos\phi = kp/\Delta_\alpha$ is used. In this form of the transform relation it is seen that the transform of the sampled periodic signal is also a sampled and periodic

signal with a sampling interval of $1/\Delta_\alpha$. This is an important property that allows us to claim that the DFrFT being the relation between the multitudes of the impulsive sequences in respective domains. This leads us to the following form for the discrete definition of the FrFT [86]

$$F^a\left[f\left(\frac{n}{\Delta_\alpha}\right)\right] = \sum_{k=-N/2}^{N/2-1} T_\phi\left(\frac{n}{\Delta_0},\frac{k}{\Delta_0}\right) f\left(\frac{k}{\Delta_0}\right) \tag{3.47}$$

where, $N=\Delta_0^2$ is used to get the above symmetric form of the transform, and the discrete transformation kernel T_ϕ is given by:

$$T_\phi\left(\frac{n}{\Delta_\alpha},\frac{k}{\Delta_0}\right) = \sqrt{\frac{2}{pqN}} A_\phi \exp\left(j\pi\left(Z\right)\right) \tag{3.48}$$

where, $Z = \left(\frac{n}{\Delta_\alpha}\right)^2 \cot\phi - 2\frac{n}{\Delta_\alpha}\frac{k}{\Delta_0}\csc\phi + \cot\phi + \left(\frac{k}{\Delta_0}\right)^2 \cot\phi$

A fast algorithm for the efficient computation of the DFrFT can be obtained by following the steps:

$$F^a\left[h(k)\right] = \exp\left(j\pi\left(\cot\phi - \frac{\Delta_0}{\Delta_\alpha}\csc\phi\right)\left(\frac{k}{\Delta_0}\right)^2\right) f\left(\frac{k}{\Delta_0}\right) \tag{3.49}$$

$$F^a\left[g(n)\right] = \sqrt{\frac{2}{pqN}} A_\phi \sum_{k=-N/2}^{N/2-1} \exp\left(j\pi \frac{(n-k)^2\Delta_0}{\Delta_\alpha\Delta_0}\csc\phi\right) F^a\left[h(k)\right] \tag{3.50}$$

$$F^a\left[f(n)\right] = \exp\left(-j\pi\left(\cot\phi - \frac{\Delta_\alpha}{\Delta_0}\csc\phi\right)\left(\frac{n}{\Delta_\alpha}\right)^2\right) F^a\left[g(n\right] \tag{3.51}$$

where in the first step $F^a\left[h(k)\right]$ can be obtained by computing N multiplications, in the second step the required convolution can be performed by using FFTs with a requirement of $O(N\log N)$ multiplications, and in the final step $f^a(n)$ for $-N/2 \le n \le N/2-1$ can be computed

by using N multiplications. Hence, the total number of multiplications required by the above algorithm is $O(N \log N)$ which are the same as that of FFT [86].

3.2.6 Eigenvectors Decomposition DFrFT

Pie *et al.* [22] suggested another type of DFrFT by searching the eigenvectors and eigenvalues of the DFT matrix and computed the fractional power of the DFT matrix. This type of DFrFT works similarly to the continuous FrFT and also satisfies the properties of orthogonality, additivity and reversibility. This DFrFT can be further improvised by modifying their eigenvectors more similarly to the continuous Hermite function (the eigen functions of the FrFT). The eigenvectors cannot be expressed in closed form and it also lacks the fast computational algorithms [21], [24].

The development of this DFrFT is based on the eigen decomposition of the DFT kernel, and many properties of the DFT matrix eigenvalues and eigenvectors have been discussed in [88] and [89]. The eigenvalues of DFT are $\{1,-j,-1,j\}$, and its multiplicities are shown in Table-3.1.

Table-3.1: Multiplicities of the eigenvalues of DFT kernel matrix.

N	$\#(N,0)$ multiplicity of 1	$\#(N,1)$ multiplicity of -j	$\#(N,2)$ Multiplicity of -1	$\#(N,3)$ multiplicity of +j
$4m$	$m+1$	m	m	$m-1$
$4m+1$	$m+1$	m	m	m
$4m+2$	$m+1$	m	$m+1$	m
$4m+3$	$m+1$	$m+1$	$m+1$	m

In Table-3.1, a multiplicity function $\#(N,k)$ is defined. This function is used to denote the DFT eigenvalue multiplicity for *N*. The parameter k is the index for the DFT eignvalue $e^{-j(\pi/2)k}$. The eigenvectors of the DFT matrix constitute four major eigensubspaces - E_0, E_1, E_2 and E_3, and each is corresponding to one of the four eigenvalues – 1, *-j*, -1 and *j* respectively. The eigenvalue multiplicities of DFT matrix indicate the ranks of the DFT subspaces [89], [90].

In [99], a method for computing the DFT eigenvectors has been introduced, but it cannot obtain the real-valued DFT eigenvectors. In [88], a novel matrix S is introduced to compute the real and complete set of DFT eigenvectors very elegantly and is defined as

$$S = \begin{bmatrix} 2 & 1 & 0 & 0 & \mathrm{i} & 1 \\ 1 & 2\cos\omega & 1 & 0 & \mathrm{i} & 0 \\ 0 & 1 & 2\cos 2\omega & 1 & \mathrm{i} & 0 \\ \mathrm{j} & \mathrm{j} & \mathrm{j} & \mathrm{l} & & \mathrm{j} \\ 1 & 0 & 0 & 0 & \mathrm{i} & 2\cos(N-1)\omega \end{bmatrix} \tag{3.52}$$

where, $\omega = 2\pi / N$. The matrix S commutes with the DFT kernel matrix F, and then, it satisfies the commutative property.

$$SF = FS \tag{3.53}$$

The eigenvectors of matrix S will also be the eigenvectors of the DFT kernel matrix F, but they correspond to different eigenvalues.

The continuous FrFT has a Hermite function with unitary variance as its eigenfunction. The corresponding eigenfunction property for the DFT would be like [22]

$$F^{2\alpha/\pi}[\hat{u}_n] = e^{-jn\alpha}\hat{u}_n \tag{3.54}$$

where $\hat{u}_n$ is the eigenvector of DFT corresponding to the n^{th} order discrete Hermite function.

It is known that the eigendecomposition of the DFT kernel matrix is not unique. The DFT can have the eigenvectors with the similar shapes as the Hermite functions. These DFT eigenvectors are known as DFT Hermite eigenvectors. DFT Hermite eigenvectors should have the associated continuous spread variance $\sqrt{(N/2\pi)}T_s$, where, T_s is the sampling intervals of signal. If the Hermite function are sampled in this way, then

$$\phi_n(k) = \frac{1}{\sqrt{2^n n! \sqrt{N/2}}} h_n\left(\frac{k}{\sqrt{N/2}}\right) e^{-\left(k^2\pi/N\right)} \tag{3.55}$$

where $h_n(.)$ is the n^{th} order Hermite polynomial.

If the sequence $\phi_n(k)$ is obtained by sampling interval $T = \sqrt{2\pi/N}$, then it can be shown that

If N is even

$$(-j)^n \phi_n(k) \approx \sqrt{\frac{1}{N}} \sum_{m=-((N-1)/2)}^{(N/2)-1} \phi_n(m) e^{-j(2\pi km/N)} \tag{3.56}$$

If N is odd

$$(-j)^n \phi_n(k) \approx \sqrt{\frac{1}{N}} \sum_{m=-((N-1)/2)}^{(N-1)/2} \phi_n(m) e^{-j(2\pi km/N)} \tag{3.57}$$

for sufficiently large N [22].

It is clear that there are two approximation errors in (3.56). One is the truncation error and the other is the numerical error. When the value of N approaches infinity, both errors approach zero. Thus, the larger N is, the better approximation (3.56). Next because the degree of Hermite

polynomial $h_n(t)$ is n, the decay rate of the Hermite function $h_n(t)$ is proportional to $t^n e^{-t^2}$ for sufficiently large t [22].

Thus larger the order n, the slower is the decay rate of Hermite function. This implies that the truncation error is larger for high order n. Thus, when order becomes large, the approximation becomes worse.

The n^{th} order continuous Hermite function should have n zeroes [91]. However, these functions are not band limited, and the sampling cannot guarantee that the number of the sign changes in this sampled n^{th} order Hermite function are also n. The small aliasing will occur while n is closer to N but this will not influence the development of the DFrFT. The sampled Hermite functions still can be used to construct the DFrFT kernel because they have the similar shapes and good approximations to the continuous Hermite functions.

If the sequence $\bar{\phi}_n(k)$ defined in the range $[0, N-1]$ is obtained by shifting Hermite Gauss samples, $\phi_n(k)$ is obtained in the following way:

If N is even

$$\bar{\phi}_n(k) = \begin{cases} \phi_n(k), & for 0 \le k \le \dfrac{N}{2} - 1 \\ \phi_n(k-N), & for \dfrac{N}{2} \le k \le N-1 \end{cases} \tag{3.58}$$

and if N is odd

$$\bar{\phi}_n(k) = \begin{cases} \phi_n(k), & for 0 \le k \le \dfrac{N-1}{2} \\ \phi_n(k-N), & for \dfrac{N+1}{2} \le k \le N-1 \end{cases} \tag{3.59}$$

then the DFT of the $\bar{\phi}_n(k)$ can be approximated by $(-j)^n \bar{\phi}_n(k)$ i.e,

$$(-j)^n \bar{\phi}_n(m) \approx \sqrt{\frac{1}{N}} \sum_{k=0}^{N-1} \bar{\phi}_n(k) e^{-j(2\pi km/N)} \tag{3.60}$$

for sufficiently large N .

The normalized vectors for the samplings of Hermite functions are defined as-

$$u_n = \frac{\left[\bar{\phi}_n(0), \bar{\phi}_n(1), \text{ i }, \bar{\phi}_n(N-1)\right]^T}{\left\| \left[\bar{\phi}_n(0), \bar{\phi}_n(1), \text{ i }, \bar{\phi}_n(N-1)\right]^T \right\|} \tag{3.61}$$

Table-3.2: Eigenvalues assignment rule of DFrFT kernel matrix.

N	The eigenvalues
$4m$	$e^{-jk\alpha}, k = 0,1,2, \text{ i }, (4m-2), 4m$
$4m+1$	$e^{-jk\alpha}, k = 0,1,2, \text{ i }, (4m-1), 4m$
$4m+2$	$e^{-jk\alpha}, k = 0,1,2, \text{ i }, 4m, (4m+2)$
$4m+3$	$e^{-jk\alpha}, k = 0,1,2, \text{ i }, (4m+1), (4m+2)$

Because matrix S can have complete real orthogonal DFT eigenvectors, the eigenvectors can be used as bases for individual DFT eigensubspaces. In addition, the projections of u_n in its DFT eigensubspace can be computed to obtain a Hermite like DFT eigenvector

$$\bar{u}_n = \sum_{(n-k) \bmod 4 = 0} < u_n v_k > v_k \tag{3.62}$$

where $k = (n \bmod 4)$, and v_k is the eigenvector of matrix S. $\bar{u}_n$ will be a DFT Hermite eigenvector. In (3.62), the DFT Hermite eigenvector $\bar{u}_n$ is computed from the eigenvectors of matrix S in the same DFT eigensubspace [22].

The fractional power of matrix can be calculated from its eigen decomposition and the powers of eigenvalues. Unfortunately, there exist two types of ambiguity in deciding the fractional power of the DFT kernel matrix.

- *Ambiguity in deciding the Fractional Powers of the Eigenvalues:* The square roots of unity are 1 and -1 which follows from elementary mathematics. This indicates that there exists root ambiguity in deciding the fractional power of eigenvalues.
- *Ambiguity in deciding the Fractional Eigenvectors of the DFT Kernel Matrix:* The DFT eigenvectors constitute four major eigensubspaces; therefore, the choices for the DFT eigenvectors to construct the DFrFT kernel are multiple and not unique.

Because of the above ambiguity, there are several DFrFT kernel matrices that can obey the rotation properties. The idea for developing our DFrFT is to find the discrete form for

$$K^{a}(x,x') = \sum_{n=0}^{\infty} e^{-jn\alpha} H_n(x) H_n(x') \qquad (3.63)$$

In order to retain the eigenfunction property in (3.54), the unit variance Hermite functions are sampled with a period of $T_s = \sqrt{2\pi / N}$ in the following discussions. In the case of continuous FrFT, the terms of the Hermite functions are summed up from order zero to infinity. However, for the discrete case, only eigenvectors for the DFT Hermite eigenvectors can be added. Table-3.2 shows the eigenvalues assignment rules for the DFrFT. This assignment rule matches the multiplicities of the eigenvalues of the DFT kernel matrix in Table-3.1. The selections of the DFT Hermite eigenvectors are from low to high orders as the approximation error for the low Hermite eigenvectors are small. In addition, it should not be expected that a finite vector can express oscillating behavior of the very high-order Hermite function very well.

The transform kernel of the DFrFT can be defined as [22]

$$F^{2\alpha/\pi} = \hat{U}D^{2\alpha/\pi}\hat{U}^T = \begin{cases} \sum_{k=0}^{N-1} e^{-jk\alpha}\hat{u}_k\hat{u}_k^T & for N = 4m+1 \;\; and \;\; 4m+3 \;\; (odd) \\ \sum_{k=0}^{N-2} e^{-jk\alpha}\hat{u}_k\hat{u}_k^T & for N = 4m \\ + e^{-jN\alpha}\hat{u}_N\hat{u}_N^T & 4m+2 (even) \end{cases} \tag{3.64}$$

where, $\hat{U} = [\hat{u}_0 | \hat{u}_1 | \text{ i } | \hat{u}_{N-1}]$, whereas N is odd, and $\hat{U} = [\hat{u}_0 | \hat{u}_1 | \text{ i } | \hat{u}_{N-2} | \hat{u}_N]$ for N is even. $\hat{u}_k$ is the normalized eigenvector corresponding to the k^{th} order Hermite function, where D is defined as follows:

For N odd

$$D^{2\alpha/\pi} = \begin{bmatrix} e^{-j0} & & & 0 \\ & e^{-j\alpha} & & \\ & & \text{I} & \\ & & & e^{-j\alpha(N-2)} & \\ 0 & & & & e^{-j\alpha(N-1)} \end{bmatrix} \tag{3.65}$$

and for N even

$$D^{2\alpha/\pi} = \begin{bmatrix} e^{-j0} & & & 0 \\ & e^{-j\alpha} & & \\ & & \text{I} & \\ & & & e^{-j\alpha(N-2)} & \\ 0 & & & & e^{-j\alpha N} \end{bmatrix} \tag{3.66}$$

An eigenbased method for computing the DFrFT to have similar continuous results has been proposed by Pei *et al* in [18]-[20]. The eigenvectors obtained from matrix S are directly considered to be the discrete Hermite functions [18]. In addition, the eigenvalue-eigenfunction is retained in defining the DFrFT. This means that $\hat{u}$ is replaced by v_k in (3.64). Such a method is called the S method.

Equation (3.62) provides a method for finding DFT Hermite eigenvectors. The role of matrix S in (3.62) is just as a tool to find a complete set of real and orthogonal DFT eigenvectors. However, the DFT Hermite eigenvectors obtained from (3.62) cannot constitute an orthogonal basis for DFT eigenspace. It is easy to verify that the angle rotation property of the DFrFT can be preserved only while the DFT eigenvectors are orthogonal. Therefore, vector orthogonalization is required for the DFT Hermite eignvectors obtained from (3.62). Two methods for vector orthogonalization are discussed here. The DFT eigenvectors are orthogonalized for each eigensubspace. This is because the eigenvectors located in different eignsubspaces will be always orthogonal.

It is easy to show that the eigenvectors located in different eigensubspaces will be orthogonal. So the DFT Hermite eigenvectors can be orthogonalized for every eigensubspace individually to obtain orthogonal eigenvectors in the whole subspace of DFT. The symbol notation in developing the two algorithms are as follows:

u_n continuous Hermite samples vector;

$\tilde{u}_n$ nonorthogonalized Hermite eigenvector;

$\hat{u}_n$ orthogonalized Hermite eigenvector;

The Gram-Schmidt Algorithm (GSA): The Gram-Schmidt method [92] is a well known orthogonalization approach for vectors. The DFT Hermite eigenvectors in each DFT eignsubspace can be orthogonalized by the Gram-Schdmidt method.

Algorithm

Calculate the continuous samples of Hermite functions: u_n

Compute the eigenvectors of matrix $S : v_n$

Use (3.62) to compute Hermite eigenvectors by projections: $\tilde{u}_n$

For $k = 0$ *to* 3

$\hat{u}_k = \tilde{u}_k$

For $m = 1$ *to* $\#(N,k) - 1$

$p = 4m + k$

$$\hat{u}_p = \tilde{u}_p - \sum_{l}^{m-1} < \hat{u}_p, \tilde{u}_{4l+k} > \hat{u}_{4l+k}$$

$$\hat{u}_p = \frac{\hat{u}_p}{\left\| \hat{u}_p \right\|}$$

end

Orthogonal Procrustes Algorithm (OPA): A traditional mathematical problem known as the *Orthogonal Procrustes Algorithm* [93] can be used to find the least Frobenius norm for the two given spaces. The OPA finds the least Frobenius norm between the samples of Hermite functions and orthogonal DFT Hermite eigenvectors.

For $k = 0,1,2,3$

$$\min \left\| U_k - \hat{U}_k \right\|_F = \min \left\| U_k - Q_k V_k \right\|_F \quad \text{Subject to } Q_k^T Q_k = I$$

where $\| \|_F$ is the Frobenius norm of the matrix, $V_k = \left\lfloor V_k \middle| V_{k+4} \middle| \text{ i } \middle| V_{k+(=(N,k)-1)*4} \right\rfloor$, $U_k = \left\lfloor u_k \middle| u_{k+4} \middle| \text{ i } \middle| u_{k+(=(N,k)-1)*4} \right\rfloor$ and $\hat{U}_k = \left\lfloor \hat{u}_k \middle| \hat{u}_{k+4} \middle| \text{ i } \middle| \hat{u}_{k+(=(N,k)-1)*4} \right\rfloor = Q_k V_k$ is the solution. The minimum Q_k can be found by calculating the singular value decomposition (SVD) of $V_k^T U_k$. Because $V_k^T V_k = I$, the solution $\hat{U}_k$ will also satisfy $\hat{U}_k^T \hat{U}_k = I$.

Algorithm

Calculate the continuous samples of Hermite functions: u_n

Compute the eigenvectors of $S : v_n$

Using (3.62) compute Hermite eigenvectors by projections: $\tilde{u}_n$

For $k = 0$ *to* 3

$C_k = V_k^T U_k$

Compute the SVD of $C_k, C_k = A_k D_k B_k^T$

$Q_k = A_k B_k^T$

$\hat{U}_k = Q_k V_k$

end

The GSA minimizes the errors between the samples of Hermite functions and orthogonal DFT Hermite eigenvectors from low to high orders, and the OPA minimizes the total errors between the samples of Hermite functions and orthogonal DFT Hermite eigenvectors.

3.3 PERFORMANCE ANALYSIS OF VARIOUS CLASSES OF DFrFT

The non-availability of a perfect and proper DFrFT expression in closed form still persists. The researchers have started the use of available definitions of DFrFT for convolution, filtering and multiplexing in the fractional Fourier domain [72].

From the above study it is clear that the results obtained from Direct form of DFrFT and Linear combination type DFrFT are not reversible and additive. They also are not similar to the continuous FrFT. Both these types of DFrFT lose various important characterisctics of continuous FrFT. The Direct form of DFrFT lacks a closed form expression also and it has a very limited use. Besides this the Linear combination type looses the most important property of 'fractionalisation' and it is very hard to filter out chirp noise. This concludes that both these DFrFT's are not useful for DSP applications. Therefore, these DFrFT's are discarded and not considered for the present performance analysis.

The analysis of remaining four classes i.e. improved sampling type, group theory type, impulse train type and eigenvector decomposition type is taken in the present study. The analysis of these four classes of DFrFT can be done by taking into consideration the evaluation time, the existence of closed form expression, complexity involved in computation and whether or not the various properties of FrFT are satisfied. A comparative analysis of these four DFrFT based on these performance metrics has been reported by Pei *et al* [24]. In [94] eigenvector decomposition type has been concluded to provide optimum performance. To substantiate this conclusion a parameter, namely, deviation factor, has been used in this study to compare the four classes of DFrFTs. A 32 point Hanning window function [95] is taken and is padded with zeros on both sides. The FFT of this function is calculated and compared with the result obtained using four classes of DFrFTs for a =1. To provide a quantitative measure deviation factor is used which is defined by (3.67).

$$\text{Deviation factor} = \frac{\sum_{i=-N}^{N} \left| fft(i) - Dfrft(i) \right|}{2N+1} \qquad (3.67)$$

where *fft(i)* = The i^{th} sample of FFT of the function.

Dfrft(i) = The i^{th} sample of DFrFT of the function for '*a*'=1.

2N+1 = The length of window function after zero padding.

The deviation factor is calculated by varying the length of the function and the results are shown in Table-3.3 and Table-3.4.

Table-3.3: Deviation factor for various DFrFT's of radix-2 length.

	Deviation factor			
No. of points	64 points	128 points	256 points	512 points
Impulse Train type	2.3362×10^{-7}	1.7038×10^{-8}	2.7286×10^{-12}	8.6808×10^{-10}
Group theory type	2.3362×10^{-7}	1.7038×10^{-8}	2.7286×10^{-12}	2.0760×10^{-10}
Improved Sampling type	2.3362×10^{-7}	1.7039×10^{-8}	2.7286×10^{-12}	2.0760×10^{-10}
Eigenvector decomposition type	7.5021×10^{-8}	1.1238×10^{-9}	1.2835×10^{-18}	1.12375×10^{-16}

Table-3.4: Deviation factor for various DFrFT's of arbitrary length.

	Deviation factor				
No. of points	55 points	100 points	200 points	300 points	400 points
Impulse Train type	3.9056×10^{-7}	9.9275×10^{-8}	1.0501×10^{-8}	1.5506×10^{-9}	1.4495×10^{-9}
Group theory type	1.4447×10^{-7}	4.8310×10^{-8}	1.5073×10^{-9}	2.6535×10^{-10}	2.9607×10^{-10}
Improved Sampling type	1.4444×10^{-7}	4.8310×10^{-8}	1.5073×10^{-9}	2.6535×10^{-10}	2.9607×10^{-10}
Eigenvector decomposition type	1.4444×10^{-7}	4.8301×10^{-8}	1.5070×10^{-9}	2.6535×10^{-10}	2.9604×10^{-10}

Following conclusions can be drawn from the tabulated values of deviation factors.

i) The deviation factor is very small for eigenvector decomposition type of DFrFT when the number of points is of the order of radix-2.

ii) For the radix-2 case eigenvector type of DFrFT outclasses the other three types of DFrFT types by a wide margin.

iii) When the number of points is not of the order of radix-2 the performance of eigenvector decomposition type is better than the impulse train type and at par with the other two types.

The Group theory type DFrFT is additive, reversible and rotational but it imposes certain constraints on the signal. It cannot be calculated for all the orders. The Improved sampling type DFrFT does not satisfies the orthogonality and additivity property. It also puts a lot many constraints (e.g. band limited) on the input signal. Moreover, it cannot be calculated for all orders. The impulse train type of DFrFT obeys many properties of continuous FrFT, it can be calculated for all orders but the deviation factor is large as compared to all other DFrFT's. It also puts certain constraints on the signal. The eigenvector decomposition type DFrFT puts least possible constraints on the signals as compared to any other class of DFrFT. It obeys many properties of continuous FrFT and it can be calculated for all orders. Although the computational complexity is higher than any other type it can be calculated in real time because of parallel processing and high speed available with the DSP processors. Also the deviation factor is smallest. Thus, it can be concluded from the above discussion that the Eigenvector decomposition type DFrFT provides optimum performance, and is preferred over others in the following chapters for the computation of DFrFT.

3.4 ANALYSIS OF WINDOW FUNCTIONS IN DISCRETE FRACTIONAL DOMAIN

Window functions are real, non-zero, time-limited and even functions. They are basically used in signal processing for power spectral estimation and FIR filtering applications [96]. A good classification of window functions is done by Gautam *et al*. [97]. As per the convention, all the windows are divided into two main categories. They are –

i) Fixed windows: The window belonging to this category is having all the parameters constant or fixed, hence the name. The windows generated either with the help of standard functions or by some combination of them. Rectangular, Triangular, Cosine, Hanning, Hamming, Blackman window are some commonly used fixed windows.

ii) Variable windows: The window functions with variable parameters are grouped together and termed as variable windows. They are parameterized on a single variable. The variable is chosen as per requirements and/or specifications of a particular application. For some windows, there are well-established relations to enumerate this variable, on the basis of the given specifications. Kaiser-Bessel, Dolph-Chebyshev, Poisson, Gaussian, Tseng window come under variable windows.

The parameters of window function which are generally used for its evaluation are [97]:

i) **Maximum Side Lobe Level** (MSLL): This is the peak ripple value of the side lobes and it is evaluated from the lobe magnitude plot of transformed window. This is also known as Selectivity amplitude ratio (SAR).

ii) **Selectivity** (S) **or Main Lobe Width** (MLW): This is the frequency at which the Main Lobe drops to the peak ripple value of the side lobes. For convenience half main lobe width (HMLW) or S/2 is computed.

iii) **Side Lobe Fall off Rate** (SLFOR): This is the asymptotic decay rate of the side lobe level. This is also called asymptotic attenuation

The definition of the parameters HMLW (S/2), MSLL (SAR) & SLFOR are illustrated using Kaiser Window as shown in Figure-3.1.

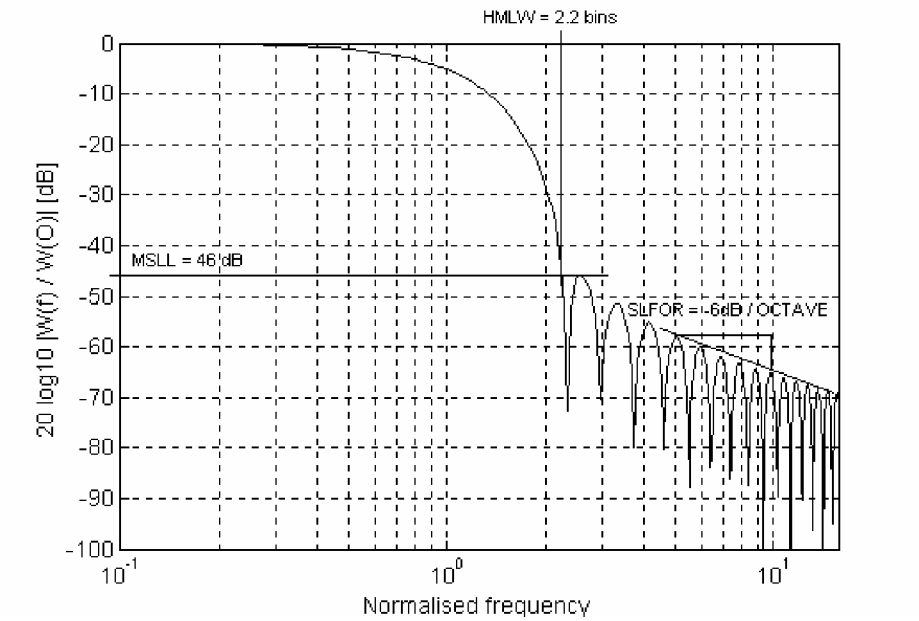

Figure-3.1: Log magnitude plot of Kaiser window to illustrate the definition of the parameters HMLW (S/2), MSLL (SAR) & SLFOR.

Four window functions, Triangular, Hanning, Blackman and Kaiser have been selected for the analysis in the fractional Fourier domain. The behavior of these windows in fractional domain is shown in Figure-3.2 to Figure-3.5.

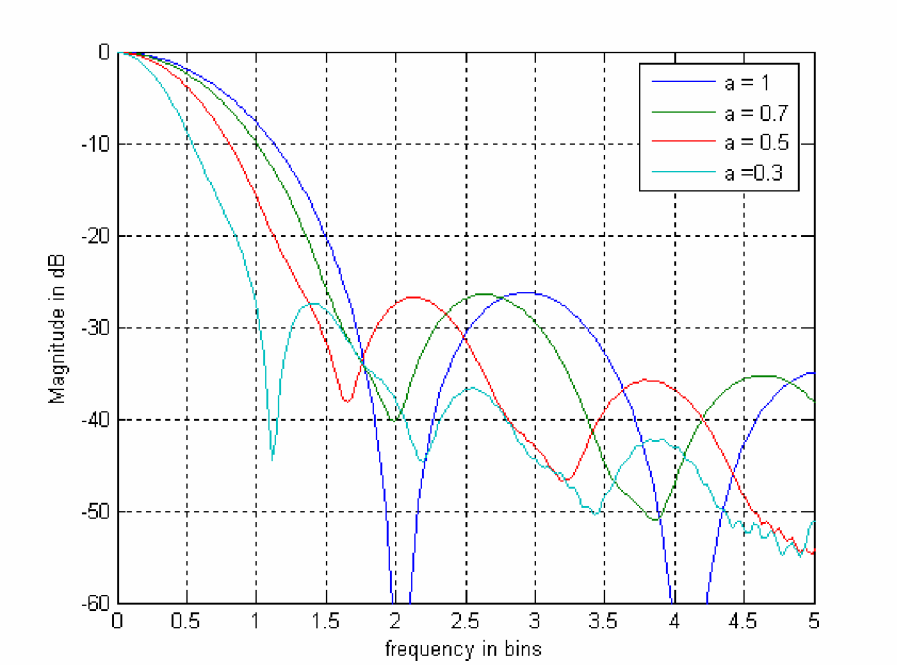

Figure–3.2: Parameters of Triangular window.

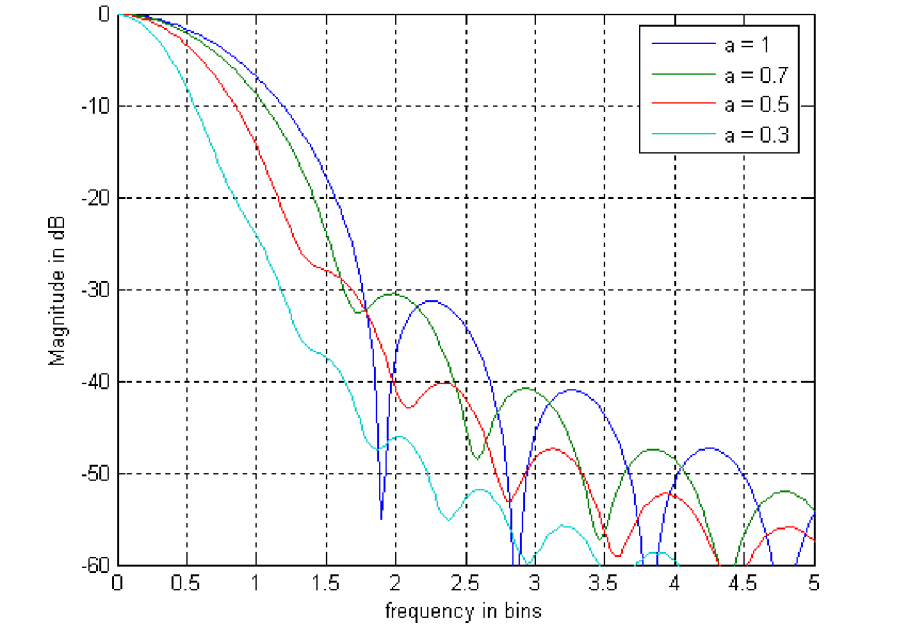

Figure–3.3: Parameters of Hanning window.

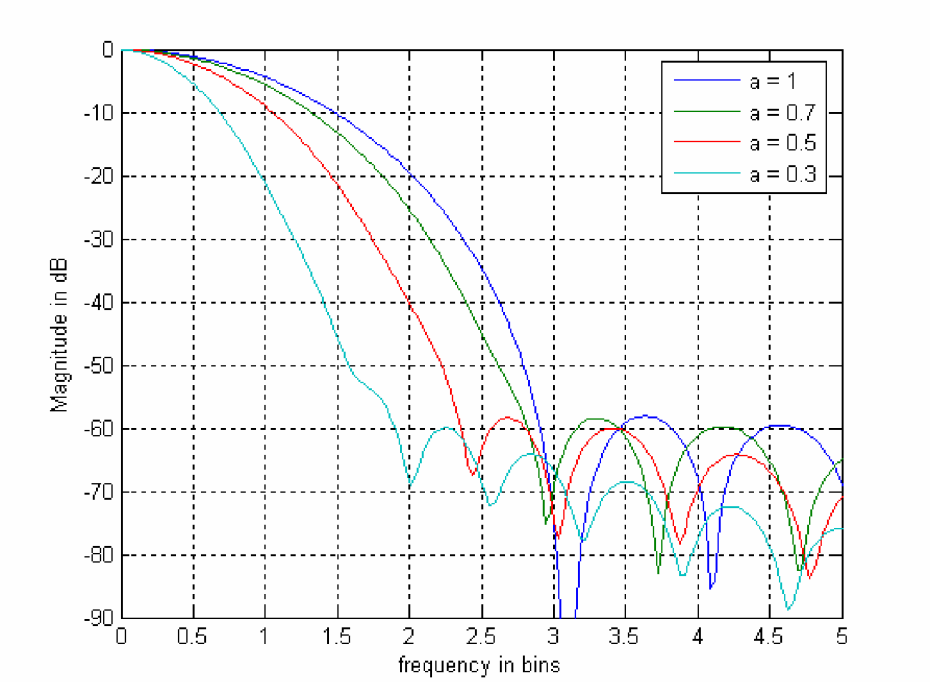

Figure–3.4: Parameters of Blackman window.

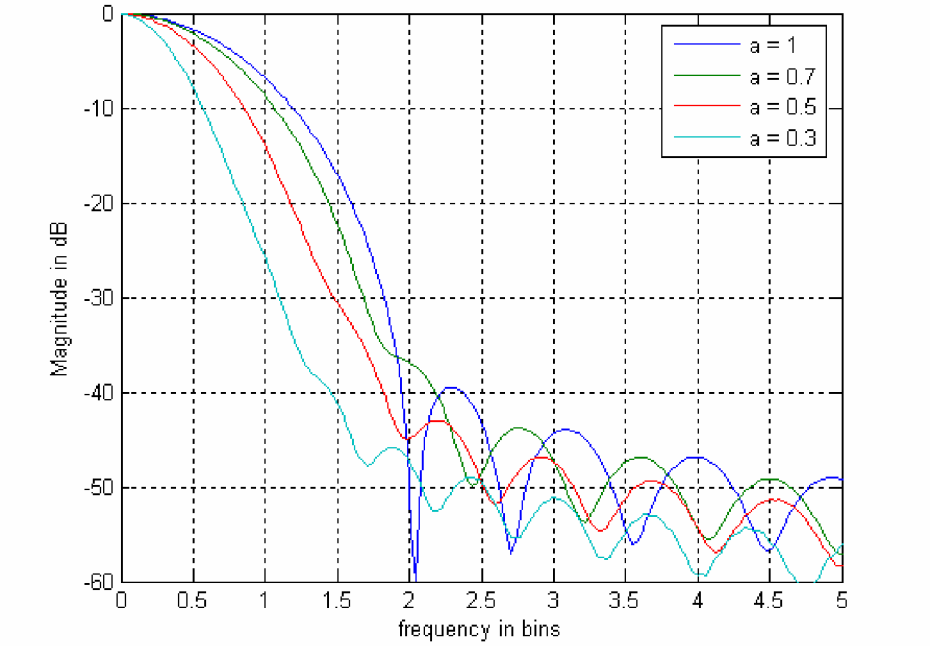

Figure–3.5: Parameters of Kaiser window at β=5.44.

Using these figures variations in MSLL, SLFOR and MSLW with FrFt order *a*, for the four windows, have been obtained and the results are shown in Table-3.5, Table-3.6, Table-3.7 and Table-3.8.

Table–3.5: Parameters of Triangular window.

S. No.	*a*	MSLL (dB)	SLFOR dB/Octave	HMLW (bins)
1.	1.0	-26	-12	1.63
2.	.9	-25.7	-12	1.61
3.	.8	-25.6	-12.6	1.57
4.	.7	-25.4	-12.8	1.50
5.	.6	-25.3	-13.2	1.50
6.	.5	-25.1	-13.7	1.41
7.	.4	-25	-13.65	1.36
8.	.3	-24.6	-13.7	1.31
9.	.2	-24.4	-13.83	1.29
10.	.1	-24.2	-13.81	1.25

Table–3.6 : Parameters of Hanning window.

S. No.	*a*	MSLL (dB)	SLFOR dB/Octave	HMLW (bins)
1.	1.0	-32	-18	1.87
2.	.9	-30.7	-18	1.77
3.	.8	-30.5	-18.1	1.71
4.	.7	-30.5	-18.17	1.61
5.	.6	-30.4	-18.2	1.51
6.	.5	-30.2	-18.3	1.50
7.	.4	-29.9	-18.32	1.44
8.	.3	-29.6	-18.35	1.36
9.	.2	-40.5	-17.03	1.22
10.	.1	-47.2	-17	*

- not observable

Table–3.7 : Parameters of Blackman window.

S. No.	*a*	MSLL (dB)	SLFOR dB/Octave	HMLW (bins)
1.	1.0	-58	-18	2.82
2.	.9	-57.5	-18.4	2.65
3.	.8	-57.3	-18.45	2.55
4.	.7	-57.1	-18.49	2.51
5.	.6	-57	-18.60	2.50
6.	.5	-56.8	-18.70	2.25
7.	.4	-56.5	-19	2.24
8.	.3	-56.3	-19.50	2.21
9.	.2	-56	-19.71	2.19
10.	.1	-55.8	*	2.15

* not observable

Table–3.8 : Parameters of Kaiser window at β=5.44.

S. No.	*a*	MSLL (dB)	HMLW (bins)	SLFOR (dB/octave)
1	1.0	-43	1.91	-6
2	0.9	-42.7	1.85	-6.03
3	0.8	-42.6	1.8	-6.08
4	0.7	-42.3	1.67	-6.09
5	0.6	-41.9	1.66	-6.10
6	0.5	-41.8	1.62	6.11
7	0.4	-41.3	1.60	6.12
8	0.3	-52.4	1.70	6.14
9	0.2	-49.3	1.63	6.20
10	0.1	-44	*	6.21

* not observable

These results lead to following conclusions –

i) As the DFrFT order is reduced MSLL increases. However, for Kaiser and Hanning windows the MSLL decreases when *a* is decreased to a particular value and then again starts increasing. This is because of the fact that as the FrFT order is reduced window response shrinks and gradually the first side lobe merges with the main lobe. Second side lobe then becomes the first side lobe, which again starts decreasing as the FrFT order is further reduced.

ii) A slight increase in the SLFOR value is observed as the value of FrFT order is reduced.

iii) HMLW of window reduces as FrFT order is reduced.

3.5 SUMMARY

In this chapter various available definitions of DFrFT have been discussed. A comparative study of these definitions of DFrFT has been carried out. A parameter 'deviation factor' has been devised and evaluated for this comparative study. Eigenvector decomposition type DFrFT emerged as the best one with least constraints and smallest deviation factor. Also analysis of window functions has been performed in fractional domain using this DFrFT. Characterization of three window parameters HMLW, SLFOR and MSLL is done in fractional domain. As the eigenvector type can be calculated for all orders and obeys many properties of continuous FrFT it has been selected to compute the DFrFTs for the applications discussed in chapter 4 and 5.

CHAPTER 4

APPLICATIONS OF DFrFT IN FILTERING AND BEAMFORMING

4.1 INTRODUCTION

FrFT has many applications in optics, especially in wave and beam propagation [39], [40], wave field reconstruction [50], phase retrieval and phase-space tomography [47], [56], [62]. It has also been used for study of time- or space-frequency distributions [26], [78]. Its applications in biometrics for iris verification are also reported [58]. In signal processing applications this transform is basically used for filtering [55], signal recovery, signal reconstruction, signal synthesis, beam forming [55], signal detectors [68], correlators [16], image recovery [51], [57], restoration and enhancement [60], pattern recognition, optimal Wiener filtering [70] and matched filtering [59]. It can also be used for multistage and multi channel filtering, multiplexing in fractional Fourier domains [72], fractional joint-transform correlators [64] and adaptive windowed FrFT. In general, the FrFT is likely to have something to offer in every area in which FT and related concepts are used. In this chapter applications of FrFT for filtering of signals that overlap in both time and frequency domains is introduced. The concepts of this filtering scheme are then applied to filtering of such signals with associated fading using FrFT. Studies with stationary as well as moving sources is carried out. Beamforming is another one dimensional signal processing application discussed in this chapter. FrFT has been used for beamforming in faded channels and

its superiority has been established over time and frequency domain beamformers. Also a performance comparison of two types of DFrFTs in optimal beamforming is carried out.

4.2 OPTIMAL FILTERING IN FRACTIONAL DOMAIN

In most of the signal processing applications, the signal which is to be recovered is degraded by known distortion, blur and/or noise and the problem is to reduce or eliminate these degradations. The concept of filtering in fractional Fourier domain is to realize flexible and efficient, general shift-variant linear filters for a variety of applications. Figure-4.1 shows WD of a desired signal and noise superimposed in a single plot. It is clear from this figure that signals with significant overlap in both time and frequency domains may have little or no overlap in fractional Fourier domain of some order. The solution of such problems depends on the observation model and the objectives, as well as the prior knowledge available about the desired signal, degradation process and noise. The problem is then to find the optimal estimation operators with respect to some design criteria that removes or minimizes these degradations. The most commonly used observation model is:

$$g(x) = h(x) * f(x) + \eta(x) \tag{4.1}$$

where, $h(x)$ is a system that degrades the desired signal $f(x)$, and $\eta(x)$ is additive noise, possibly non stationary noise, and $g(x)$ is the signal at the input of the filter.

The effect of FrFT on a signal can be seen easily in a time-frequency plane. One of the most popular time-frequency distributions, the WD that gives the idea about the energy distribution of a signal in time-frequency can be used to illustrate this effect [51], [78]. The effect of FrFT on the WD of a signal is simply a clockwise rotation by an angle in time-frequency plane. It is also seen

from Figure-4.1 (which shows WD of a desired signal and noise superimposed in single plot) that signals with significant overlap in both time and frequency domains may have little or no overlap in a particular fractional Fourier domain.

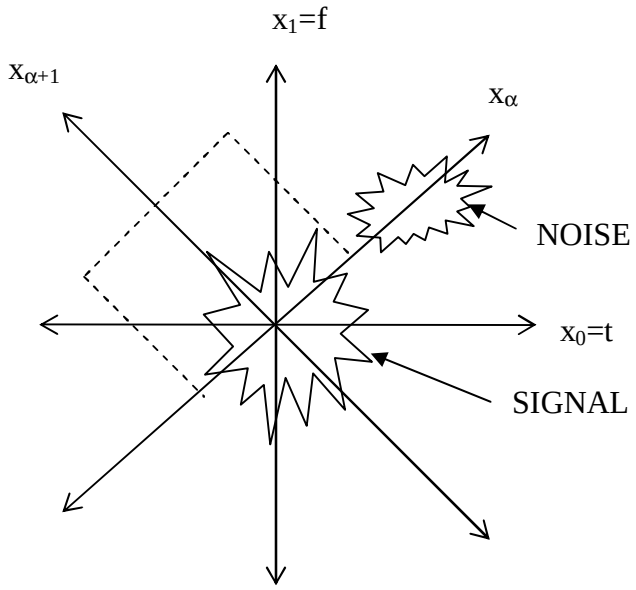

Figure-4.1: Filtering in fractional Fourier domain as observed in time-frequency plane at $\alpha = \pi/4$.

The problem now is of the determination of the FrFT order that can provide best filtering results. The filtering process in this particular domain is termed as optimal filtering. For an arbitrary degradation model (non stationary processes), the resulting optimal recovery will not be time invariant and thus cannot be expressed as a convolution and so cannot be realized by filtering in conventional Fourier domain (multiplying the Fourier transform of a function with their filter function in that domain). The optimal filtering can be obtained depending upon the criterion of optimization. The main criterions of optimization are minimum mean squared error (MMSE), maximum signal to noise ratio (SNR) and minimum variance [99]. Each criterion has its own

advantages and disadvantages. The problem considered here is to minimize the MSE for arbitrary degradation model and non-stationary processes by filtering in fractional Fourier domains. The MMSE method has been used to obtain the optimum filter. The objective here is to recover the desired signal free from noise and fading from the received signal, in stationary and moving source problems. The MMSE, which is obtained in frequency or time domain, can now be optimized over this parameter *a*. It has been shown that FrFT filter improves the performance in case of sources that may be stationary or moving at a constant velocity in additive white Gaussian noise (AWGN) signals. In above cases it has been shown that the space or frequency domain filtering does not serve the purpose so it is required to optimize filtering in an appropriate fractional Fourier domain [59]. The extra degree of freedom given by FrFT as parameter *a*, improves the performance of a large class of signal processing applications in space or time variant filtering [59].

Let the filter input be $g(x)$ and the reference signal be $f(x)$. The observation model in fractional Fourier domain becomes:

$$g(x) = \int h_d(x, x_a) f(x_a) dx_a + \eta(x). \tag{4.2}$$

where, $h_d(x, x_a)$ is the kernel of the linear system that distorts or blurs the desired signal $f(x)$, and $\eta(x)$ is an additive white Gaussian noise term.

The problem is to find an estimation operator represented by kernel $h(x, x_a)$ such that the estimated signal

$$f_{est}(x) = \int h(x, x_a) g(x_a) dx_a \tag{4.3}$$

minimizes the mean square error σ_{err}^2 as

$$\sigma_{err}^2 = \left\langle \int \left| f_{est}(x) - f(x) \right|^2 dx \right\rangle, \tag{4.4}$$

where, the angle brackets denote ensemble average. The estimation or recovery operator minimizing σ_{err}^2 is known as optimal Wiener Filter. It is assumed that the $h(x, x_a)$ as well as the correlation function $R_{ff}(x, x_a) = \langle f(x) f^*(x_a) \rangle$ and $R_{\eta\eta}(x, x_a) = \langle \eta(x) \eta^*(x_a) \rangle$ of the random signals $f(x)$ and $\eta(x)$ are known. It is further assumed that the noise $\eta(x)$ is independent of $f(x)$ and that it has zero mean all the time, i.e., $\langle \eta(x) \rangle = 0$. Under these assumptions the cross correlation function $R_{fg}(x, x_a) = \langle f(x) g^*(x_a) \rangle$ and autocorrelation function $R_{gg}(x, x_a) = \langle g(x) g^*(x_a) \rangle$ can be obtained using (4.2). Restricting the problem to the class of linear estimators which corresponds to filtering in a single fractional Fourier domain the estimate can be expressed as [59]

$$f_{\mathbf{est}(x)} = F^{-\mathbf{a}} \Lambda_h F^{\mathbf{a}} g(x) \tag{4.5}$$

where, Λ_h corresponds to operator corresponding to multiplication by the filter function $h(x)$. According to (4.5), first the a^{th} order FrFT of the observed signal *g(x)* is taken, then the resultant is multiplied with the filter $h(x)$ and finally inverse a^{th} order FrFT of the product is taken.

Since the FrFT is unitary, σ_{err}^2 can be expressed in a^{th} domain as

$$\sigma_{err}^2 = \left\langle \int \left| f^{a}{}_{est}(x_a) - f^{a}(x_a) \right|^2 dx_a \right\rangle \quad , \tag{4.6}$$

where, $f^{a}{}_{est}(x_a) = h(x_a) g(x_a)$. If the value of a is assumed to be constant σ_{err}^2 is to be minimized with respect to $h(x_a)$. The expression of optimal filter function is then obtained by equating the partial derivative of σ_{err}^2, with respect to $h(x_a)$, equal to zero as [59]

$$h(x_a) = \frac{R_{f^a g^a}(x, x_a)}{R_{g^a g^a}(x, x_a)} \tag{4.7}$$

where, the above correlation functions are related to the correlation functions $R_{fg}(x, x_a)$ and $R_{gg}(x, x_a)$ through

$$R_{f^a g^a}(x, x_a) = \int\int K^a(x_a, x)\ K^{-a}(x_a, x_{a1})\, R_{fg}(x, x_{a1}) dx_{a1} dx,$$

$$R_{g^a g^a}(x, x_a) = \int\int K^a(x_a, x)\ K^{-a}(x_a, x_{a1})\, R_{gg}(x, x_{a1}) dx_{a1} dx. \qquad (4.8)$$

Thus the optimal filter function in the a^{th} fractional Fourier domain is

$$h(x_a) = \frac{\int\int K^a(x_a, x) K^{-a}(x_a, x_{a1}) R_{fg}(x, x_{a1}) dx_{a1} dx}{\int\int K^a(x_a, x)\ K^{-a}(x_a, x_{a1}) R_{gg}(x, x_{a1}) dx_{a1} dx} \qquad (4.9)$$

which is the same as (4.7). In (4.9) K^a is the FrFT kernel given by (2.1).

The optimal fractional Fourier domain is found by finding the minimum of $\sigma_{err}^2(a)$. This is done by calculating σ_{err}^2 for various values of a and then taking the value of a for which σ_{err}^2 is minimum.

The problem of optimal filtering in fractional Fourier domain for the discrete time signals and systems is analogous to with the continuous case discussed above. Let an observed signal **g** be related to a signal **f,** which is to be recovered, as

$$\mathbf{g} = \mathbf{H}_d\, \mathbf{f} + \eta \qquad (4.10)$$

where, **g**, **f** and η are column vectors with N elements and $\mathbf{H}_d$ is an $N \times N$ matrix. It is assumed that $\mathbf{H}_d$, as well as the coorelation matrix $\mathbf{R}_{ff} = \langle \mathbf{f}\mathbf{f}^H \rangle$ and $\mathbf{R}_{\eta\eta} = \langle \eta\eta^H \rangle$ of the random signal **f** and the noise η are known. It is further assumed that η has zero mean and is independent of **f**. Under these assumptions the cross-correlation matrix $\mathbf{R}_{fg} = \langle \mathbf{f}\, \mathbf{g}^H \rangle$ and the autocoorelation matrix $\mathbf{R}_{gg} = \langle \mathbf{g}\, \mathbf{g}^H \rangle$ can be obtained [59].

The most general linear estimate in form of $\mathbf{f}_{est} = \mathbf{H}\mathbf{g}$ is an analogy with (4.3), then the optimal general linear estimator **H** minimizing the mean square error

$$\sigma_{err}^2 = \frac{1}{N}\left\langle \left\| \mathbf{f}_{\mathbf{est}} - \mathbf{f} \right\|^2 \right\rangle \tag{4.11}$$

between the actual signal **f** and the estimate $\mathbf{f}_{est}$, satisfies $\mathbf{R}_{fg} = \mathbf{H}\mathbf{R}_{gg}$.

The discussion is restricted to the class of linear estimators which corresponds to filtering in a single fractional Fourier domain and the estimate is expressed as

$$\mathbf{f}_{\mathbf{est}} = \mathbf{F}^{-\mathbf{a}} \mathbf{\Lambda}_{\mathbf{h}} \mathbf{F}^{\mathbf{a}} \mathbf{g}\,, \tag{4.12}$$

where, $\mathbf{F}^a$ is the a^{th} order DFrFT matrix, $\mathbf{F}^{-a} = (\mathbf{F}^a)^{\text{H}}$ and $\mathbf{\Lambda}_{\mathbf{h}}$ is a diagonal matrix whose diagonal consists of the elements of the vector **h**. When $a = 1$ the matrix $\mathbf{F}^a$ reduces to the DFT matrix and the overall operation corresponds to conventional Fourier domain filtering.

Since the FrFT is unitary, σ_{err}^2 can be expressed in a^{th} domain as

$$\sigma_{err}^2 = \frac{1}{N}\left\langle \left\| \mathbf{f}_{\mathbf{est}_a} - \mathbf{f}_a \right\|^2 \right\rangle \tag{4.13}$$

where $\mathbf{f}^{a} = \mathbf{F}^a\mathbf{f}$ and $\mathbf{f}_{est} = \mathbf{F}^a\mathbf{f}_{est} = \mathbf{\Lambda}_{\mathbf{h}}\mathbf{F}^{a}\mathbf{g} = \mathbf{\Lambda}_{\mathbf{h}}\mathbf{g}^{a}$. Assuming the value of a is fixed, the problem remains that of minimizing σ_{err}^2 with respect to complex vector **h**. Writing σ_{err}^2 explicitly in the form

$$\sigma_{err}^2 = \left\langle \frac{1}{N}\sum_{l=1}^{N} \left| f_l^{\,a} - h_l g_l^{\,a} \right|^2 \right\rangle \tag{4.14}$$

where, f^a, g^a and $h_l = h_{lr} + h_{li}$ are the elements of the vector $\mathbf{f}^a$, $\mathbf{g}^a$ and **h** where h_{ir} and h_{li} are real & imaginary parts of h. The partial derivates can be evaluated as

$$\frac{\partial \sigma_{err}^2}{\partial h_{lr}} = \frac{1}{N}\left\langle -2\Re\left[f_l^{\,a} g_l^{a*} \right] + 2h_{lr}\left| g_l^{\,a} \right|^2 \right\rangle \text{and} \qquad \frac{\partial \sigma_{err}^2}{\partial h_{li}} = \frac{1}{N}\left\langle -2\Re\left[f_l^{\,a} g_l^{a*} \right] + 2h_{li}\left| g_l^{\,a} \right|^2 \right\rangle. \tag{4.15}$$

Setting these to zero the elements of the optimal filter vector are obtained

$$h_l = \frac{\left\langle f_l^{\,a} g_l^{a*} \right\rangle}{\left\langle \left| g_l^{a} \right|^2 \right\rangle}. \tag{4.16}$$

The numerator is simply the $(l,l)^{\text{th}}$ element of $\mathbf{R}_{\mathbf{f}^a\mathbf{g}^a}$ and the denominator is simply the $(l,l)^{\text{th}}$ element of $\mathbf{R}_{\mathbf{g}^a\mathbf{g}^a}$, where

$$\mathbf{R}_{\mathbf{f}^a\mathbf{g}^a} = \left\langle \mathbf{f}^{\,a}\mathbf{g}^{\,a} \right\rangle = \mathbf{F}^{\,a}\mathbf{R}_{\mathbf{ff}}\mathbf{H}_{\mathbf{d}}^{\mathbf{H}}\mathbf{F}^{-a} \tag{4.17}$$

$$\mathbf{R}_{\mathbf{g}^a\mathbf{g}^a} = \left\langle \mathbf{g}^{\,a}\mathbf{g}^{\,a} \right\rangle = \mathbf{F}^{\,a}\left(\mathbf{H}_{\mathbf{d}}\mathbf{R}_{\mathbf{ff}}\mathbf{H}_{\mathbf{d}}^{\mathbf{H}} + \mathbf{R}_{\boldsymbol{\eta}\boldsymbol{\eta}}\right)\mathbf{F}^{-a} \tag{4.18}$$

(4.18) is fully analogous to (4.8).

4.2.1 Simulation Results for a Stationary Source

A computer simulation that illustrates the applications and performance of fractional Fourier domain filtering is presented. The filter configuration discussed in section 4.2 is used for stationary targets. The harmonic source is in far field emitting frequency 1MHz. The signal is assumed to be associated with additive white Gaussian noise.

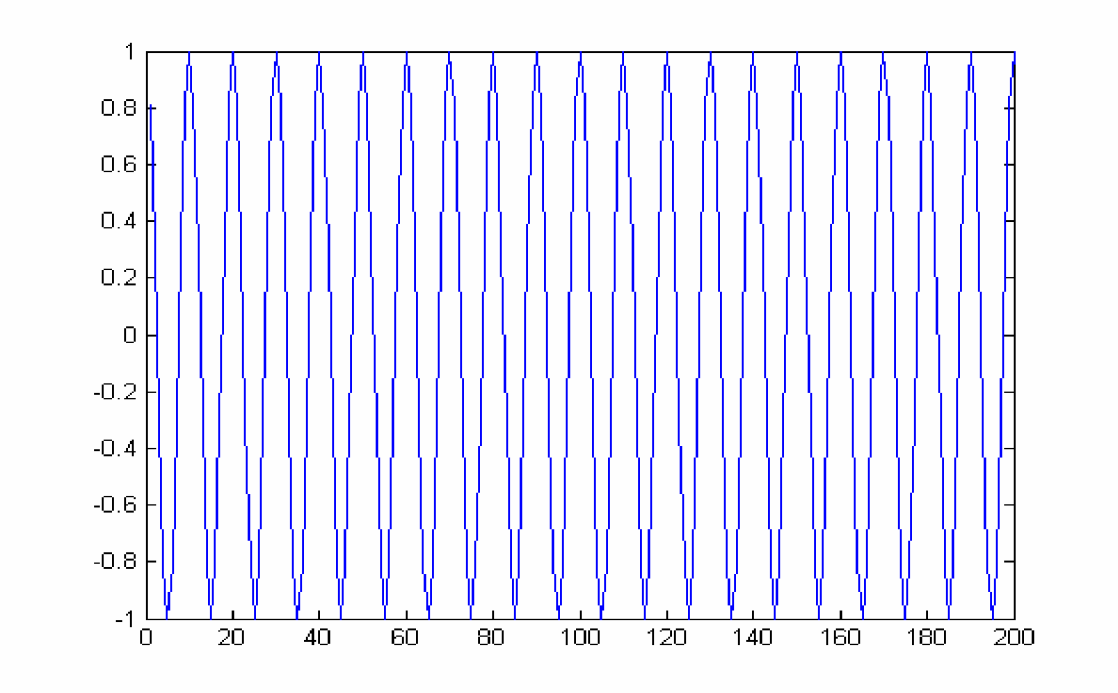

Figure-4.2: Original signal transmitted by source.

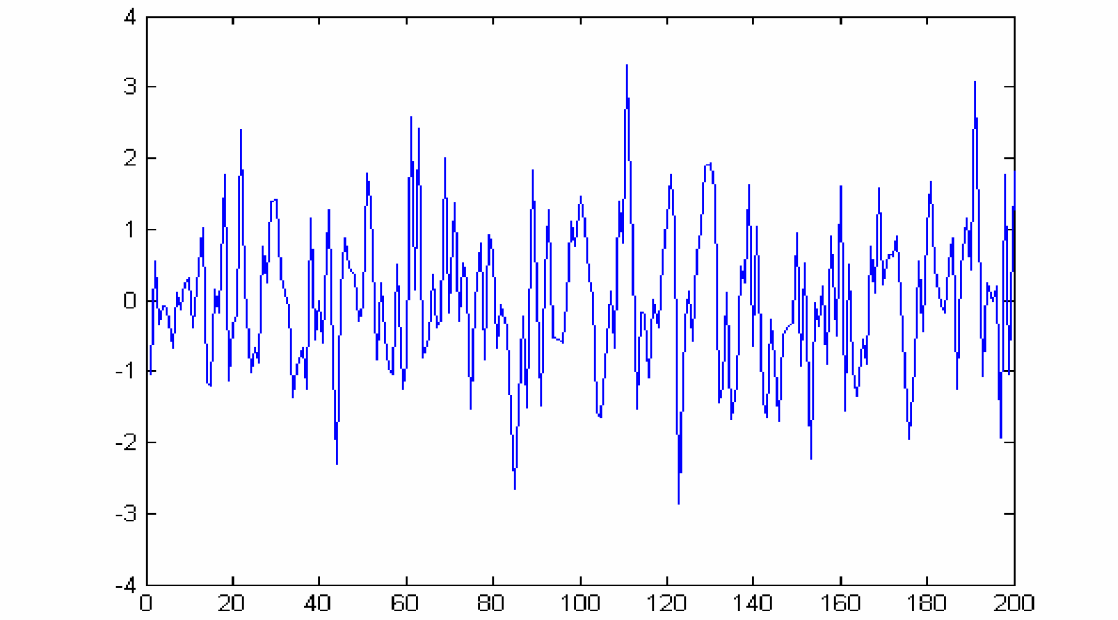

Figure-4.3: Original signal with additive white Gaussian noise.

The original sinusoidal signal sent by the transmitter is shown in Figure-4.2. Figure-4.3 shows the signal with additive white Gaussian noise. Plots shown in Figure-4.4 and Figure-4.5

correspond to the filtering of the signal in time and frequency domain respectively. Results for the filtering of the signal using FrFT are shown in Figure-4.6. These results corresponds to the recovery of the signal in optimum FrFT domain. The value of *a* for this simulation example which resulted in optimum domain filtering is -0.7. The value of SNR is 20 for time, frequency as well as FrFT domain filtering results.

To perform a comparative analysis of time, frequency and FrFT domain filtering corresponding to $a = 0$, $a = 1$, and $a = -0.7$ respectively, MSE Vs SNR for the three cases is plotted in Figure-4.7. Results shown in Figure-4.6 and Figure-4.7 are for a stationary source. From these plots it is clear that there is a significant improvement in the performance of filter in optimum FrFT domain as compared to time and frequency domains.

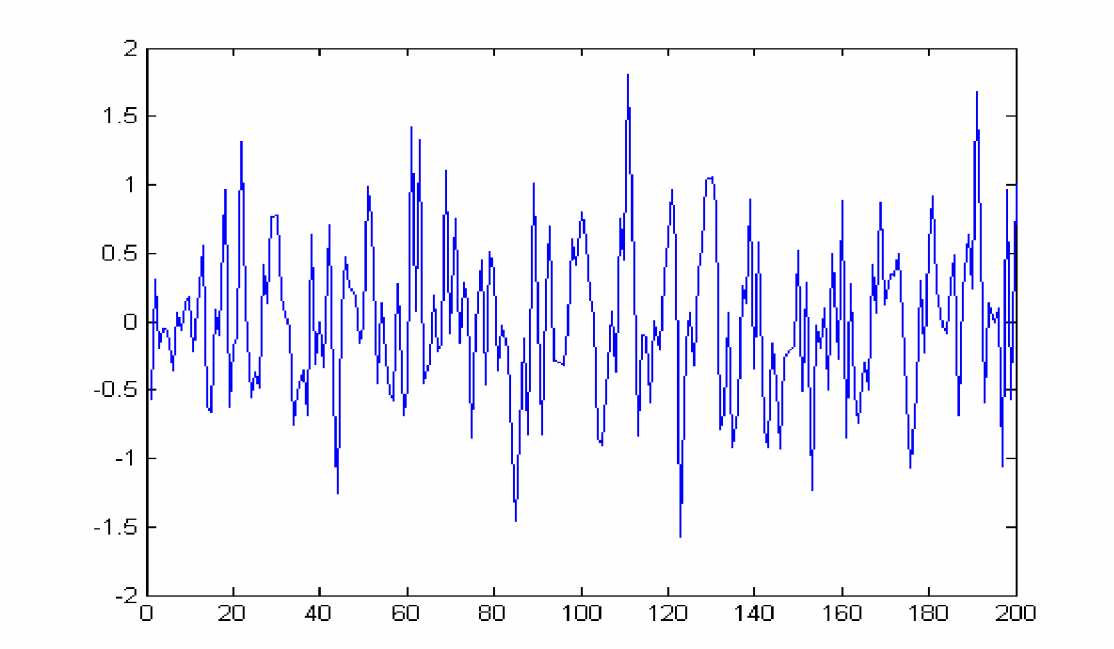

Figure-4.4: Filtering of received signal in time domain.

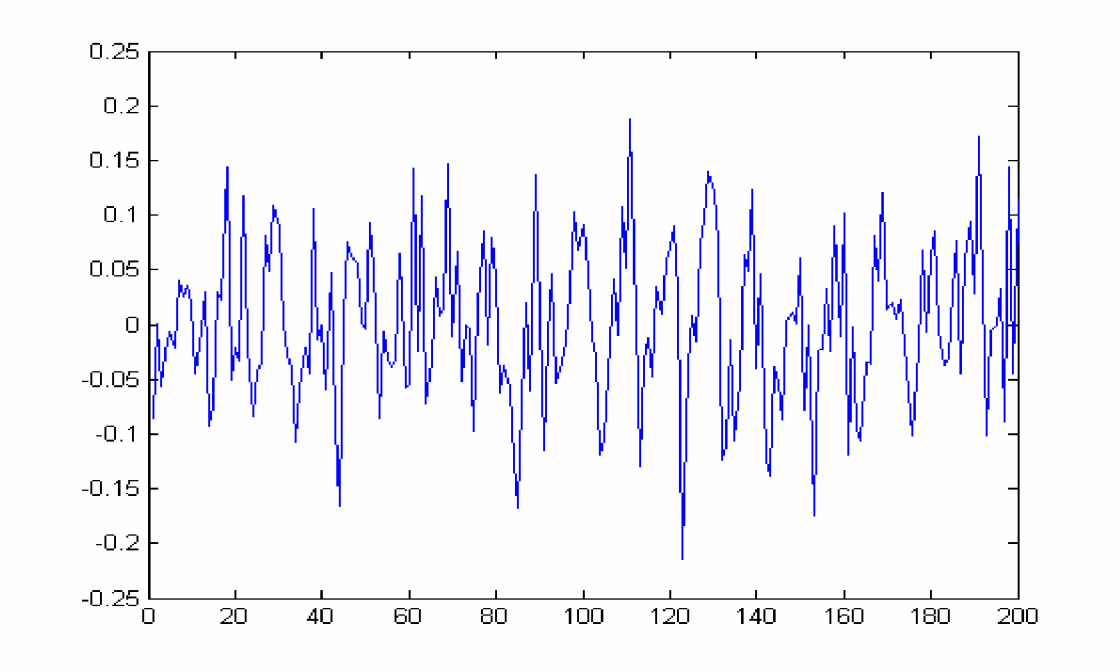

Figure-4.5: Filtering of received signal in frequency domain.

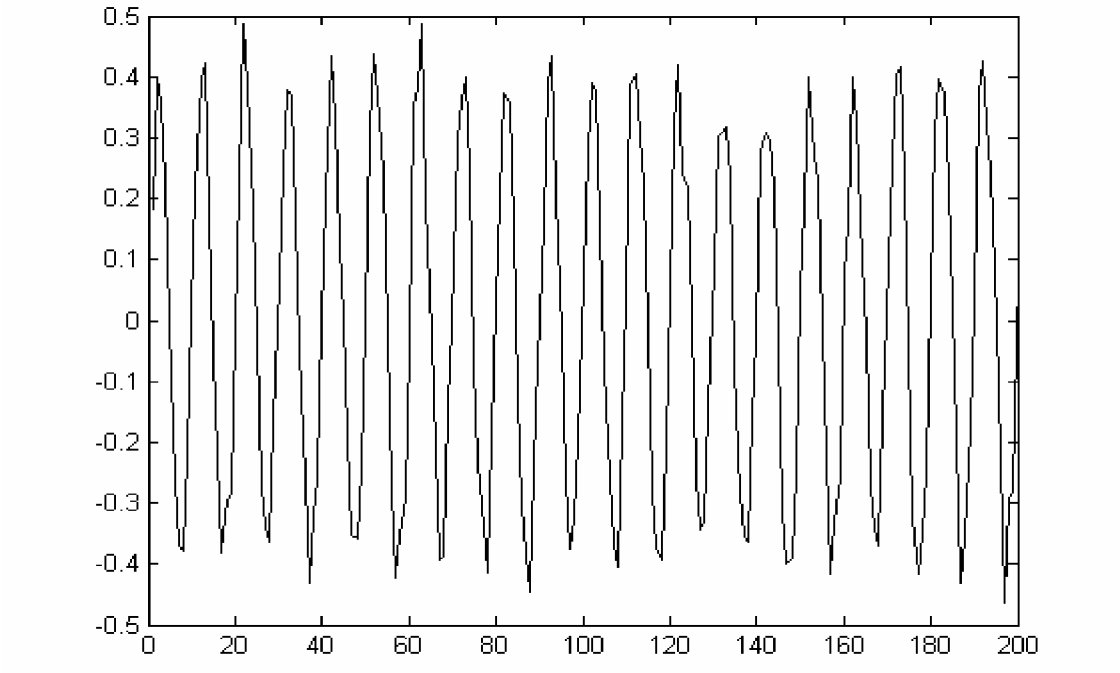

Figure-4.6: Recovered signal after filtering in optimum domain (a = 0.7).

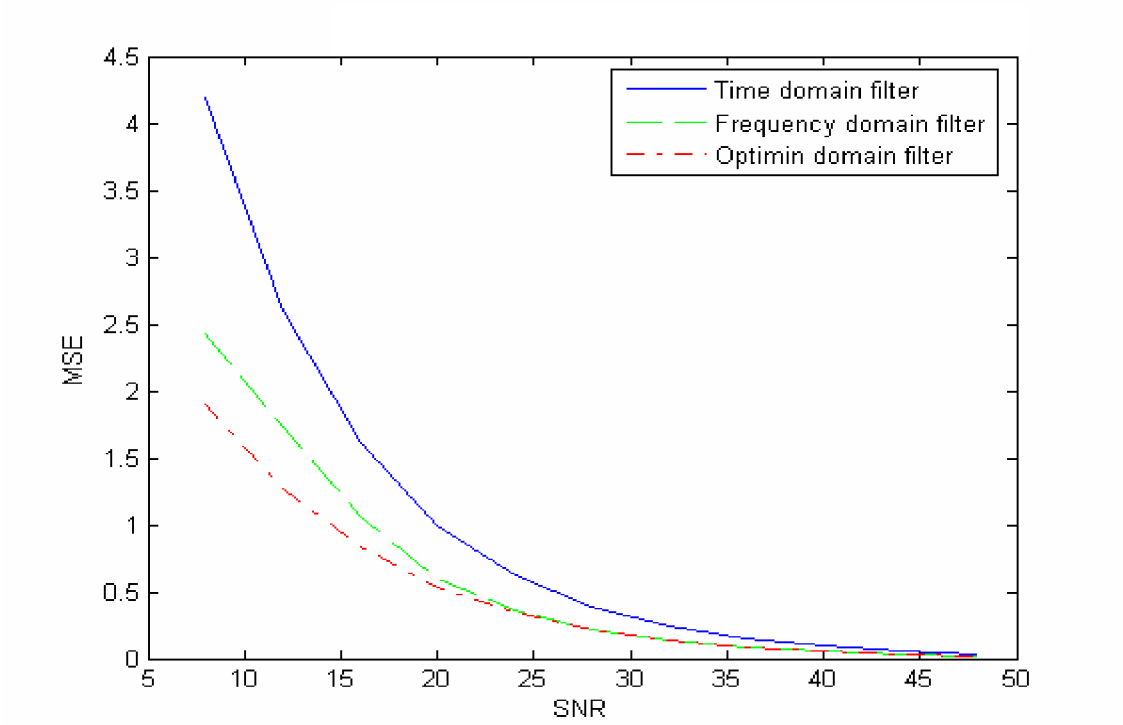

Figure-4.7: MSE vs SNR for time, frequency and optimum FrFT domain filter in case of stationary source.

4.2.2 Simulation Results for a Moving Source

The results for stationary source can be extended to the case when there is a relative notion between transmitter and receiver with a constant velocity which leads to Doppler shift in the frequency domain.

The received signal $g(t)$ can be expressed as [100]

$$g(t) = \Re\left\{Ae^{j(\omega_c t+\phi)}\right\} = A\cos(\omega_c t+\phi) \qquad (4.19)$$

where, ω_c is the frequency of unmodulated carrier.

The phase ϕ depends on the path lengths, changing by 2π when the path length changes by a wavelength. Let the reflected wave with amplitude A and phase ϕ arrive at the receiver at an angle ψ relative to the direction of motion of the antenna. The Doppler shift of the wave is given by

$$\omega_d = \frac{\omega_c v}{c}\cos\psi \qquad (4.20)$$

where, v is the velocity of the mobile, c is the speed of light ($3x10^8$ m/s). The received signal $g(x)$ can now be written as [100]

$$g(t) = A\cos(\omega_c t + \omega_d t + \phi) \qquad (4.21)$$

$$g(t) = A\cos\{(\omega_c + \omega_d)t + \phi)\} \qquad (4.22)$$

From here it is clear that the frequency of the source is added in the frequency of the signal at the receiver end.

The filtering scheme discussed in section 4.2 and used for the optimal filtering in section 4.2.1 is used for the case when the source is moving with a constant velocity.

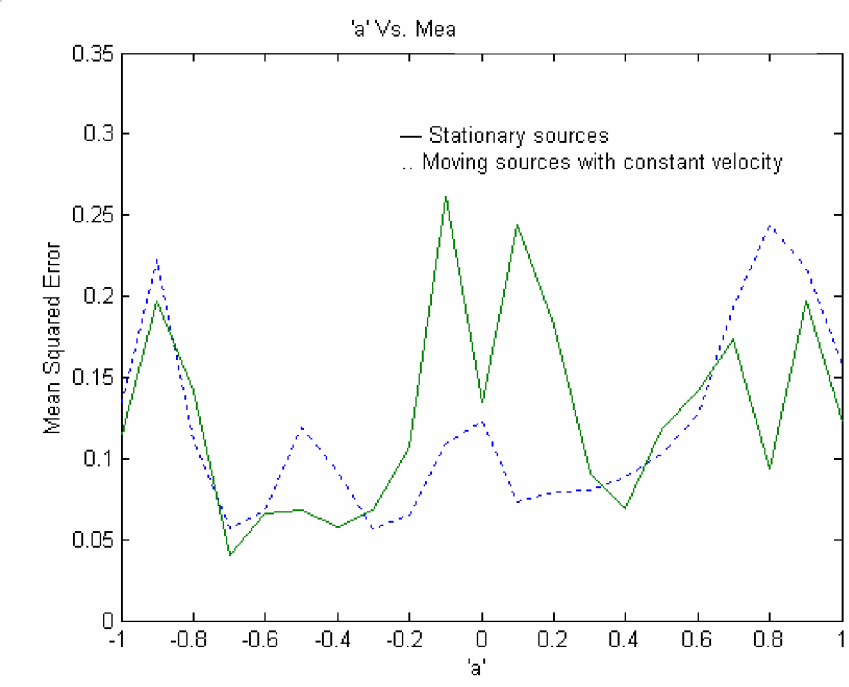

Figure-4.8: Fractional order '*a*' Vs MSE for stationary and moving sources with constant velocity.

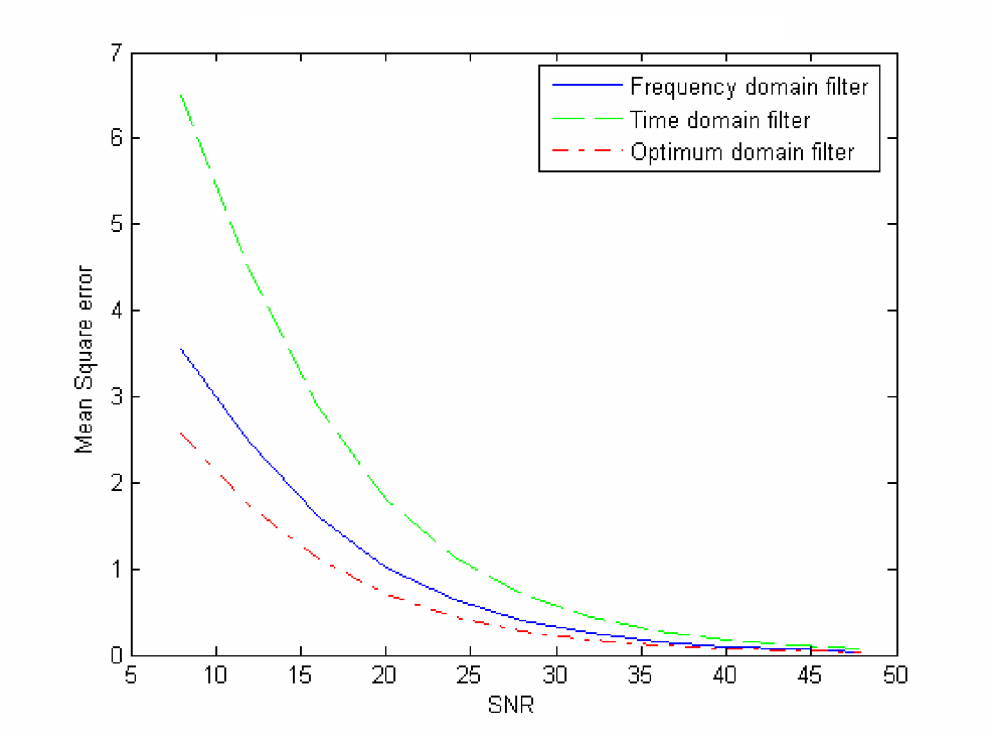

Figure-4.9: SNR Vs MSE for time , frequency and optimum FrFT domain filter in case of moving sources.

Figure-4.8 shows the variation of MSE with a in case of stationary and moving source with a constant velocity of 100m/s. In both cases the MSE is smaller in optimum FrFT domain ($a = a_{opt}$) as compared to space domain ($a = 0$) and frequency domain ($a = 1$). For a stationary source the optimum FrFT domain is $a = -0.7$ and for moving source the optimum FrFT domain is $a = -0.3$. In Figure-4.9 MSE is shown as a function of SNR in case of moving source with a constant velocity in time, frequency and optimum FrFT domain. From these plots it can be concluded that there is a significant improvement in the performance of filter in optimum FrFT domain as compared to time and frequency domains.

4.3 SIGNAL FADING IN MOBILE COMMUNICATION

In most of the communication systems, the height of the antenna is much lower than the surrounding structures, thus, the existence of a direct or line-of-sight path between the transmitter and the receiver is highly unlikely. In such a case, propagation of the signal is mainly due to reflection and scattering from the buildings and by diffraction over and/or around them. So, in practice, the transmitted signal arrives at the receiver via several paths with different time delays creating a multipath situation and these paths cannot be individually resolved if the difference in the time delay of the number of paths is less than the reciprocal of the transmission bandwidth. Moreover, these paths also have random phases and they add up at the receiver according to their relative strengths and phases. The envelope of the received signal is therefore a random variable and this random nature of the received signal envelope is referred to as fading [101].

There are two types of fading which characterize mobile communication: large scale fading and small scale fading. Large scale fading represents average signal power attenuation or the path loss due to motion over large areas. This phenomenon is affected by prominent terrain contours (e.g. hills, forests, clumps of buildings etc.) between transmitter and receiver. The receiver is often said to be shadowed by such prominences. The statistics of the large scale fading provides a way of computing an estimate of path loss as a function of distance. This is often described in terms of mean path loss and a log-normally distributed variation about mean. Small scale fading refers to the dramatic changes in signal amplitude and phase that can be experienced as a result of small changes (as small as half wavelength) in the spatial positioning between transmitter and receiver. The small scale fading manifests itself in two mechanisms – time spreading of signal (signal dispersion) and time-variant behavior of the channel. For mobile-radio applications, the channel is time variant because the relative motion between transmitter and

receiver results in propagation path changes. The rate of change of these propagation conditions account for fading rapidity (rate of change of fading impairments). Small scale fading is also called Rayleigh fading if there are multiple reflective paths that are large in number and if there is no line of sight component; the envelope of such received signals is statistically described by Rayleigh probability density function. A mobile-radio roaming over a large area must process signals that experience both type of fading. In the present work a mobile radio roaming over a small area is considered which should be able to process small scale fading that is more prominent in mobile radios. The Rayleigh faded signals have been successfully filtered in fractional fourier domain to get the desired signal at the receiver [101].

In the case of an un modulated carrier, the transmitted signal at angular frequency ω_c reaches the receiver via a number of paths, the i^{th} path having an amplitude A_i, and a phase ϕ_i. The received signal $g(x)$ can be expressed as [101]

$$g(t) = \Re\left\{\sum_{i=1}^{L} A_i e^{j\left(\omega_{c_i} t + \phi_i\right)}\right\} = \sum_{i=1}^{L} A_i \cos(\omega_c t + \phi_i) \tag{4.23}$$

where, L is the number of paths. The phase ϕ_i depends on the varying path lengths, changing by 2π when the path length changes by a wavelength. Therefore, the phases are uniformly distributed over $[0,2\pi]$. Let the i^{th} reflected wave with amplitude A_i and phase ϕ_i arrive at the receiver at an angle ψ_i relative to the direction of motion of the antenna. The Doppler shift of this wave is given by

$$\omega_{d_i} = \frac{\omega_c v}{c} \cos\psi_i \tag{4.24}$$

where, v is the velocity of the mobile, c is the speed of light ($3\text{x}10^8$ m/s), and the ψ_i's are uniformly distributed over $[0,2\pi]$. The received signal $g(t)$ can now be written as

$$g(t) = \sum_{i=1}^{L} A_i \cos(\omega_c t + \omega_{d_i} t + \phi_i) \tag{4.25}$$

Expressing the signal in terms of its in phase and quadrature form, equation (4.25) can be written as

$$g(t) = I(t)\cos\omega_c t - Q(t)\sin\omega_c t \tag{4.26}$$

where the in phase and quadrature components are respectively given as

$$I(t) = \sum_{i=1}^{L} A_i \cos(\omega_{d_i} t + \phi_i) \quad \text{and} \quad Q(t) = \sum_{i=1}^{L} A_i \sin(\omega_{d_i} t + \phi_i) \tag{4.27}$$

If l is sufficiently large, by virtue of the central limit theorem, the in phase and quadrature components $I(t)$ and $Q(t)$ will be independent Gaussian processes which can be completely characterized by their mean and autocorrelation function. In this case, the means of $I(t)$ and $Q(t)$ are zero. Furthermore, $I(t)$ and $Q(t)$ will have equal variances, σ^2, given by the mean-square value or the mean power. The envelope, $r(t)$, of $I(t)$ and $Q(t)$ is obtained by demodulating the signal $g(t)$. The received signal envelope is given by [101]

$$r(t) = \sqrt{I^2(t) + Q^2(t)} \tag{4.28}$$

and the phase θ is given by

$$\theta = \arctan\left(\frac{Q(t)}{I(t)}\right) \tag{4.29}$$

The probability density function (pdf) of the received signal amplitude (envelope), *f(r)*, can be shown to be Rayleigh given by [101]

$$f_A(r) = \frac{r}{\sigma^2}\exp\left\{-\frac{r^2}{2\sigma^2}\right\}, \qquad r \geq 0 \tag{4.30}$$

The cumulative distribution function (cdf) for the envelope is given by

$$F(r) = \int_0^r f(r)dr = 1 - \exp\left\{-\frac{r^2}{2\sigma^2}\right\} \qquad (4.31)$$

The mean and the variance of the Rayleigh distribution are $\sigma\sqrt{\pi/2}$ and $(2-\pi/2)\sigma^2$, respectively. The phase θ is uniformly distributed over $[0,2\pi]$. The instantaneous power is thus exponential. The Rayleigh distribution is a commonly accepted model for small-scale amplitude fluctuations in the absence of a direct line-of-sight (LOS) path, due to its simple theoretical and empirical justifications [101].

4.3.1 Filtering of Rayleigh Faded Signal Using DFrFT

The filter model discussed in Section 4.2 is used for the filtering of Rayleigh faded signals for stationary as well as the sources moving with constant velocity.

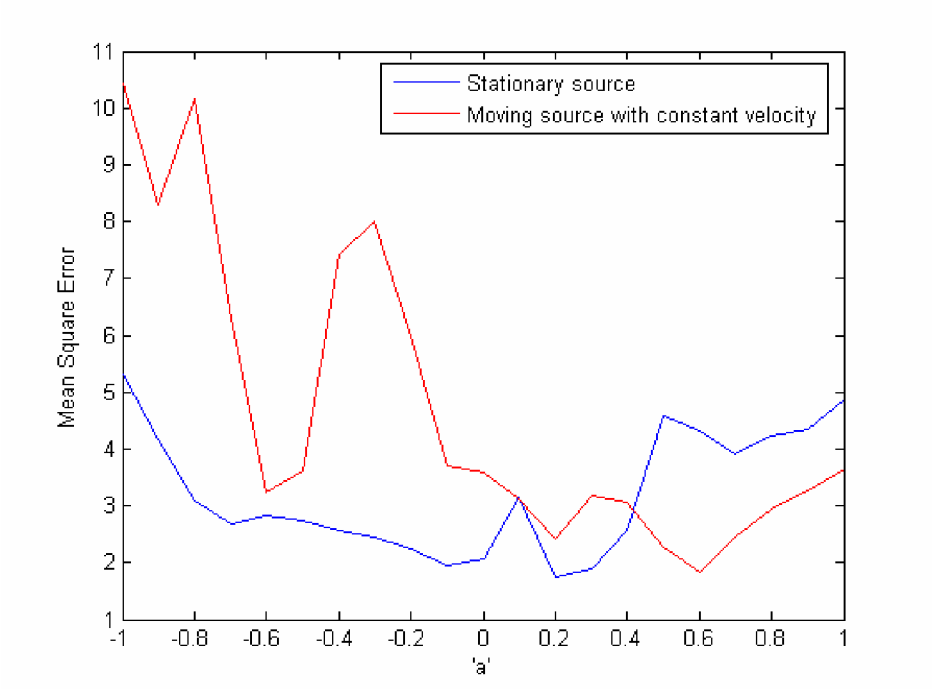

Figure-4.10: MSE Vs *a* for stationary and moving source for faded signal.

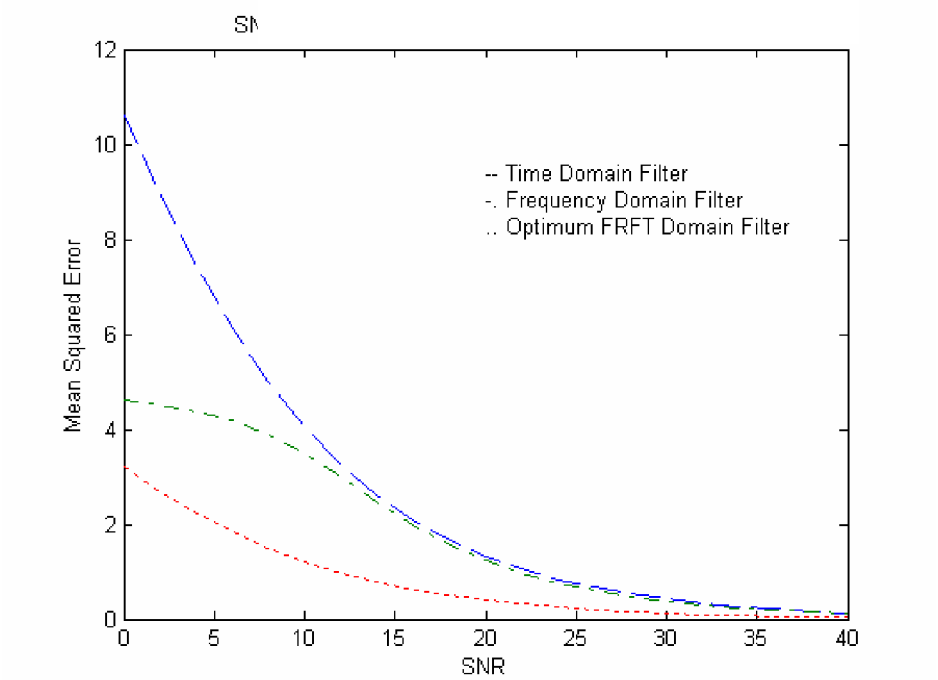

Figure-4.11: MSE Vs SNR for time, frequency and optimum FrFT domain filter in case of stationary source for faded channel

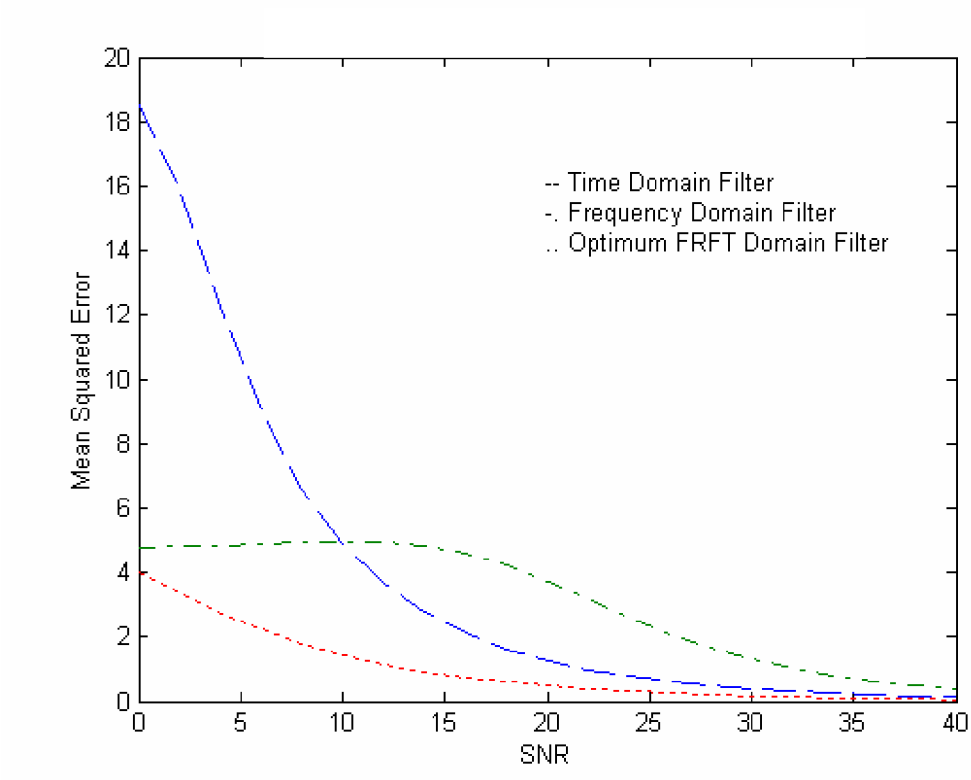

Figure-4.13: MSE Vs SNR for time, frequency and optimum FrFT domain filter in case of a moving source for faded channel

Figure-4.10 shows the variation of MSE with a for Rayleigh faded signals in case of stationary and moving source with a constant velocity of 100m/s. In both cases the MSE is smaller in optimum FrFT domain ($a = a_{opt}$) as compared to space domain ($a = 0$) and frequency domain ($a = 1$). In Figure-4.11and Figure-4.12 MSE is shown as a function of SNR in case of stationary source and moving source with a constant velocity respectively for Rayleigh faded signals in time, frequency and optimum FrFT domain. For a stationary source the optimum FrFT domain is $a = 0.2$ and for moving source the optimum FrFT domain is $a = 0.6$. It is observed that optimum domain is different from 0 and 1 in both the cases. From these plots it is clear that there is a significant improvement in the performance of filter for a Rayleigh faded signal in optimum FrFT domain as compared to time and frequency domains. The results for stationary and moving source with constant velocity in Rayleigh faded signals, shown in Figures-4.11 and Figure-4.13 substantiate this conclusion.

The optimum multiplicative filter function, which minimizes the MSE in optimum fractional Fourier domain, has been derived for Rayleigh faded time frequency varying signals. This optimum FrFT domain filter can be used for yielding small errors in case of moving source problems. This method of obtaining optimum a is based upon frame by frame basis. In practice the optimum 'a' that gives minimum MSE requires an efficient on-line procedure for its computation for which fast computation algorithm DFrFT is required.

As a conclusion, filtering in optimum fractional Fourier domain enables significant reduction of MSE compared to the ordinary Fourier domain filtering.

4.4 BEAMFORMING

Beamforming is a very useful tool in sensor array signal processing and is used widely for direction of arrival estimation, interference suppression and signal enhancement. The FT based method of beamforming is not in use these days because of its inherent short coming to handle time varying signals. In the active radar problem where the chirp signals are transmitted or an accelerating source reflects the sinusoidal signal as a chirp signal FrFT can be applied because of the ability of FrFT to handle chirp signals better than the FT. Therefore, as discussed earlier, the replacement of FT with FrFT should improve the performance considerably [55].

Beamforming provides an effective and versatile means of spatial filtering of signals arriving at distributed array of sensors. The sensor array collects spatial samples of propagating waves, which are processed by beamformer. To find the spectral differences a beamformer performs temporal filtering along with spatial filtering. It is applicable to either reception or radiation of energy. A beamformer linearly combines the spatially sampled time series from each sensor to obtain a scalar output time series as in the case of FIR filter. Mathematically a general beamformer process can be expressed as

$$f(t) = \sum_{m=1}^{M} \sum_{n=0}^{N-1} w_{m,n}^{*} g_m(t - nT) \tag{4.32}$$

where, $y(t)$ is the beamformer output, $x_m(t)$'s are the signals arriving at the sensors, N-1 is the number of delays in each of sensor channels, T is the duration of single time delay, M is the number of sensors, $w_{m,n}$'s are the weights of the beamformer and the subscript * denotes complex conjugation. The $w_{m,n}$'s are chosen to achieve the required cost function. The equation (4.32) can be written in the vector form as

$$f(t) = w^H g(t) \tag{4.33}$$

where, $g(t) = \left[g_1(t), g_1(t-T), ..., g_1(t-(N-1)T), g_2(t), ..., g_M(t-(N-1)T)\right]^T$

and $w = \left[w_{1,0}, w_{1,1}, ..., w_{1,N-1}, w_{2,0}, ..., w_{M,N-1}\right]^H$

where the subscript "T" denotes transpose and "H" denotes Hermitian conjugate.

This beamforming problem can be optimally solved by considering it to be multichannel filtering in Fractional Fourier domain [55]. The structure of this multichannel filter in Fractional Fourier Domain is given in Figure-4.13. The methodology is to transform the signal in an optimal a^{th} domain, then process the filtering in this domain and again transforming back into the time domain. The process requires online determination of the optimum a^{th} domain that is left as an open area of research.

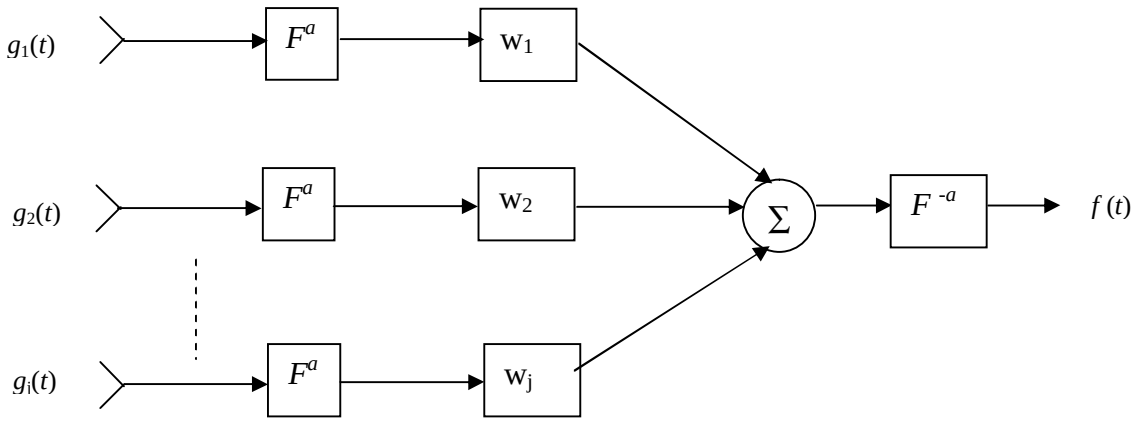

'*a*' denotes order of the FRFT

Figure-4.13: Block diagram of optimum FRFT domain filter.

The output of the filter can be expressed as:

$$f(t) = F^{-a}\left\| w^{H}(F^{a}\{g(t)\})\right\| \tag{4.34}$$

where, F^{a} denotes the a^{th} order FrFT. For FrFT filter the cost function *J(w)* is minimized and the optimum weights are given by:

$$w_{opt} = R_{g^{a}g^{a}}^{-1} r_{f^{a}g^{a}} \tag{4.35}$$

where $R_{y^{a}}$ is the covariance of the a^{th} order FrFT of the signals arriving at sensors and $r_{g^{a}f^{a}}$ is the cross-covariance between a^{th} order FrFT of the desired signal and FrFT of the signal arriving at the sensor. The $R_{y^{a}}$ and $r_{y^{a}x}$ can be computed using the covariance as follows:

$$R_{g^{a}g^{a}} = R_{g^{a}g^{a}}(x, x_a) = \int_{-\infty}^{\infty}\int_{-\infty}^{\infty} K^{a}(x, x_{a1})\, K^{-a}(x_a, x_{a2})\, R_{gg}(x_{a1}, x_{a2}) dx_{a1} dx_{a2} \tag{4.36}$$

$$r_{f^{a}g^{a}} = r_{f^{a}g^{a}}(x, x_a) = \int_{-\infty}^{\infty}\int_{-\infty}^{\infty} K^{a}(x, x_{a1})\, K^{-a}(x_a, x_{a2})\, r_{fg}(x_{a1}, x_{a2}) dx_{a1} dx_{a2} \tag{4.37}$$

The filter configuration, is as discussed in Figure-4.13, and multipath fading environment is simulated for stationary sources and sources moving with constant velocity. The harmonic source is in far field emitting frequency 1MHz. The signal is assumed to be Rayleigh faded with additive Gaussian noise.

The optimal beamformer can be obtained depending upon the criteria of optimization. The main criteria's of optimization are MMSE, Maximum SNR to Noise Ratio and Minimum Variance. Each criterion has its own advantages and disadvantages. The MMSE requires the reference signal and there is no requirement of the information about Direction of Arrival (DOA) of the signal. The maximum SNR requires direction of arrival of both desired and interfering signals. In this the weights are chosen so that the SNR at the output of the beamformer is optimized. The Minimum Variance method does not require knowledge of the angle of arrival of interferences but it requires

the angle of arrival of desired signal. In this the output power is minimized to ensure the effect of noise is minimized. The method proposed can be viewed as the generalization of MSE, which minimizes error between its output and the desired signal.

As FrFT gives rotational effect to time-frequency plane, a chirp signal that is a oblique line in time-frequency plane transforms into a harmonic which is vertical line in this plane. The WD gives the idea about the energy distribution of a signal in time-frequency plane and FrFT rotates the WD in clockwise direction by an angle α in the time frequency plane. This way the chirp signal (which are not compact in either spatial or time domain) is converted to harmonic signal as there exists an order for which the signal is compact. After this the MSE is calculated for various FrFT domains from $a = -1$ to $a = 1$. The optimal domain is searched where the MSE is least. Beamforming in this optimal domain is seen to be significantly better than in conventional Fourier domain. From Figure-4.14 it is clear that there is a significant improvement in the performance of beamformer in optimum FrFT domain as compared to space and frequency domains.

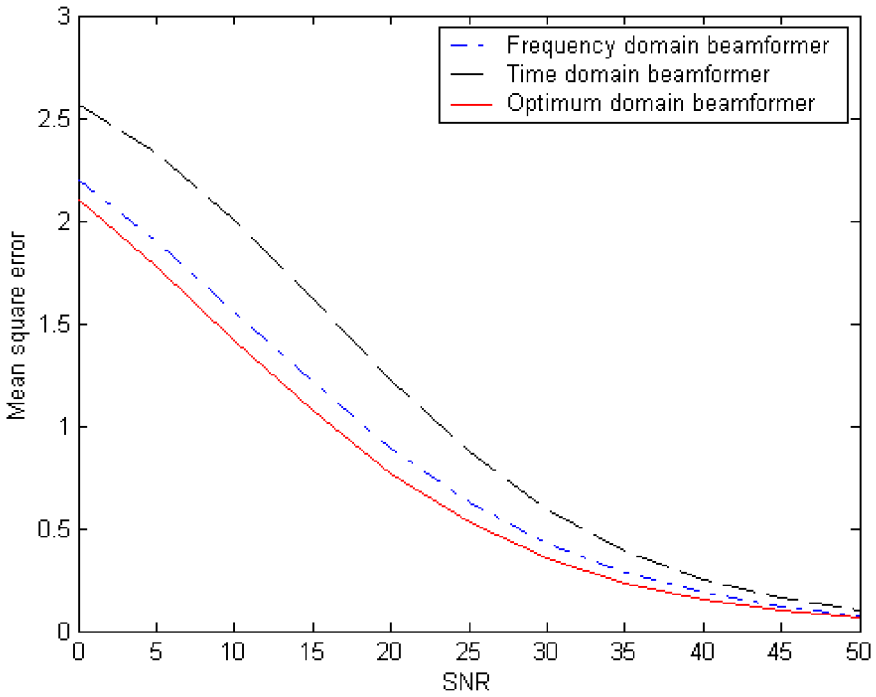

Figure-4.14: Comparison of MSE with varying SNR for different beam formers.

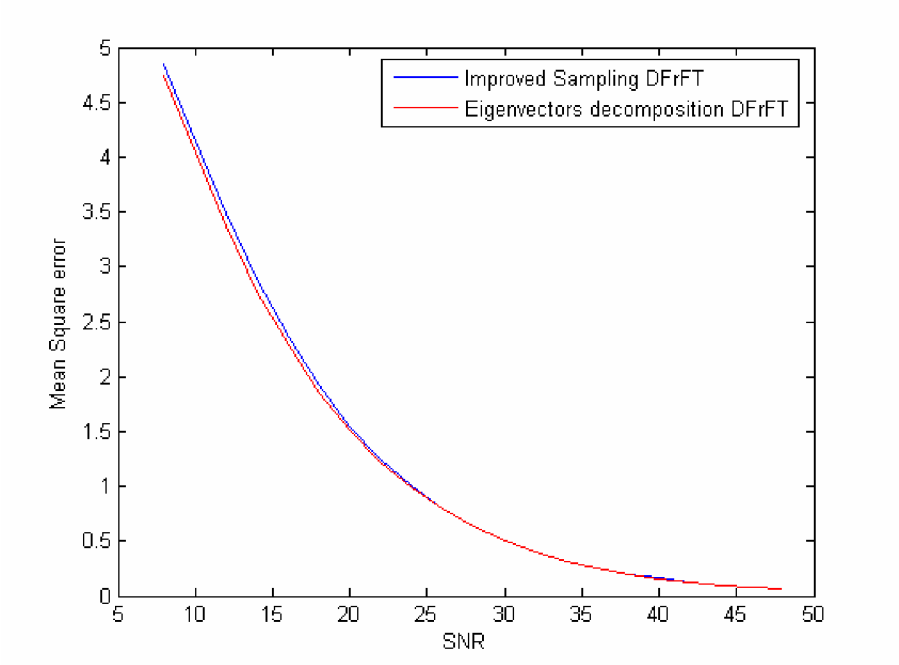

Figure 4.15: Comparitive plot for optimum domain beamforming using improved sampling and eigenvector decomposition type DFrFT.

The method of obtaining optimum *a* discussed in this work is based on frame by frame basis. In practice the optimum *a* that gives minimum MSE require an efficient on-line fast algorithm for computation of DFrFT.

Also in Figure-4.15 performance of eigenvector decomposition type DFrFT is compared with improved sampling DFrFT for optimum domain beamforming. Eigenvector decomposition excels over improved sampling type, which once again justifies the usage of eigenvector decomposition type in our work.

4.5 SUMMARY

In this chapter one dimensional signal processing applications, namely, filtering and beamforming have been discussed. Filtering of signals overlapping in both time and frequency domain using DFrFT is performed. Performance of DFrFT in filtering with a relative motion between source and receiver is also studied. The results so obtained of proposed filtering clearly establish the superiority of DFrFT for filtering of such signals. These studies have been then extended for the filtering of faded signals. Rayleigh faded time-frequency varying signals are filtered using DFrFT. Filtering in the optimum domain outclasses both time and frequency domain filtering. Beamforming is another application of DFrFT successfully attempted using FrFT. For both applications determination of optimum domain is mandatory. The optimum multiplicative filter function then minimizes the MSE. The method of obtaining optimum a is based upon frame by frame basis. In practice the optimum a that gives minimum MSE requires an efficient on-line procedure for its computation.

As a conclusion, filtering in optimum fractional Fourier domain enables significant reduction of MSE compared with ordinary Fourier domain filtering. This reduction in MSE comes at no additional cost and computation complexity.

CHAPTER 5

TWO DIMENSIONAL APPLICATIONS

5.1 INTRODUCTION

One dimensional applications of DFrFT have been discussed in previous chapter. Image compression and image encryption are two very important applications in two dimensional signal processing. In this chapter these two dimensional applications have been successfully discussed using DFrFT and DFrCT respectively. The performance of these fractional transforms in these two application areas has also been compared with wavelet transform.

5.2 IMAGE COMPRESSION

An image is a visual representation of an object or a group of objects. It may also be defined as a two-dimensional function, $f(x, y)$, where x and y are spatial coordinates and the magnitude of $f(.)$ at any pair of coordinates (x, y) is called the intensity of the image at that point. When x, y and the magnitude value of $f(.)$ are all finite discrete quantities, it is called a digital image. A digital image is composed of a finite number of elements each of which has a particular location and value. Normally, a digital image is a rectangular array of elements (referred as picture elements, image element, pels or pixels) sometimes called a bitmap. It is represented by

an array of N rows and M columns and usually $N = M$. Typically values of N and M are 128, 256, 512 and 1024 etc [102].

Image compression addresses the problem of reducing the amount of data required to represent a digital image. The underlying basis of the reduction process is the removal of redundant data. According to mathematical point of view, this amounts to transforming a two-dimensional pixel array into a statistically uncorrelated data set. The transformation is applied prior to storage or transmission of the image. At receiver, the compressed image is decompressed to reconstruct the original image or an approximation to it. The initial focus of research efforts in this field was on the development of analog methods for reducing video transmission bandwidth, a process called bandwidth compression [102]. The advent of digital computer and subsequent development of advanced integrated circuits, however, caused interest to shift from analog to digital compression approaches. With the recent adoption of several key international image compression standards, the field is now poised for significant growth through the practical application of the theoretical work that began in the 1940s, when C.E. Shannon and others first formulated the probabilistic view of information and its representation, transmission, and compression [102].The term data compression refers to reducing amount of data required to represent a given amount of information. There should be a clear distinction between data and information. In fact, data are the form of information representation. Thus the same information may be represented by a completely different data set. If certain information has two representations differing in size, one of them is said to have data redundancy [103].

The data redundancy is a quantifiable entity. If n_1 and n_2 are the number of information units in two data sets representing the same information, the relative data redundancy R_D of the first data set (the one characterized by n_1) is defined as-

$$R_D = 1 - \frac{1}{C_R} \tag{5.1}$$

where, C_R commonly called the compression ratio (CR), is

$$C_R = \frac{n_1}{n_2} \tag{5.2}$$

For the case $n_2 = n_1, C_R = 1$ and $R_D = 0$ indicating that (relative to the second data set) the first representation of the information contains no redundant data. When $n_2 << n_1, C_R$ and R_D, implying significant compression and highly redundant data. In the final case, $n_2 >> n_1, C_R$ and R_D, indicating that the second data set contains much more data than the original representation. This is of course, is the normally undesirable case of data expansion. In general C_R and R_D lie in the open intervals (0,∞) and (-∞, 1) respectively. A compression ratio 8:1 means that the first data set has 8 information carrying units per every 1 unit in the second or compressed data set. The corresponding redundancy of 0.875 implies that 87.5 percent of the data in the first data set is redundant [102].

A common characteristic of most images is that the neighboring pixels are correlated and therefore contain redundant information. The foremost task then is to find less correlated representation of the image. Two fundamental components of compression are redundancy and irrelevancy reduction. Redundancy reduction aims at removing duplication from the signal source (image/video). Irrelevancy reduction omits parts of the signal that will not be noticed by the signal receiver, namely the Human Visual System.

In digital image compression, three basic data redundancies can be identified and exploited [102]:

- **Coding redundancy:** Fewer bits to represent frequent symbols.
- **Interpixel redundancy:** Neighboring pixels have similar values.
- **Psychovisual redundancy:** Human visual system cannot simultaneously distinguish all colors.

Data compression is achieved when one or more of these redundancies are reduced or eliminated.

5.2.1 Image Compression Techniques

Two general techniques for reducing the amount of data required to represent an image are lossless compression and lossy compression. In both of these techniques one or more redundancies as discussed in the last sections are removed. In lossless compression, the reconstructed image after decompression is numerically identical to the original image. In lossy compression scheme, the reconstructed image contains degradation relative to the original.

In case of video, compression causes some information to be lost, some information at a detail level is considered not essential for a reasonable reproduction of the scene. This type of compression is called lossy compression. Audio compression on the other hand, is not lossy, it is called lossless compression. An important design consideration in an algorithm that causes permanent loss of information is the impact of this loss in the future use of the stored data. Lossy technique causes image quality degradation in each compression / decompression step. Careful consideration of the human visual perception ensures that the degradation is often unrecognizable,

though this depends on the selected compression ratio. In general, lossy techniques provide far greater compression ratios than lossless techniques [103].

Following are the some of the lossless and lossy data compression techniques [102]:

a) Lossless compression techniques

i) Run length encoding

ii) Huffman encoding

iii) Arithmetic encoding

iv) Entropy encoding

v) Area encoding

b) Lossy compression techniques

i) Predictive coding

ii) Transform coding (FT / DCT / Wavelets)

However, these techniques are also combined to form practical image compression system. Generally a compression system consists of two distinct structural blocks: an encoder and a decoder. An input image $f(x, y)$ is fed into the encoder, which creates a set of symbols from the input data. After transmission over the channel, the encoded representation is fed to the decoder, where a restructured output image $g(x, y)$ is generated. In general $g(x, y)$ may or may not be an exact replica of $f(x, y)$ [103].

5.2.2 Image Compression Characteristics

There are three main characteristics by which one can evaluate an image-compression algorithm: CR, compression speed, and image quality. These characteristics can be used to determine the suitability of a given compression algorithm to the various applications. The following paragraphs discuss each of these attributes in more detail [103].

a) Compression Ratio

The CR is equal to the size of the original image divided by the size of the compressed image. This ratio gives an indication of how much compression is achieved for a particular image. The CR achieved usually indicates the picture quality. Generally, the higher the compression ratio, the poorer the quality of the resulting image. The trade-off between CR and picture quality is an important one to consider when compressing images. Furthermore, some compression schemes produce compression ratios that are highly dependent on the image content. This aspect of compression is called data dependency. Using an algorithm with a high degree of data dependency, an image of a crowd at a football game (which contains a lot of detail) may produce a very small CR, whereas an image of a blue sky (which consists mostly of constant colors and intensities) may produce a very high compression ratio.

b) Compression Speed

Compression time and decompression time are defined as the amount of time required to compress and decompress an image, respectively. Their value depends on the following considerations:

- the complexity of the compression algorithm
- the efficiency of the software or hardware implementation of the algorithm
- the speed of the utilized processor or auxiliary hardware

Generally, the algorithm performs both compression and decompression in a faster way, can be considered the better one. Fast compression time increases the speed with which material can be created. Fast decompression time increases the speed with which the user can display and interact with images.

c) Image Quality

Image quality describes the fidelity with which an image compression scheme recreates the source image data. Compression schemes can be characterized as being either lossy or lossless. Lossless schemes preserve all of the original data. Lossy compression does not preserve the data precisely; image data is lost, and it cannot be recovered after compression. Most lossy schemes try to compress the data as much as possible, without decreasing the image quality in a noticeable way. Some schemes may be either lossy or lossless, depending upon the quality level desired by the user [102].

The quality of compressed image can be measured by many parameters, which are used to compare different compression techniques. The most commonly used parameters are Mean Square error (MSE) and Peak Signal to Noise Ratio (PSNR). The PSNR value used to measure the difference between a decompressed image $g(x, y)$ and its original image $f(x, y)$ is defined as follows. In general, the larger PSNR value, the better will be the decompressed image quality.

$$MSE = \left[\frac{1}{MN} \sum_{i=0}^{M-1} \sum_{j=0}^{N-1} \left[g(i, j) - f(i, j) \right]^2 \right] \quad (5.1)$$

$$PSNR = 10 \log_{10} \left[\frac{M \times N}{MSE^2} \right] \quad (5.2)$$

where, M × N is the size of the images, $g(i, j)$ and $f(i, j)$ are the matrix elements of the decompressed and the original images at (i, j) pixel. In order to evaluate the performance of image compression systems, CR matrix is often employed.

5.3 TRANSFORM CODING

This work focuses on the performance analysis of different transforms for data compression. The Transform coding first transforms the image from its spatial domain representation to a different type of representation using some well-known transform and then codes the transformed values (coefficients). The goal of the transformation process is to decorrelate the pixels of each subimage, or to pack as much information as possible into the smallest number of transforms coefficients [102]. This method provides greater data compression compared to predictive methods, although at the expense of greater computational requirements. The choice of particular transform in a given application depends on the amount of reconstruction error that can be tolerated and the computational resources available.

A general model of transform coding system is shown in Figure-5.1 [102]. As shown in Figure-5.1(a), encoder performs three relatively straightforward operations i.e. subimage decomposition, transformation and quantization. The decoder implements the inverse sequence of steps with the exception of the quantization function of the encoder shown in Figure-5.1(b).

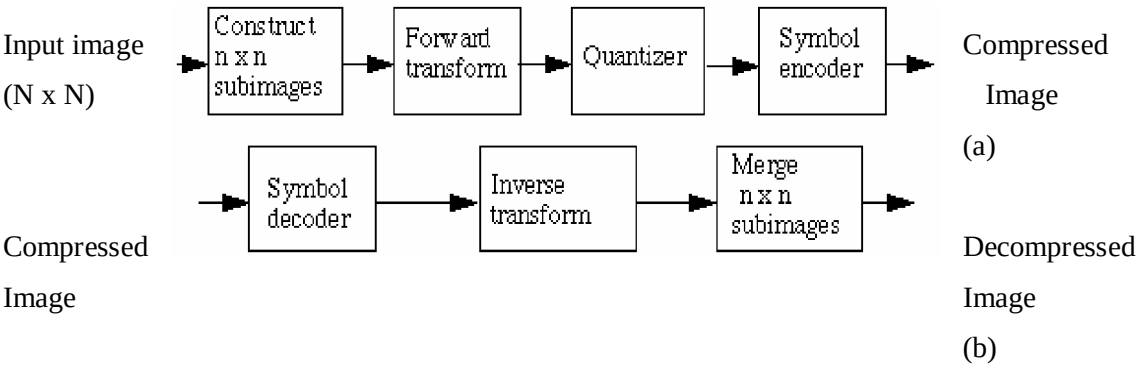

Figure-5.1: A transform compression system: (a) encoder; (b) decoder.

An $N \times N$ input image is first subdivided into sub images of size $n \times n$, which are then transformed to generat $(N/n)^2$ subimage transform arrays of $n \times n$. The quantization stage selectively eliminates or more coarsely quantize the coefficient that carry the least information. These coefficient have the smallest impact on reconstructed subimage quality. Any or all of the transform coding steps can be adapted in local image content, called adaptive transform coding, or fixed for all sub images, called non-adaptive transform coding. In the proposed implementation non-adaptive transform coding has been chosen [102].

In transform coding system any kind of transformation can be chosen, such as Karhunen Loeve (KLT), Discrete Cosine (DCT), Walsh-Hadamard (WHT), Fourier (FT) etc. The choice of a particular transformation in a given application depends on the amount of reconstruction error that can be tolerated and the computational resources available [102]. To receive good result the transform should have the following properties:

- Fast to compute.
- Decorrelate transform coefficient to remove redundancies.
- Pack energy into only a few transform coefficients.
- Preserve energy.

A significant factor affecting transform coding, error and computational complexity is function of subimage size. In most application images are subdivided so that the correlation (redundancy) between adjacent subimages is reduced to some acceptable level so that *n* can be expressed as an integral power of 2, where *n* is the subimage dimension. The latter condition simplifies the computation of the subimage transformation. In general, both the levels of compression and computational complexity increase as the subimage size increases. The most popular subimage sizes are 8 × 8 and 16 × 16. Figure-5.2 illustrates graphically the impact of subimage size on transform coding reconstruction error [102].

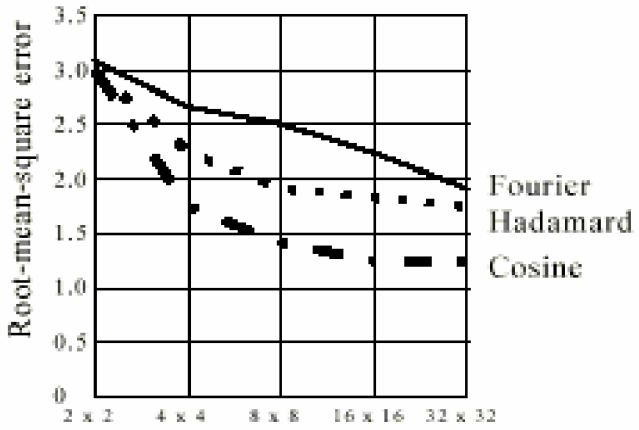

Figure-5.2: Reconstruction (root mean square) error versus subimage size.

It is clear from Figure-5.2 that the Hadamard and Cosine curves flatten as the size of the subimage becomes greater than 8×8, whereas the Fourier reconstruction error decreases more rapidly in this region [102].

5.3.1 Image compression using DFrFT

It has been recently noticed that the DFrFT can be used in the field of image processing [74]. The significant feature of discrete fractional Fourier domain image compression benefits from its extra degree of freedom that is provided by its fractional orders. The one-dimensional DFrFT is useful in processing single-dimensional signals such as speech waveforms. For analysis of two-dimensional signals such as images, a two-dimensional version of the DFrFT is needed. For an $M \times N$ matrix, the two-dimensional DFrFT is computed in a simple way: The one-dimensional DFrFT is applied to each row of matrix and then to each column of the result. Thus, the generalization of the DFrFT to two-dimension is given by taking the DFrFT of the rows of the matrix *i.e.* image in a fractional domain and then taking the DFrFT of the resultant matrix columnwise. In the case of the two-dimensional DFrFT two angles of rotation $\alpha=a\pi/2$ and $\beta=b\pi/2$ have to be considered. If one of these angles is zero, the two-dimensional transformation kernel reduces to the one-dimensional transformation kernel.

By adjusting the cutoff of the transform coefficients, a compromise can be made between image quality and CR. To exploit this method, an image is first partitioned into non-overlapped $n \times n$ subimages as shown in Figure-5.3. A two-dimensional DFrFT is applied to each block to convert the gray levels of pixels in the spatial domain into coefficients in the ath domain. The coefficients are normalized by different scales according to the cutoff selected. The quantized coefficients are

rearranged in a zigzag scan order to be further compressed by efficient lossless coding strategies. At decoder simply inverse process of encoding by using inverse two-dimensional DFrFT is performed. Because quantization results in an irreversible information loss, a lossy compression results.

5.3.1.1 DFrFT Compression Model

In image compression using DFrFT, a compression model encoder performs three relatively straightforward operations i.e. subimage decomposition, transformation and quantization. The decoder implements the inverse sequence of steps of encoder. Because quantization results in irreversible information loss, so inverse quantizer block is not included in the decoder as shown in Figure-5.3(b). Hence it is a lossy compression technique.

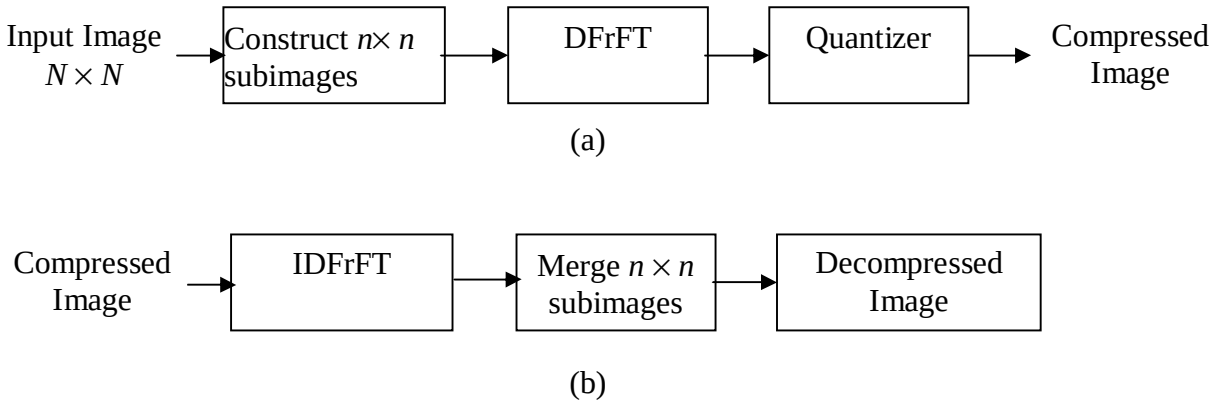

Figure-5.3: DFrFT compression model: (a) encoder; (b) decoder.

An image is first partitioned into non-overlapped n × n subimages as shown in Figure-5.3(a). The most popular subimage sizes are 8 × 8, 16 × 16. In the proposed implementation

scheme subimage size chosen is 8×8. As subimage size increases, error decreases but computational complexity increases. Compression techniques that operate on block of pixels i.e. subimages are often described as block coding techniques. The transform of a block of pixels may suffer from discontinuity effects resulting in the presence of blocking artifacts in the image after it has been decompressed.

In second step, a two-dimensional DFrFT is applied to each block to convert the gray levels of pixels in the spatial domain into coefficients in the frequency domain. By using DFrFT a large amount of information is packed into smaller number of transform coefficients, hence small amount of compression is achieved at this step.

The final step in compression process is to quantize the transformed coefficients according to cutoff selected and value of *a*. By adjusting the cutoff of the transform coefficients, a compromise can be made between image quality and compression factor. With the DFrFT by varying its free parameter *a*, high compression ratio can be achieved even for same cutoff. The quantized coefficients are then rearranged in a zig-zag scan order to form compressed image which can be stored or transmitted.

At decoder simply inverse process of encoder is performed by using inverse two-dimensional DFrFT. The non-overlapped subimages are merged to get decompressed image. As it is a lossy compression technique so there is some error between decompressed image and original image which is evaluated using (5.1).

5.3.1.2 Simulation Results

Numerical simulations have been performed to examine the validity of this image compression technique. The original images taken are the pictures of Lena, Cameraman, IC, Barbara and Rice with 256×256 pixels. These images are compressed for compression ratios of 10%, 20%, 30%, 40%, 50% and 75% for varying values of *a*. The Figures-5.4 show the decompressed images with different fractional orders for 30% CR. It is clear that as we increase the value of '*a*' image quality degrades. At $a = 1$ which corresponds to FT image quality is very poor. By using DFrFT, it is clear that for same CR, it gives better-decompressed image as compared to FT. For $a = 0.91$ best results are achieved, with a maximum PSNR of 30.51.

Figure-5.4(a): The Original Lena Image.

Figure-5.4(b): Lena image after decompression at *a*= 0.1.

Figure-5.4(c): Lena image after decompression at *a*= 0.2.

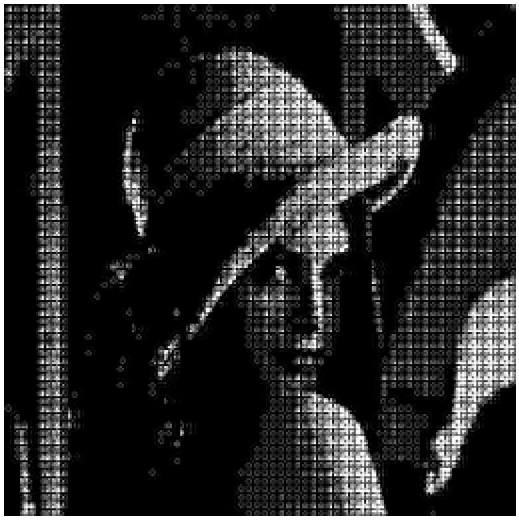

Figure-5.4(d): Lena image after decompression at *a*= 0.3.

Figure-5.4: Simulation results of the Lena image with 256x256 pixels at varying *a* using DFrFT. (contd.)

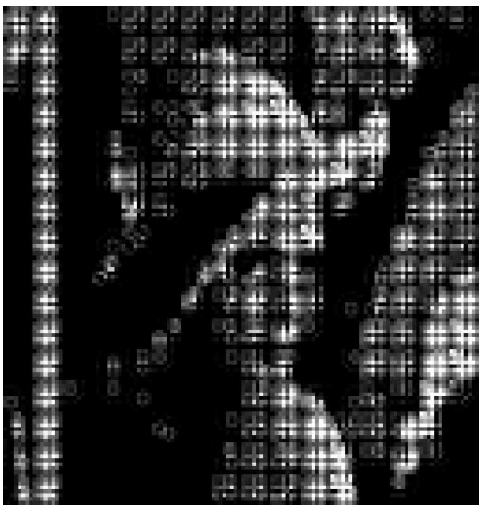

Figure-5.4(e): Lena image after decompression at *a*= 0.4.

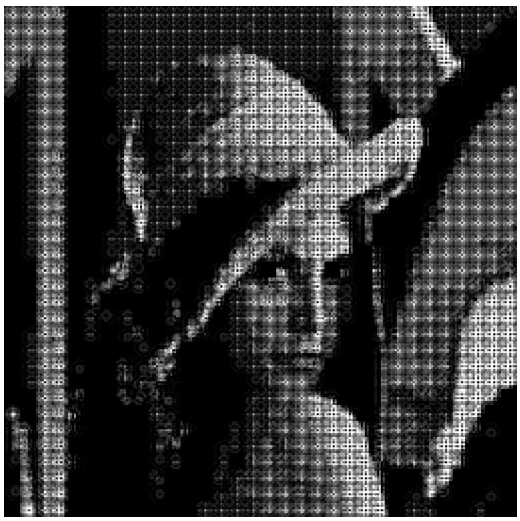

Figure-5.4(f): Lena image after decompression at *a*= 0.5.

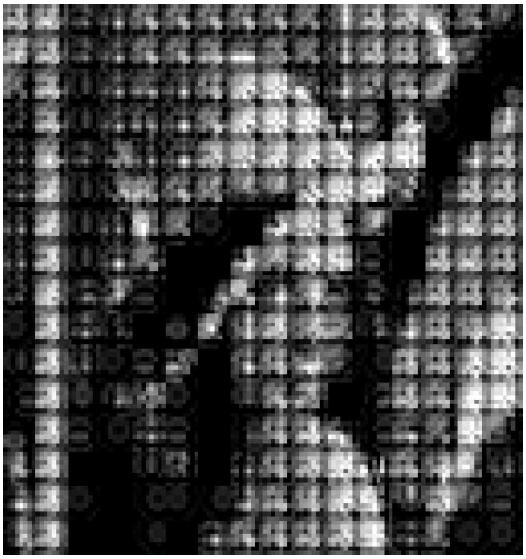

Figure-5.4(g): Lena image after decompression at *a*= 0.6.

Figure-5.4(h): Lena image after decompression at *a*= 0.7.

Figure-5.4: Simulation results of the Lena image with 256x256 pixels at varying *a* using DFrFT. (contd.)

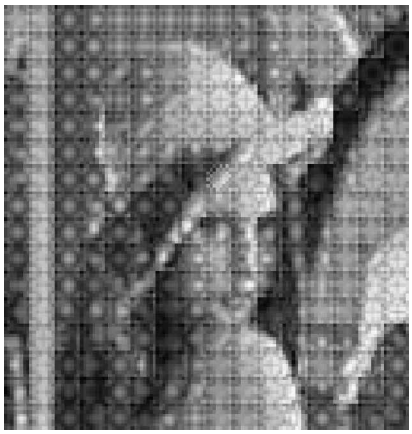

Figure-5.4(i): Lena image after Decompression at *a*= 0.8.

Figure-5.4(j): Lena image after decompression at *a*= 0.9.

Figure-5.4(k): Lena image after decompression at *a*= 0.91.

Figure-5.4(l): Lena image after decompression at *a*= 0.92.

Figure-5.4: Simulation results of the Lena image with 256x256 pixels at varying *a* using DFrFT. (contd.)

Figure-5.4(m): Lena image after decompression at *a*= 0.93.

Figure-5.4(n): Lena image after decompression at *a*= 0.94.

Figure-5.4(o): Lena image after decompression at *a*= 0.95.

Figure-5.4(p): Lena image after decompression at *a*= 0.96.

Figure-5.4: Simulation results of the Lena image with 256x256 pixels at varying *a* using DFrFT. (contd.)

Figure-5.4(q): Lena image after decompression at *a*= 0.97.

Figure-5.4(r): Lena image after decompression at *a*= 0.98.

Figure-5.4(s): Lena image after decompression at *a*= 0.99.

Figure-5.4(t): Lena image after decompression at *a* = 1.

Figure-5.4: Simulation results of the Lena image with 256x256 pixels at varying *a* using DFrFT.

5.3.1.3 Performance Analysis of DFrFT in Image Compression

To illustrate the performance of DFrFT in image compression MSE and PSNR have been selected as metric parameters. Figure-5.5 and Figure-5.6 respectively show the plots for MSE and PSNR with respect to '*a*' for different CRs. The image selected for these figures is Lena. In Figure-5.7 to Figure-5.12, comparative plots for five other images between PSNR and '*a*', for CRs of 10%, 20%, 30%, 40%, 50% and 75% respectively are shown. It is observed that the optimum compression performance is achieved for values of '*a*' varying between 0.91 and 0.97. The optimum value of '*a*' is dependent both on the image and the CR.

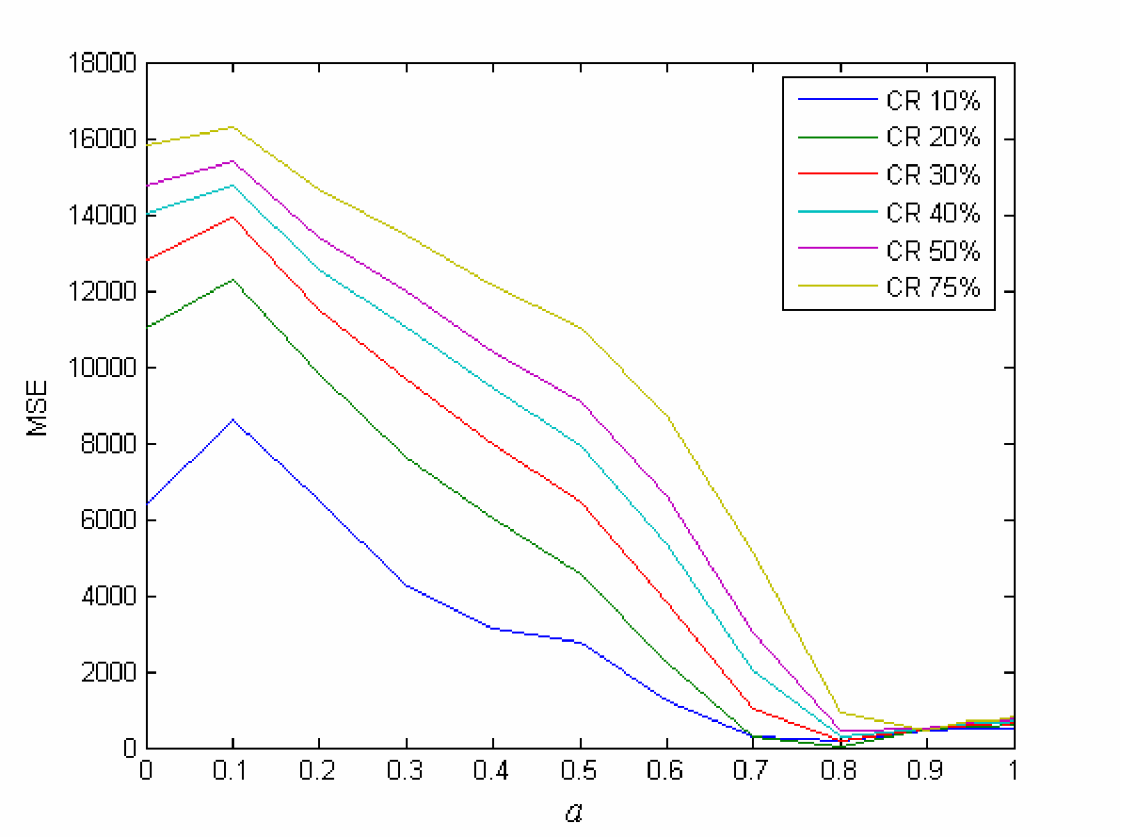

Figure-5.5: Fractional order *a* vs MSE of Lena image for different CR using DFrFT.

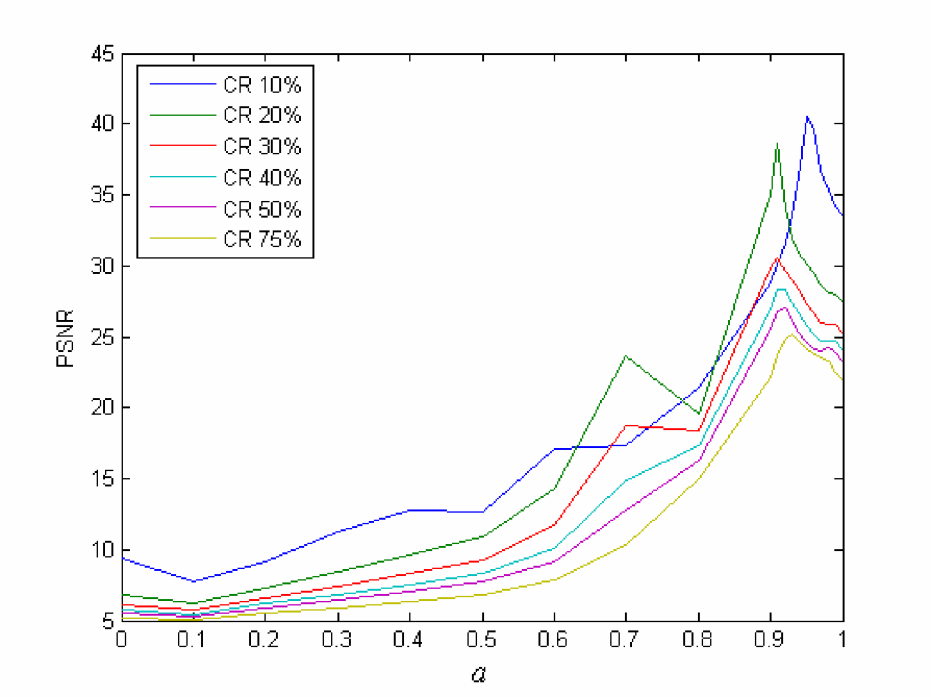

Figure-5.6: Fractional order *a* vs PSNR of Lena image for different CR using DFrFT.

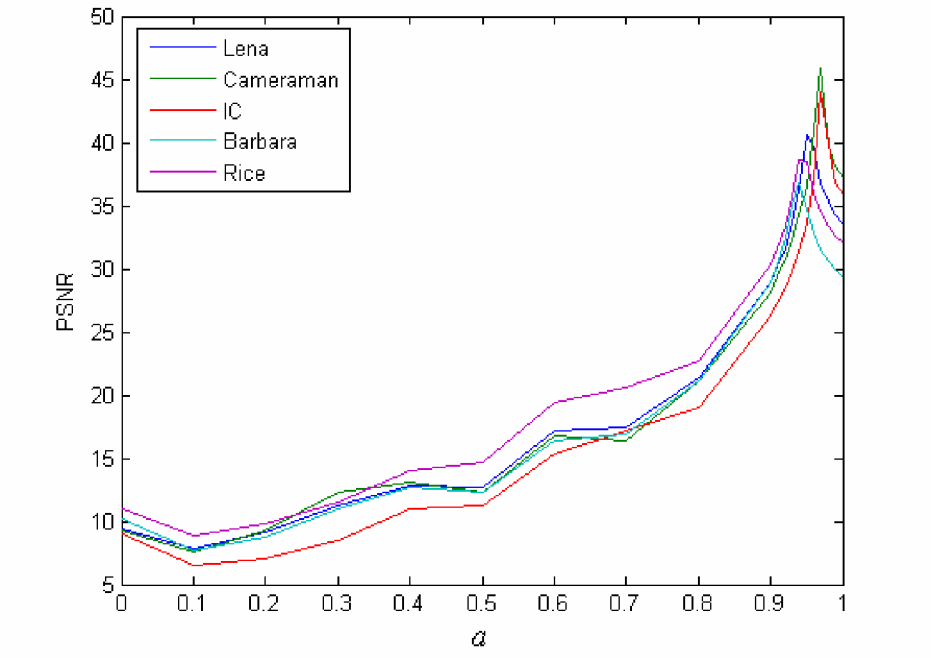

Figure-5.7: Fractional order *a* vs PSNR of different images at CR of 10% using DFrFT.

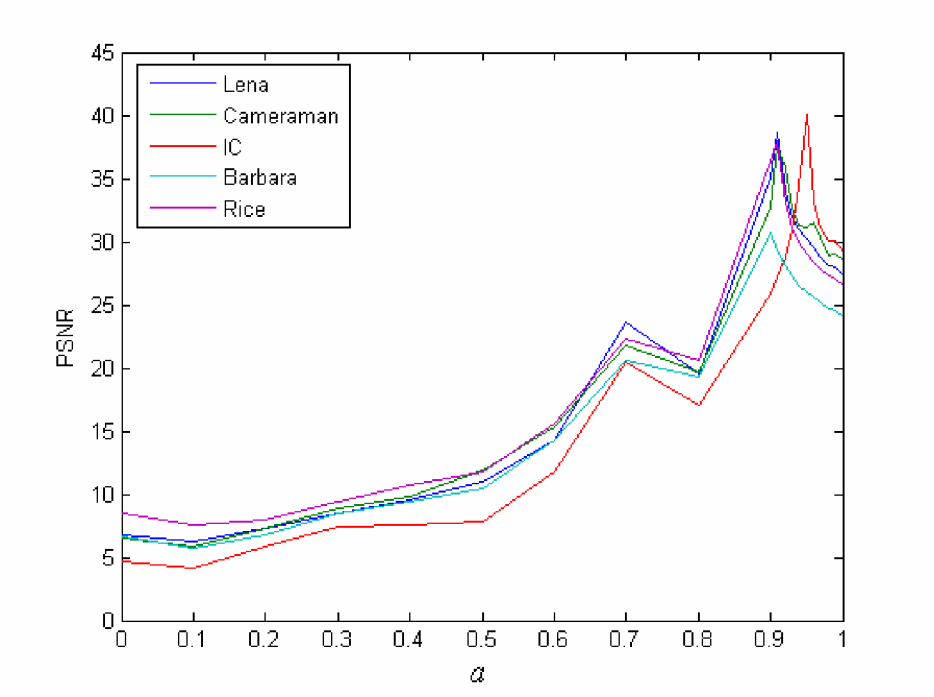

Figure-5.8: Fractional order *a* vs PSNR of different images at CR of 20% using DFrFT.

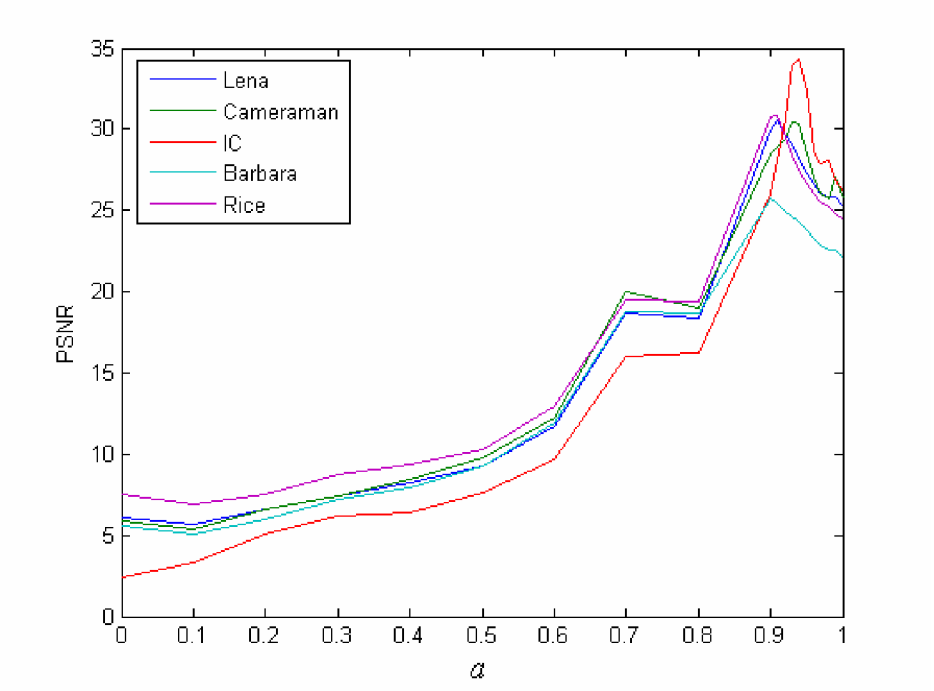

Figure-5.9: Fractional order *a* Vs PSNR of different images at CR of 30% using DFrFT.

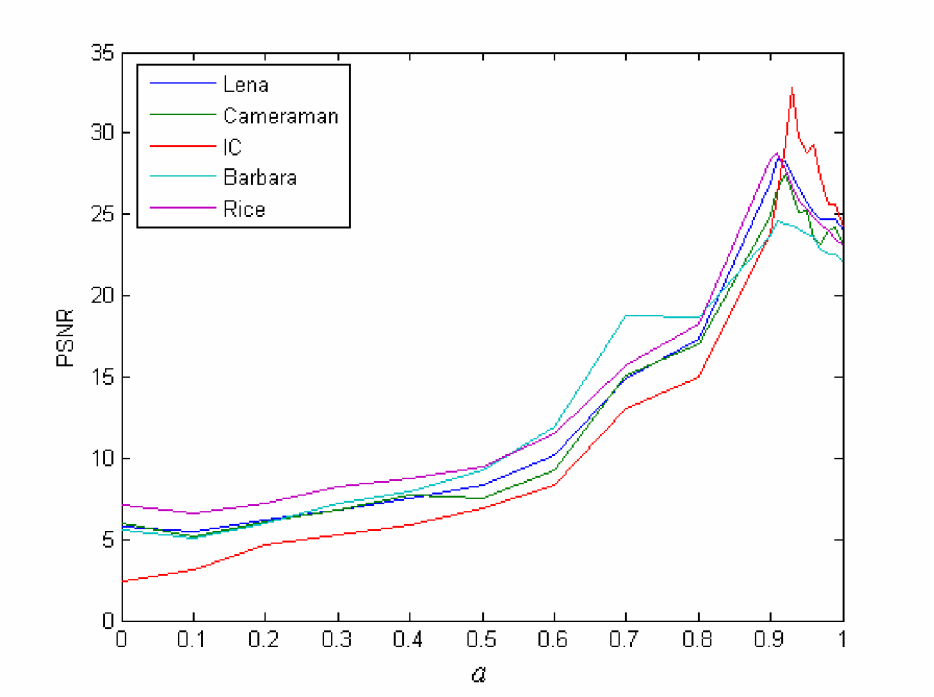

Figure-5.10: Fractional order *a* vs PSNR of different images at CR of 40% using DFrFT.

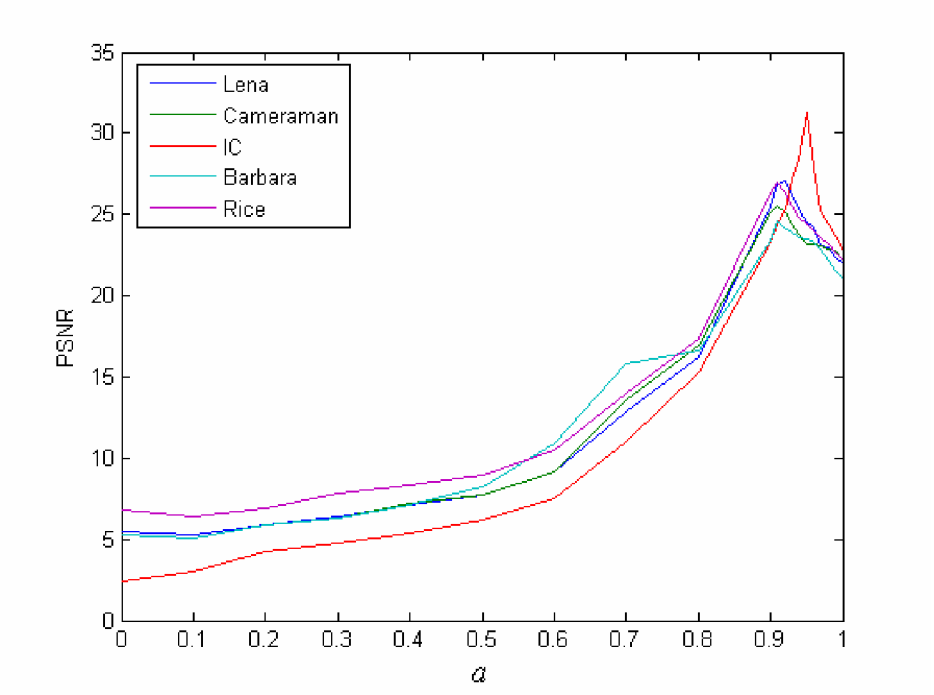

Figure-5.11: Fractional order *a* vs PSNR of different images at CR of 50% using DFrFT.

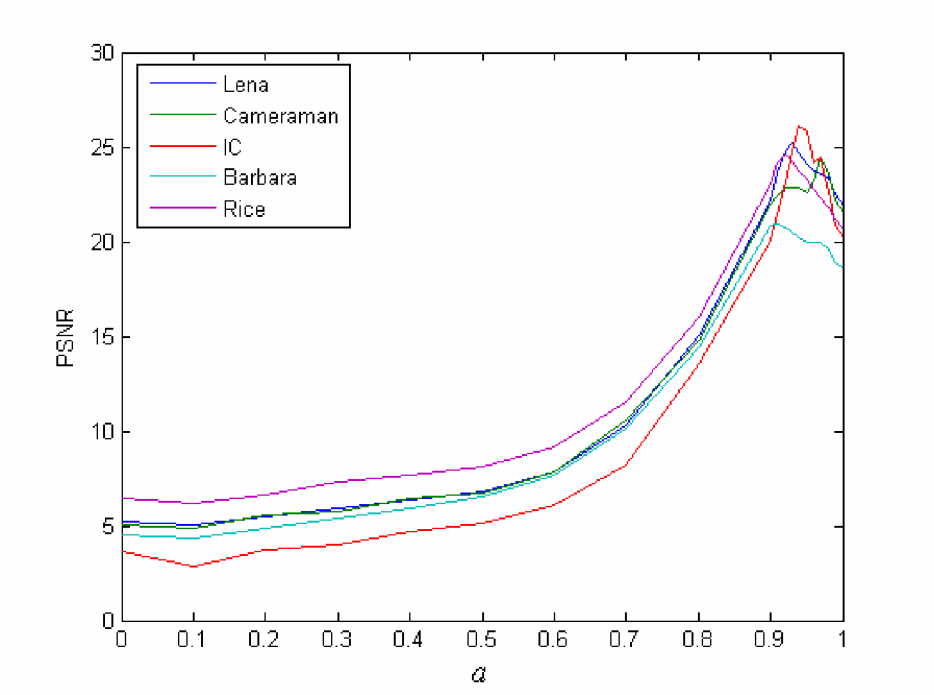

Figure-5.12: Fractional order *a* vs PSNR of different images at CR of 75% using DFrFT.

5.3.2 Image Compression Using DFrCT

Image compression has also been carried out using DFrCT. The procedure is the same as used for DFrFT. Compression results for a CR of 10% for different values of DFrCT order are shown in Figure-5.13. The image selected for this illustration is Rice.

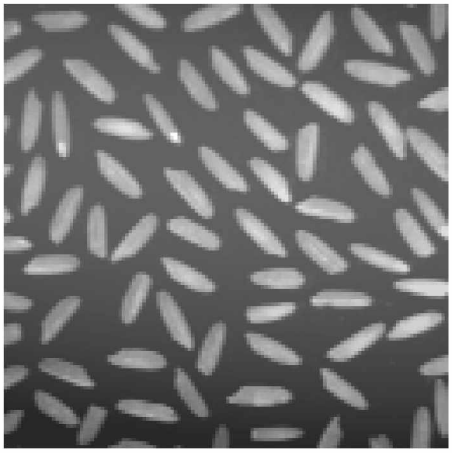

Figure-5.13(a): Original Rice image

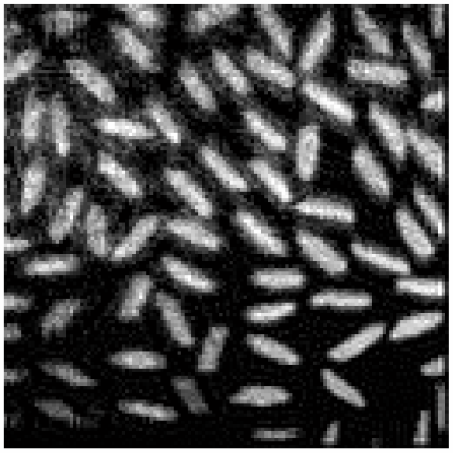

Figure-5.13(b): Rice image after decompression at *a*= 0.1.

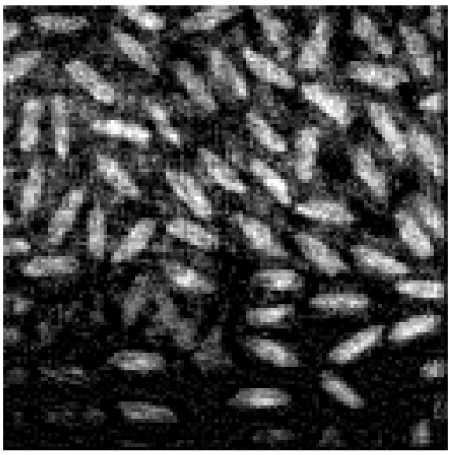

Figure-5.13(c): Rice image after decompression at *a*= 0.3.

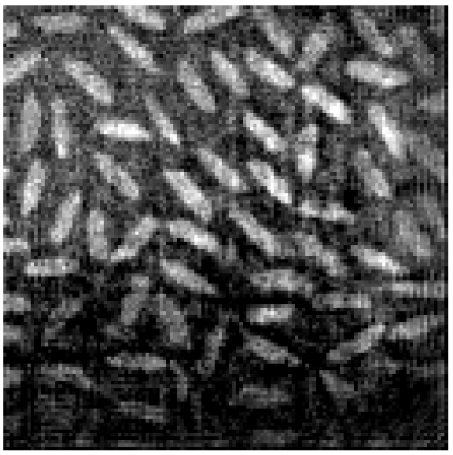

Figure-5.13(d): Rice image after decompression at *a*= 0.5.

Figure-5.13: Simulation results of the Rice image with 256x256 pixels at varying *a* using DFrCT. (contd.)

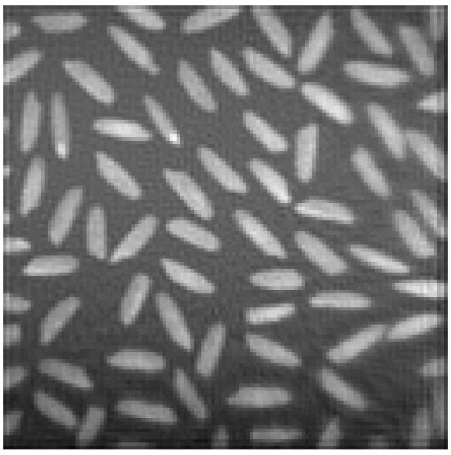

Figure-5.13(e): Rice image after decompression at *a*= 0.7.

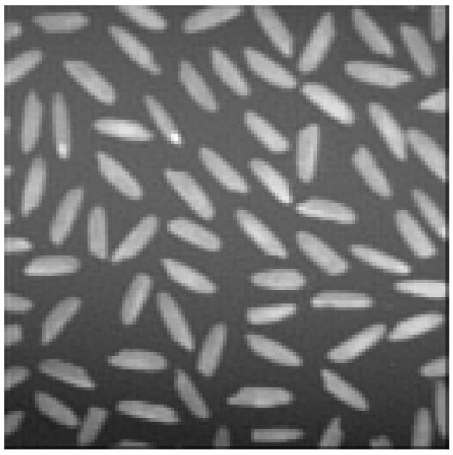

Figure-5.13(f): Rice image after decompression at *a*= 0.9.

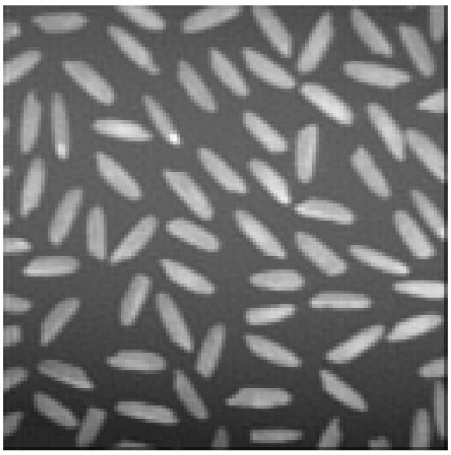

Figure-5.13(g): Rice image after decompression at *a*= 0.91.

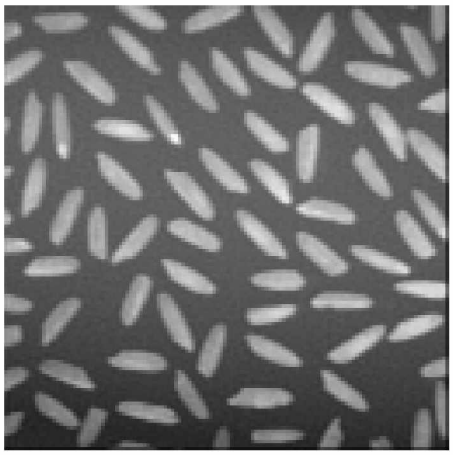

Figure-5.13(h): Rice image after decompression at *a*= 1.

Figure-5.13: Simulation results of the Rice image with 256x256 pixels at varying *a* using DFrCT.

5.3.2.1 Performance Analysis of DFrCT in Image Compression

Variation in MSE and PSNR with respect to DFrCT order 'a' for different CRs are shown in Figure-5.14 and Figure-5.15 respectively. In Figure-5.16 to Figure-.21, comparative plots for five images between PSNR and order '*a*' for different CRs are shown. Optimum value of '*a*' is to be dependent on both the CR and the image type. This optimum value varied between 0.91 and 0.99.

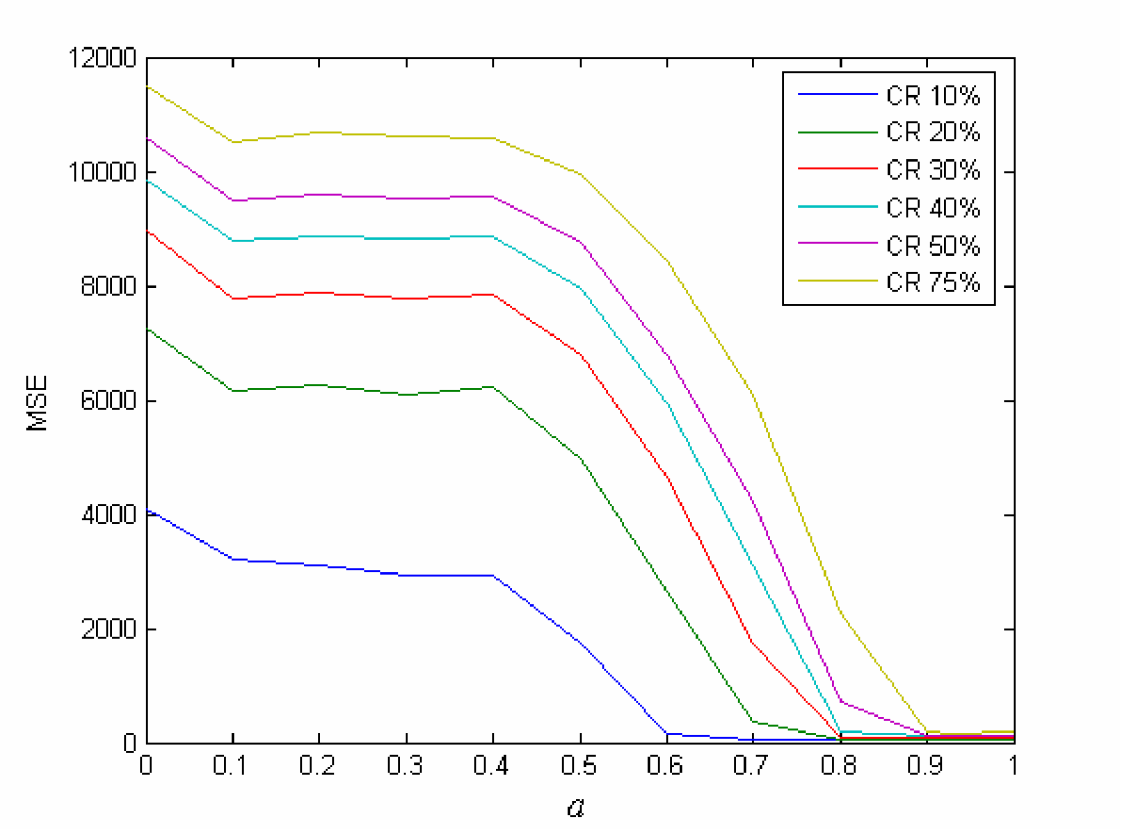

Figure-5.14: Fractional order *a* vs MSE of Rice image for different CR using DFrCT.

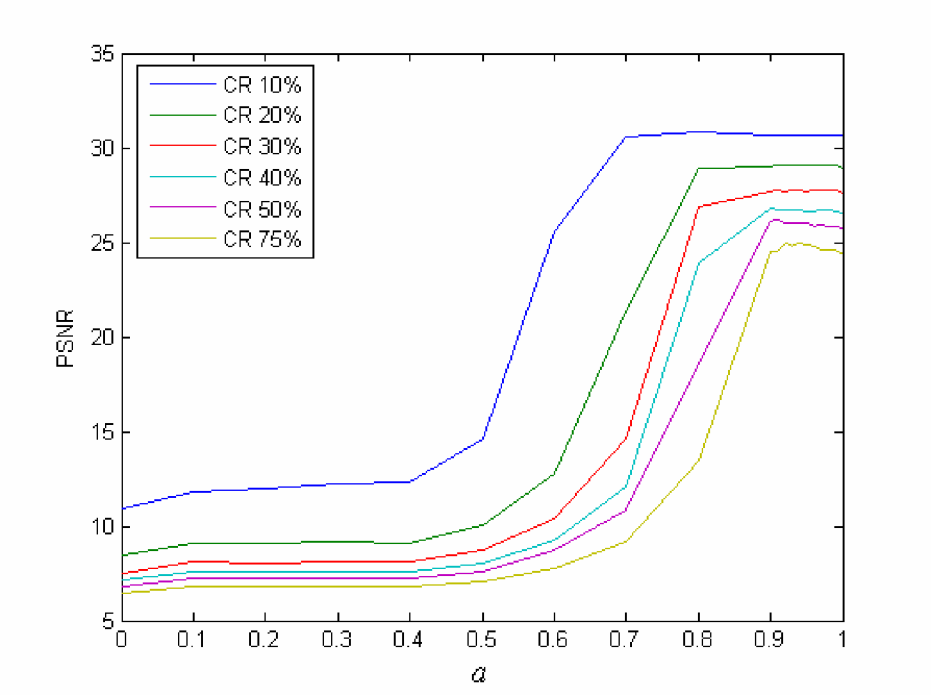

Figure-5.15: Fractional order *a* vs PSNR of Rice image for different CR using DFrCT.

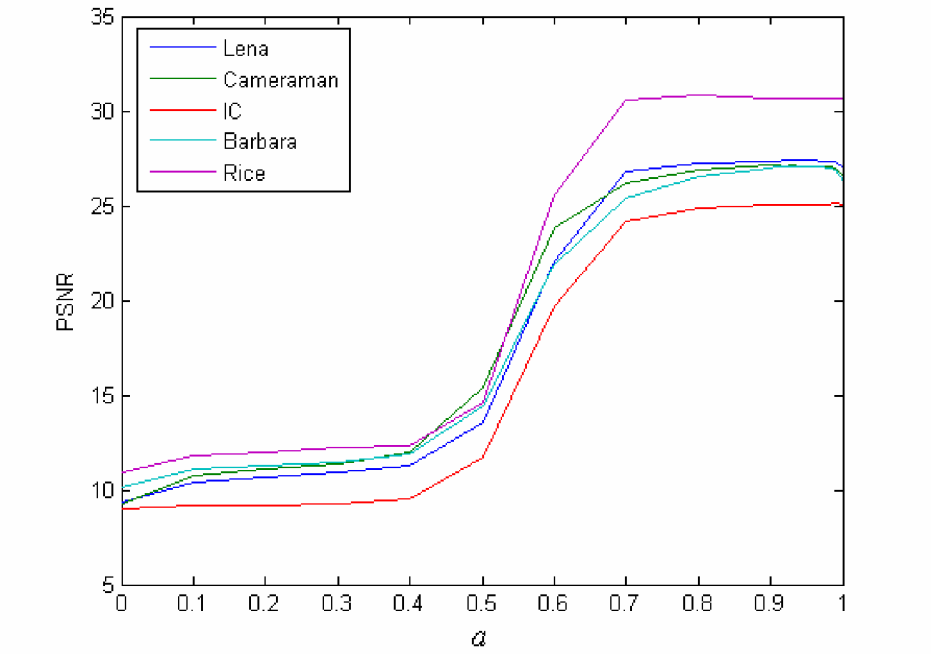

Figure-5.16: Fractional order *a* vs PSNR of different images at CR of 10% using DFrCT.

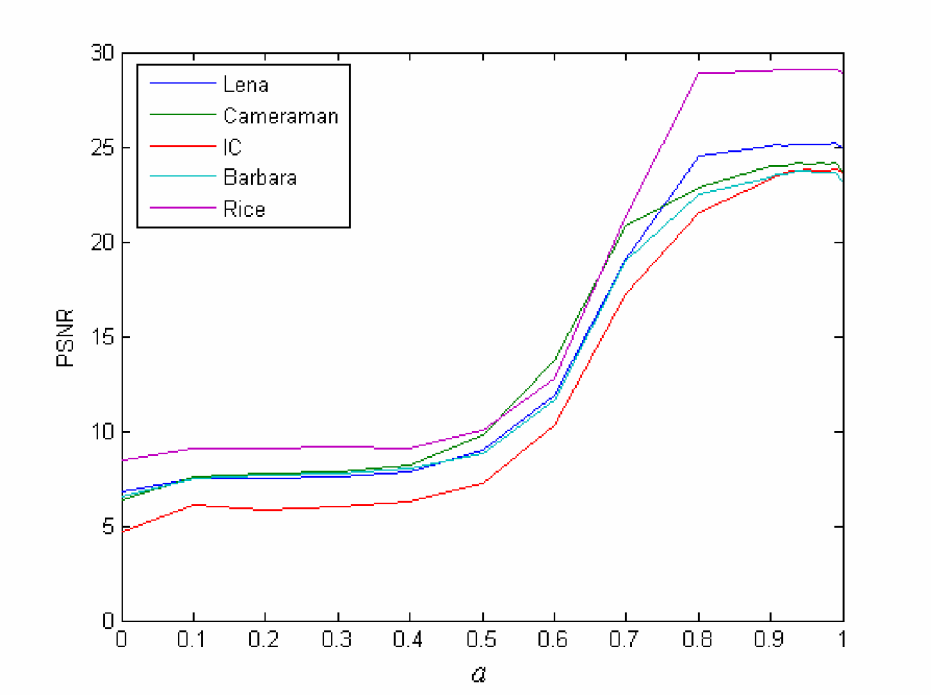

Figure-5.17: Fractional order *a* vs PSNR of different images at CR of 20% using DFrCT.

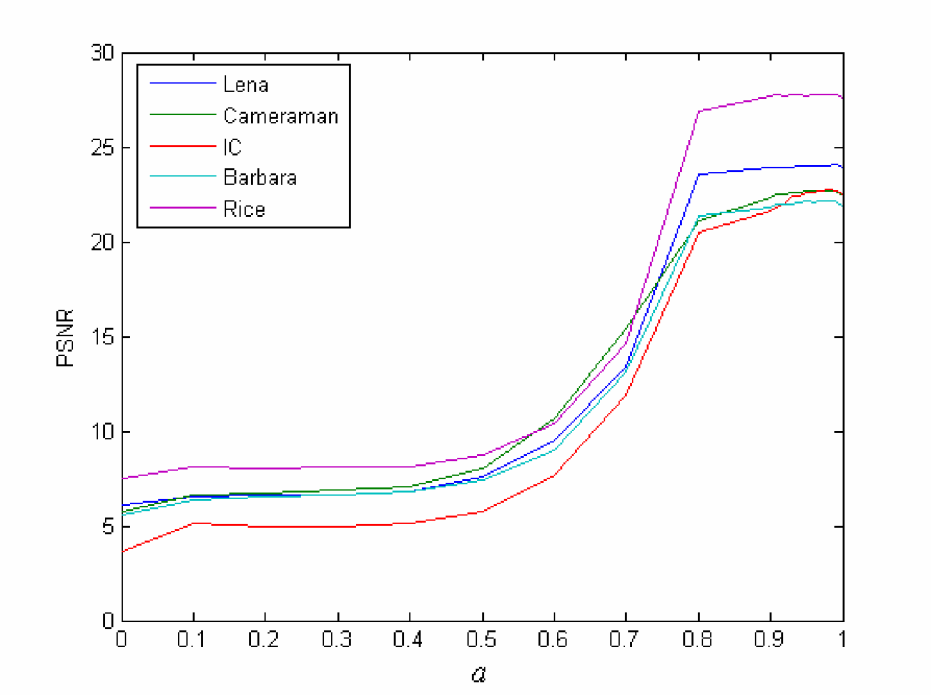

Figure-5.18: Fractional order *a* vs PSNR of different images at CR of 30% using DFrCT.

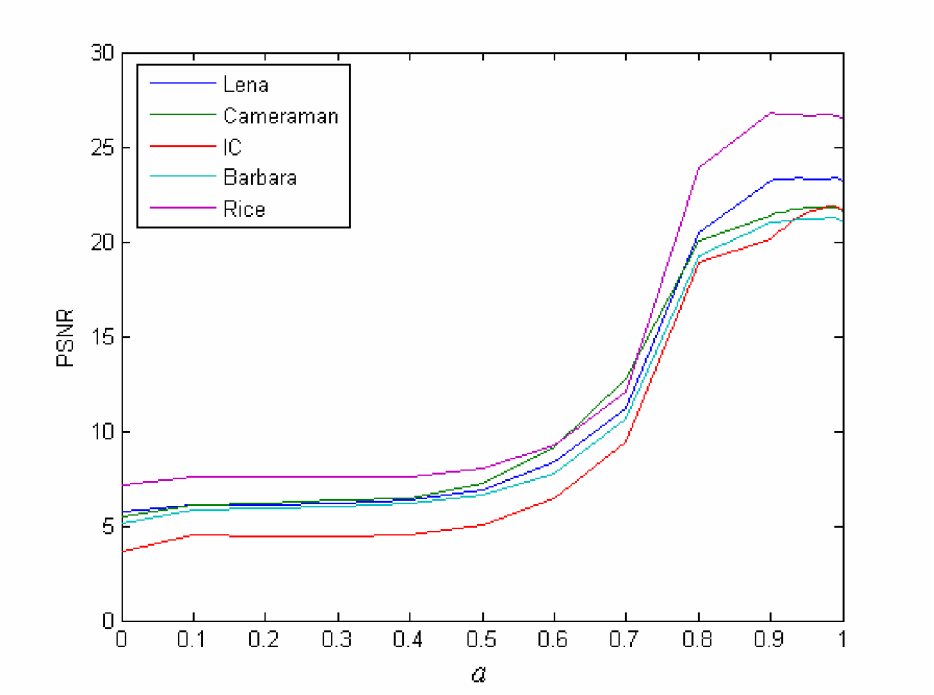

Figure-5.19: Fractional order *a* vs PSNR of different images at CR of 40% using DFrCT.

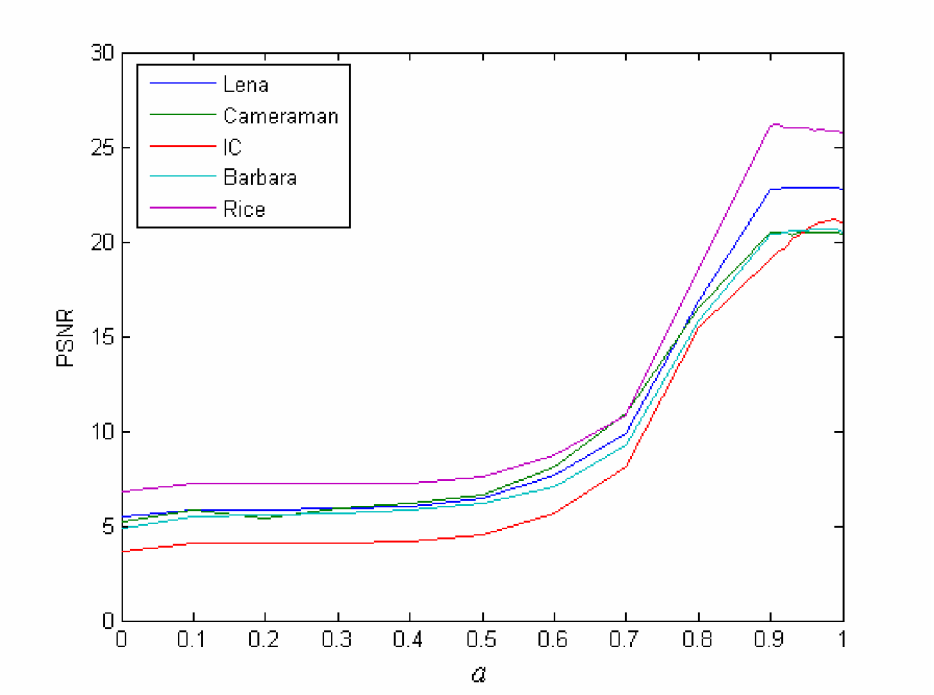

Figure-5.20: Fractional order *a* vs PSNR of different images at CR of 50% using DFrCT.

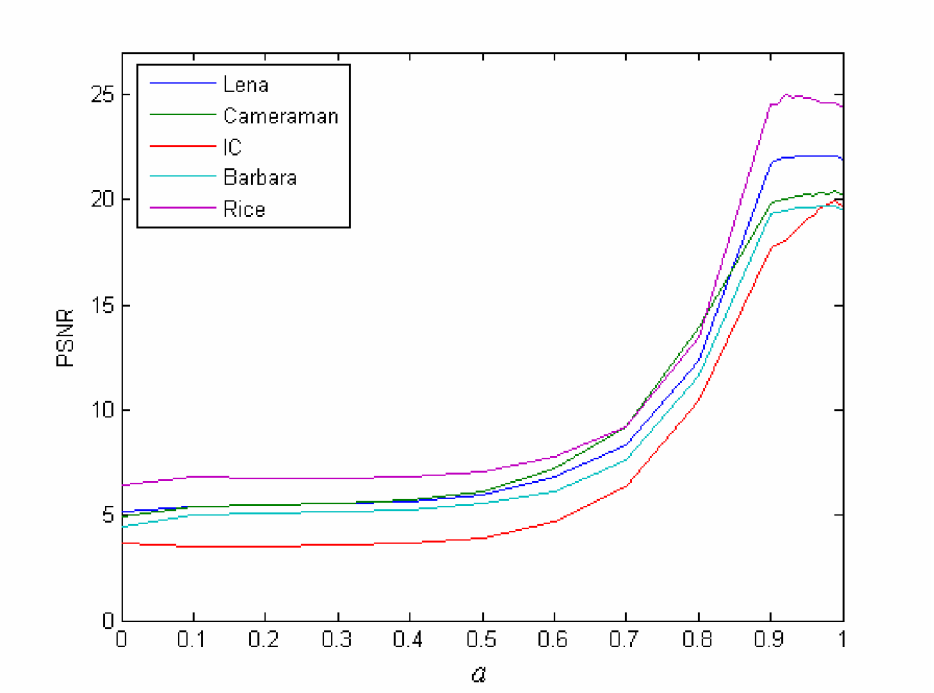

Figure-5.21: Fractional order *a* vs PSNR of different images at CR of 75% using DFrCT.

5.3.3 Comparative Performance Analysis of DFrFT and DFrCT in Image Compression

Lena, Cameraman, IC, Barbara and Rice have been selected to carry out the comparative performance analysis of DFrFT and DFrCT in image compression. The results are shown in Table-5.1 and Table–5.2. Using the data of Table–5.1 and Table–5.2 comparative plots between PSNR and CR using DFrFT and DFrCT have been plotted. The values of PSNR corresponding to optimum *a* have been used in these plots. These plots clearly reflect the superior performance of DFrFT over DFrCT.

Table 5.1 : MSE and PSNR of various images at optimum value of *a* for different compression ratios in case of DFrFT.

	LENA			BARBARA			CAMERAMAN			RICE			IC		
	a_{opt}	MSE	PSNR	a_{opt}	MSE	PSNR	a_{opt}	MSE	PSNR	a_{opt}	MSE	PSNR	a_{opt}	MSE	PSNR
CR 10%	0.95	1.3499	40.5469	0.94	5.7832	36.8319	0.97	0.0007	47.8538	0.95	6.0657	38.4368	0.97	0.0017	44.0418
CR 20%	0.91	5.5568	38.6579	0.90	33.5664	30.7666	0.91	1.7324	37.6164	0.91	8.0680	37.9580	0.95	4.9628	40.0849
CR 30%	0.91	28.2238	30.5168	0.90	100.1614	25.7415	0.93	30.8870	30.4611	0.91	32.4011	30.8283	0.94	16.0984	34.3545
CR 40%	0.91	26.8032	28.3714	0.92	103.3568	25.3873	0.92	42.0350	28.4819	0.91	43.0565	28.7661	0.93	7.4426	32.8239
CR 50%	0.92	74.2933	27.0405	0.91	155.4567	24.5672	0.91	99.9315	25.4873	0.91	54.6284	26.9971	0.95	0.5131	31.3103
CR 75%	0.93	97.8964	25.2155	0.91	339.7583	20.9184	0.97	180.7375	24.4061	0.92	122.2713	24.5787	0.94	44.8209	26.1115

Table 5.2 : MSE and PSNR of various images at optimum value of *a* for different compression ratios in case of DFrCT.

	LENA			BARBARA			CAMERAMAN			RICE			IC		
	a_{opt}	MSE	PSNR	a_{opt}	MSE	PSNR	a_{opt}	MSE	PSNR	a_{opt}	MSE	PSNR	a_{opt}	MSE	PSNR
CR 10%	0.94	91.6251	27.4230	0.94	98.7028	27.0998	0.93	98.4593	27.1111	0.91	43.0990	30.6987	0.99	156.4357	25.1003
CR 20%	0.96	153.8577	25.1723	0.95	214.8742	23.7214	0.94	194.4440	24.1557	0.91	62.0642	29.1140	0.95	210.9510	23.8018
CR 30%	0.99	197.8928	24.0793	0.97	307.5664	22.1641	0.99	272.5142	22.6896	0.97	84.1989	27.7905	0.98	270.0349	22.7293
CR 40%	0.99	234.1035	23.3495	0.98	379.4201	21.2524	0.99	331.8652	21.8339	0.98	106.9195	26.7528	0.99	327.2758	21.8938
CR 50%	0.99	261.9134	22.8620	0.98	432.8660	20.6801	0.99	345.5632	21.5674	0.91	122.8254	26.1448	0.99	383.6817	21.2036
CR 75%	0.94	313.8599	22.0750	0.99	543.0482	19.6952	0.99	464.3242	20.3753	0.92	161.5246	24.9566	0.99	512.2650	19.9487

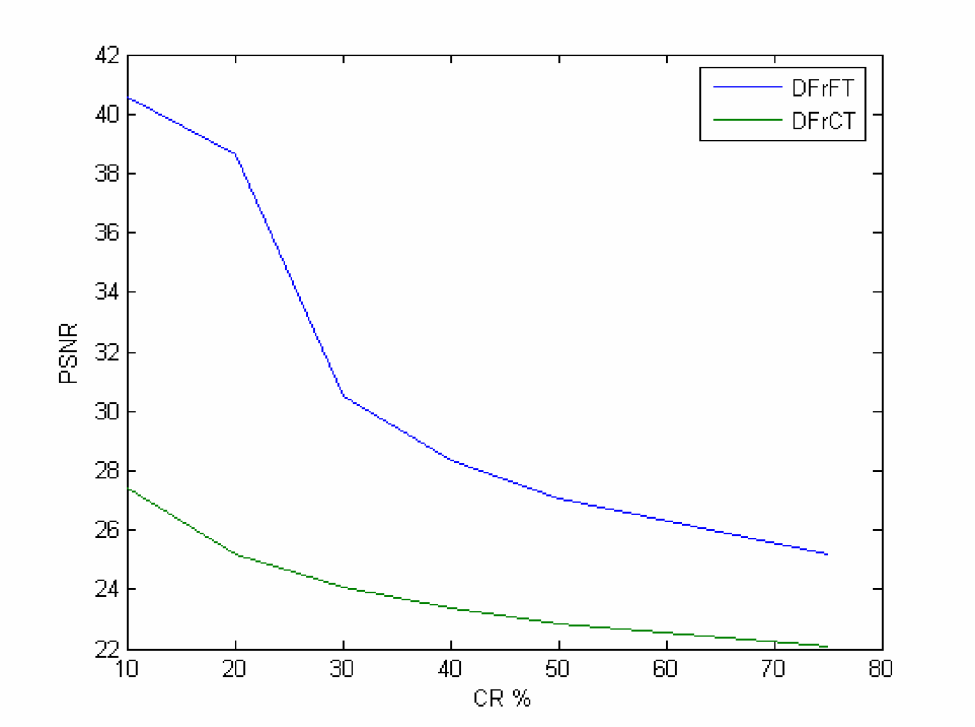

Figure-5.22: CR vs PSNR of Lena image for DFrFT and DFrCT.

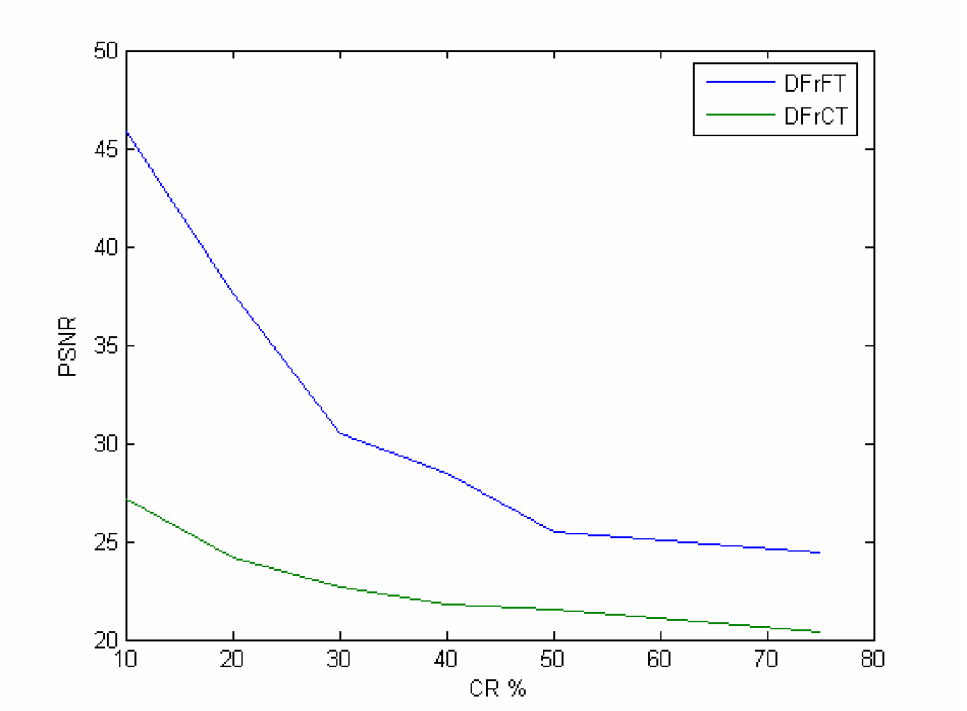

Figure-5.23: CR vs PSNR of Cameraman image for DFrFT and DFrCT.

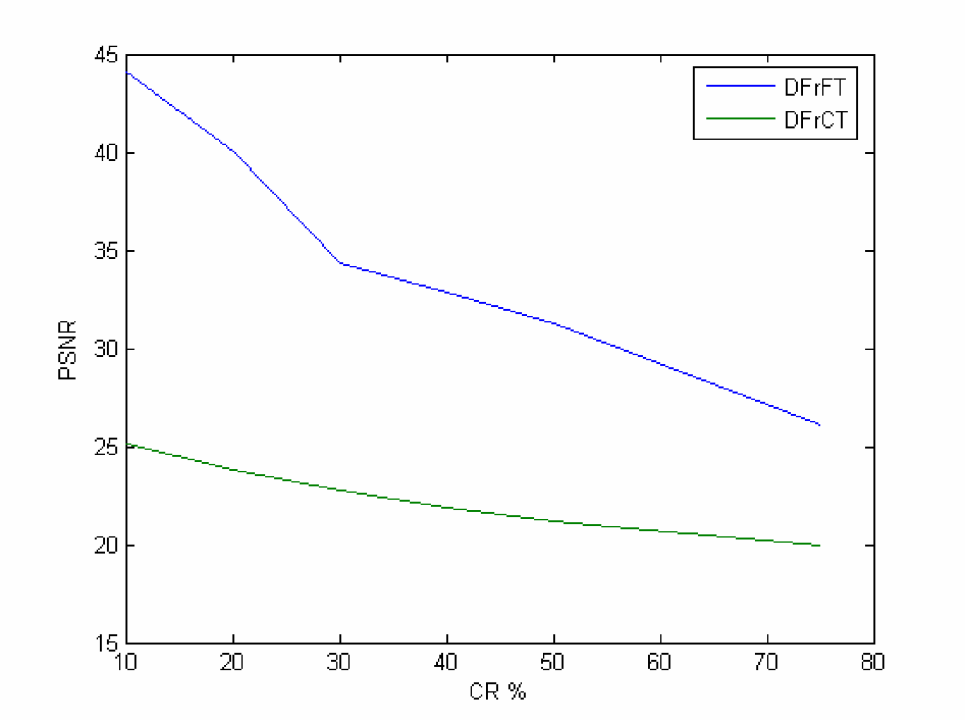

Figure-5.24: CR vs PSNR of IC image for DFrFT and DFrCT.

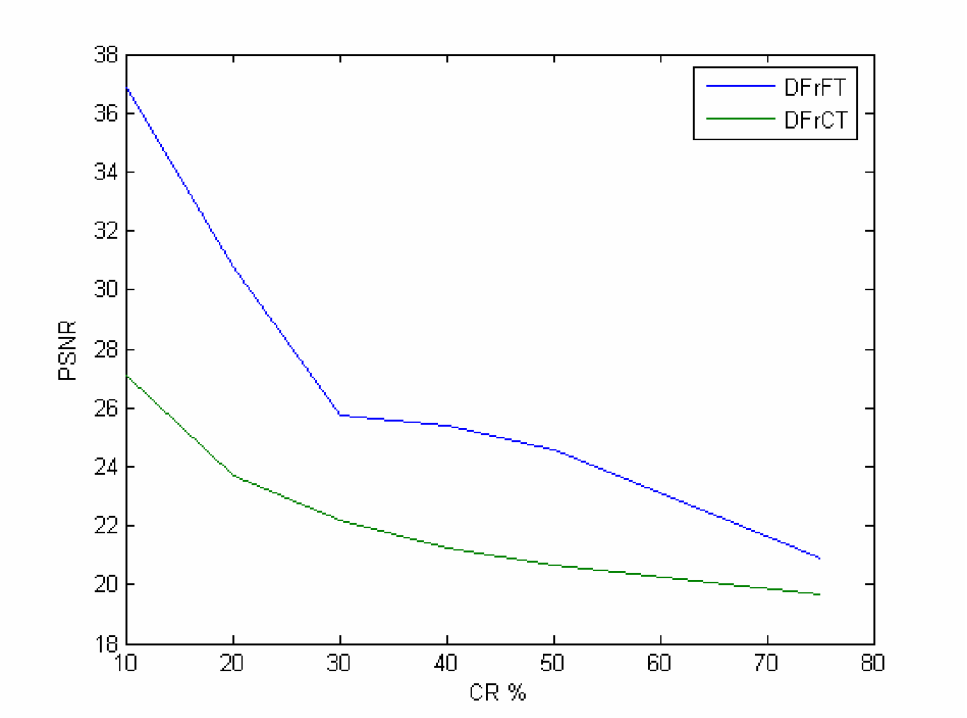

Figure-5.25: CR vs PSNR of Barbara image for DFrFT and DFrCT.

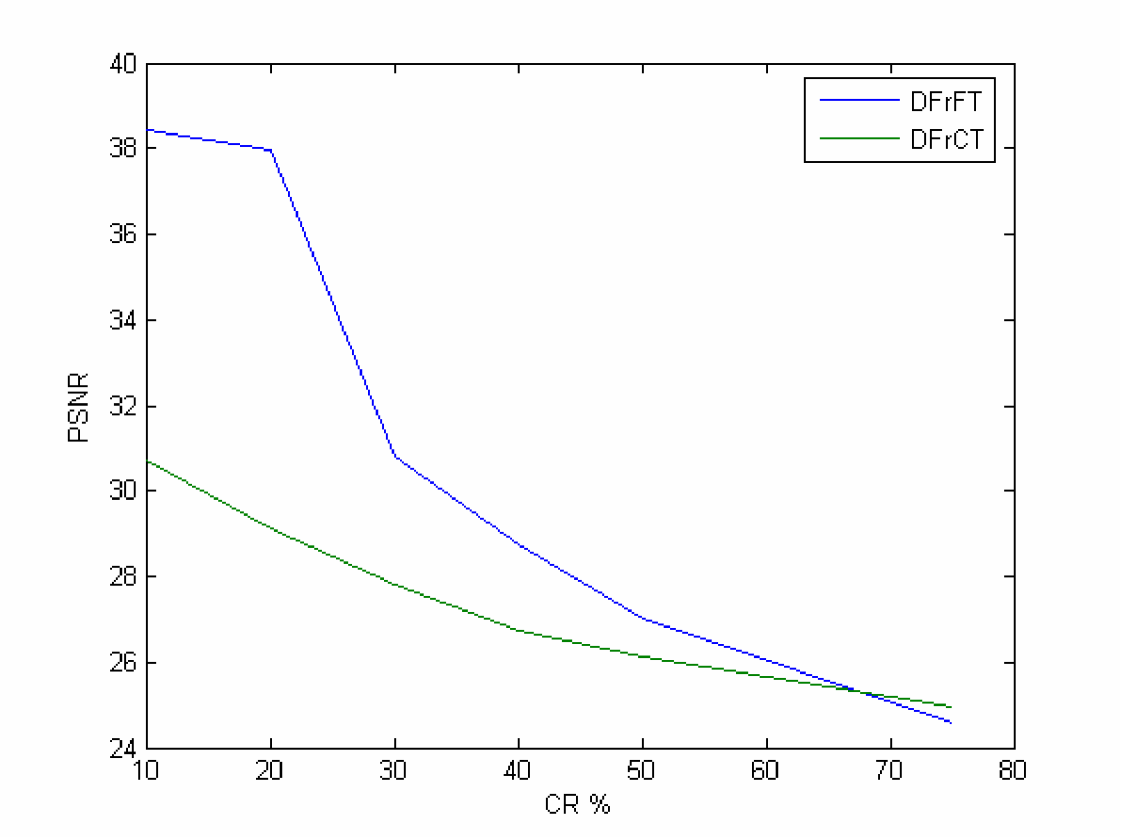

Figure-5.26: CR vs PSNR of Rice image for DFrFT and DFrCT.

The comparison of DFrFT, DFrCT and discrete wavelet transform (DWT) was also done for Barbara image using Daubechies wavelet. Figure-5.27 and Figure-5.28 shows PSNR vs CR and MSE vs CR for Barbara image using these three transforms. It is evident from here that for higher CR the DFrFT gives better PSNR than DWT and DFrCT.

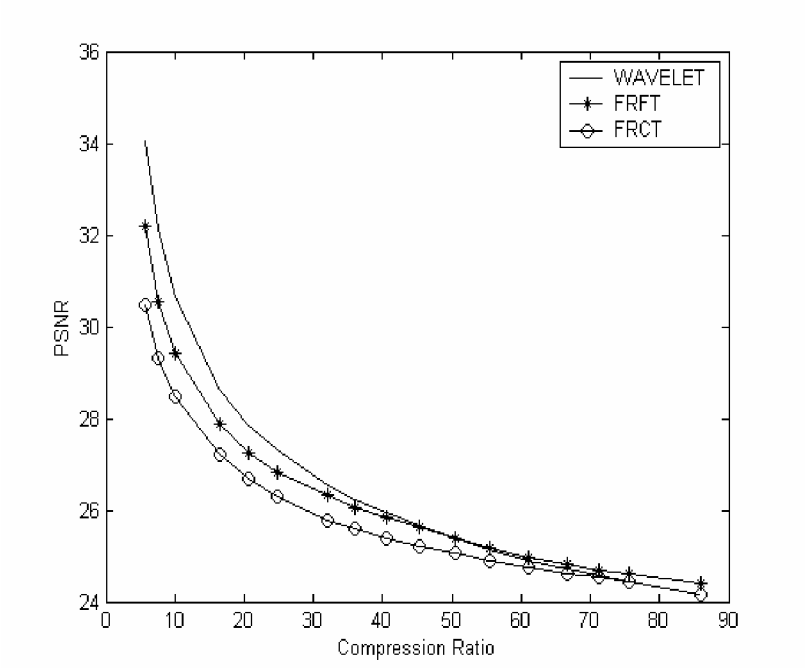

Figure-5.27: PSNR vs CR for Barbara image with 256 × 256 pixels.

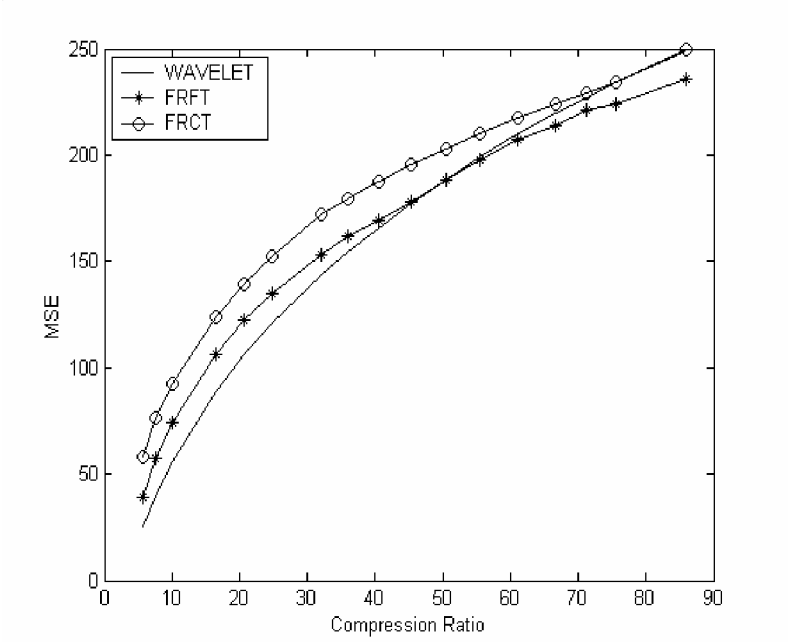

Figure-5.28: MSE vs CR for Barbara image with 256 × 256 pixels.

5.4 IMAGE ENCRYPTION

The explosive growth of information storage in computers and transmitting it via e-mail, as well as arrival of e-commerce, has led to cryptography as an essential feature of modern communications and data storage. Cryptography is the study of mathematical techniques related to aspects of information security such as confidentiality, data integrity, entity authentication and data origin authentication. Encryption is an area of cryptography involving the transformation of information into some gibberish form, thus ensuring privacy by keeping the information hidden from anyone for whom it is not intended - one may wish to encrypt files on a hard disk to prevent an intruder from reading them, or in a multi-user setting, encryption allows secure communication over an insecure channel. An example of this: A wishes to send a message to B so that no one else besides B can read it. A encrypts the message (plaintext) with an encryption key; the encrypted message (cipher text) is sent to B. B decrypts the cipher text with the decryption key and reads the message. An attacker, C, may either try to obtain the secret key or to recover the plaintext without using the secret key. In a secure cryptosystem, the plaintext cannot be recovered from the cipher text except by using the decryption key [104].

The most successful image encryption scheme is random phase encoding in fractional domain. In this thesis DFrCT with random phase masking is used as basic cryptographic tool. This double phase encoding scheme encrypts the image into different fractional orders and random distribution so that the unauthorized person by no means can access the image without keys. The significant feature of image encryption benefits from its extra degree of freedom that is provided by fractional orders. The performance of DFrCT for image encryption is compared with the reported results using DFrFT [75].

5.4.1 Image Encryption Using DFrCT

It has been very recently noticed that fractional transforms can be used in encryption of images [75]. In this encryption process cascaded multistage DFrCT with random phase filters have been utilized in between. The n-stage of DFrCT can provide n-dimensional extra keys indicated by the fractional orders. In case of two-dimensional DFrCT transform, there are two different fractional orders along x-axis and y-axis respectively. Such a system can have n-1 random phase filters, so that the total encryption keys can be increased to as many as 3n-1. Thus the security strength of the encryption keys may be greatly enhanced. For simplicity, the order *a* along x and y direction are taken to be same i.e. $\alpha_x = \alpha_y = \alpha$ and three stages of DFrCT are cascaded together. Thus in the intermediate planes two randomly encoded phase masks are used. Algorithm consists of two parts, encryption to encrypt image and decryption to retrieve image. The image encryption can be described as follows [75].

Let $f(x_0, y_0)$, a real valued two-dimensional data, denote the image that is to be encrypted. DFrCT is applied continuously three times to this data with the fractional orders α_1, α_2 and α_3, respectively. In the intermediate stages two random phase masks

$H_1(x_1, y_1) = [-i2\pi\phi_1(x_1, y_1)]$ and $H_2(x_2, y_2) = [-i2\pi\phi_2(x_2, y_2)]$ respectively are used.

where, $\phi_2(x_2, y_2)$ are randomly generated homogeneously distributed functions.

Thus the resultant transformed function $\psi(x, y)$ can be written as

$$\psi(x, y) = F_c^{\alpha 3}[\psi_2(x_2, y_2) H_2(x_2, y_2)] \tag{5.3}$$

with

$$\psi_2(x_2, y_2) = F_c^{\alpha 2}[\psi_1(x_1, y_1) H_1(x_1, y_{1)}] \tag{5.4}$$

and

$$\psi_1(x_1, y_1) = F_c^{\alpha 1}[f(x_0, y_0)]. \qquad (5.5)$$

The resultant transformed function $\psi(x, y)$ can be regarded as the encrypted image.

The decryption process is the reverse operation with respect to the encryption. Firstly, we take DFrCT of order -α_3 on the encrypted image$\psi(x, y)$ and after multiplying the random phase mask $H_2^*(x_2, y_2)$. The mid term function $\psi_2(x_2, y_2)$ is obtained. Then by performing DFrCT of order -α_2 on the function $\psi_2(x_2, y_2)$and multiplying it by the random phase mask $H_1^*(x_1, y_1)$, function $\psi_1(x_1, y_1)$is recovered. After another DFrCT of order -α_1 on the function$\psi_1(x_1, y_1)$, the original image $f(x_0, y_0)$is obtained. Here the random phase masks $H_1^*(x_1, y_1)$,and $H_2^*(x_2, y_2)$are the complex conjugates of $H_1(x_1, y_1)$and $H_2(x_2, y_2)$, respectively. Encryption and decryption results for Barbara, Cameraman, Lena and rice images are shown in Figure-5.29 to Figure-5.32 respectively.

To compare the performance of DFrCT with DFrFT for image encryption PSNRs of the images decrypted using wrong keys is compared. The value of PSNR is smaller for DFrCT, thus indicating better performance of DFrCT over DFrFT.

Figure-5.29(a): Original Barbara image.

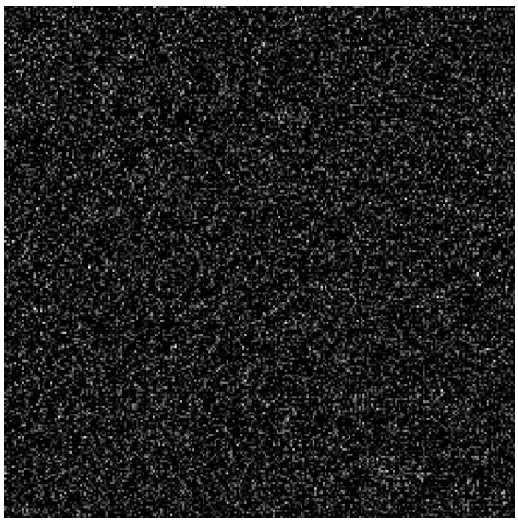

Figure-5.29(b): Encrypted Barbara image.

Figure-5.29(c): Decrypted image with right key.

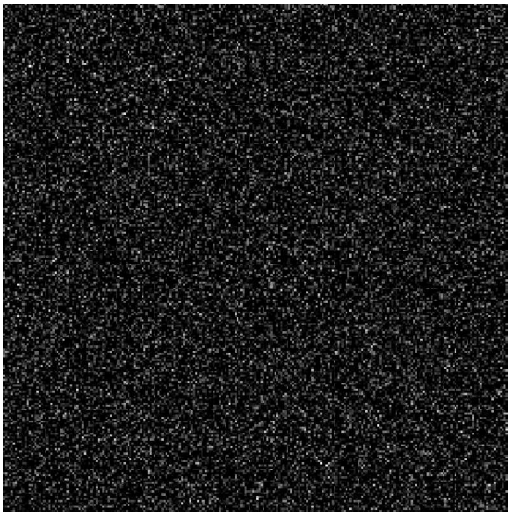

Figure-5.29(d): Decrypted Image with wrong key.

Figure-5.29: Simulation results of encryption for Barbara image using DFrCT.

Figure-5.30(a): Original Cameraman image.

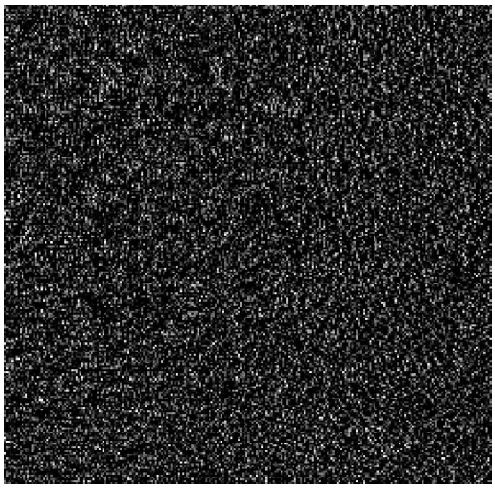

Figure-5.30(b): Encrypted Cameraman image.

Figure-5.30(c): Decrypted image with right key.

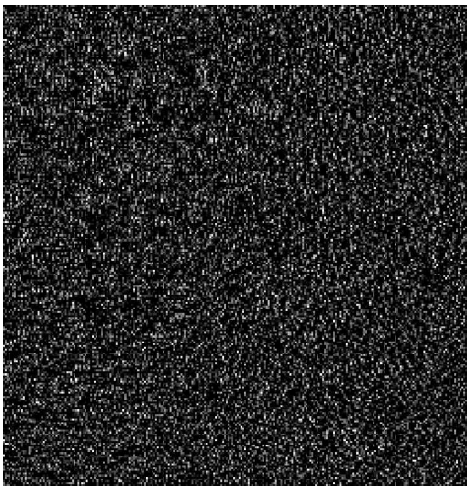

Figure-5.30(d): Decrypted Image with wrong key.

Figure-5.30: Simulation results of encryption for Cameraman image using DFrCT.

Figure-5.31(a): Original Lena image.

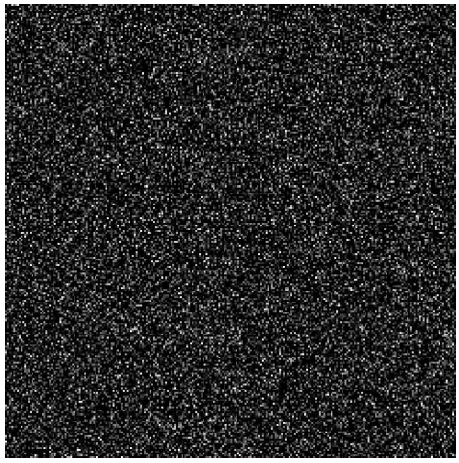

Figure-5.31(b): Encrypted Lena image.

Figure-5.31(c): Decrypted image with right key.

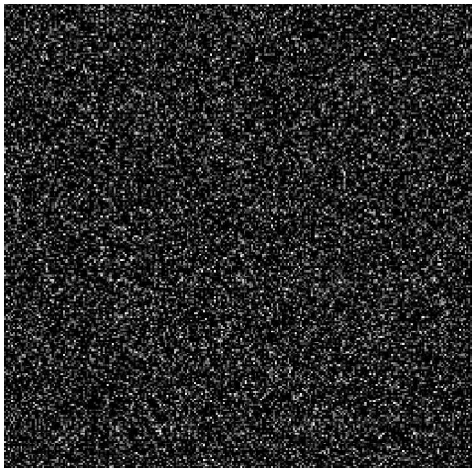

Figure-5.31(d): Decrypted Image with wrong key.

Figure-5.31: Simulation results of encryption for Lena image using DFrCT.

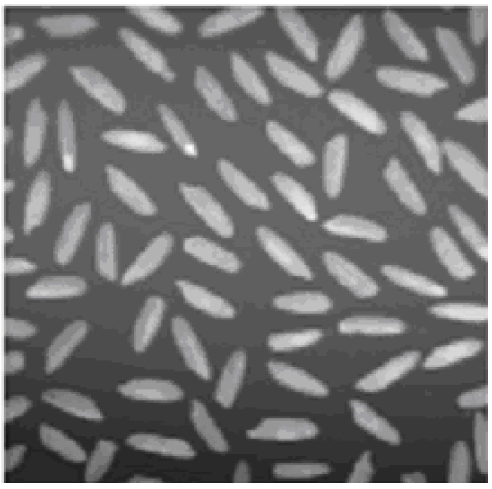

Figure-5.32(a): Original Rice image.

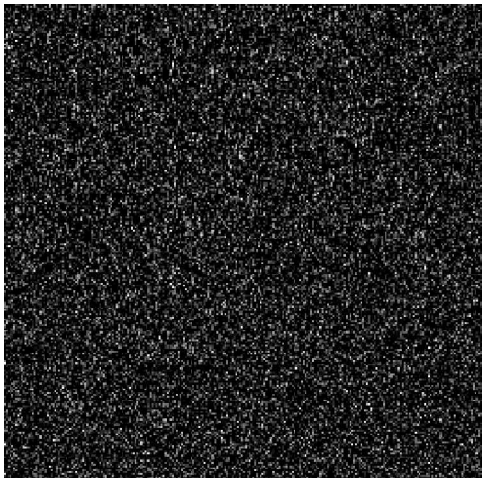

Figure-5.32(b): Encrypted Rice image.

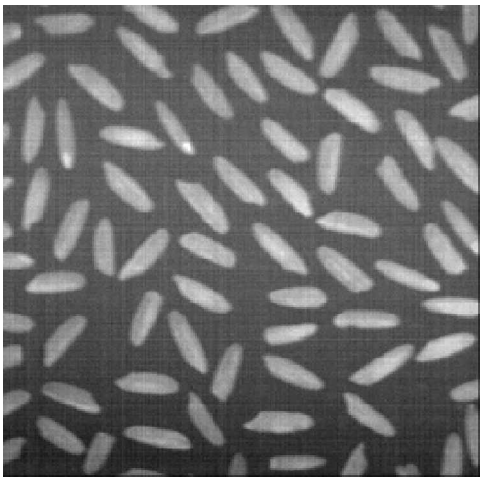

Figure-5.32(c): Decrypted image with right key.

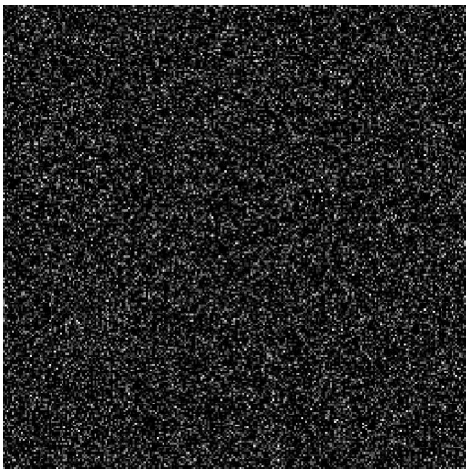

Figure-5.32(d): Decrypted Image with wrong key.

Figure-5.32: Simulation results of encryption for Rice image using DFrCT.

5.5 SUMMARY

In this chapter two fractional transform DFrFT and DFrCT have been examined for their suitability in image compressions and encryption applications. PSNR and MSE have been used as parameters to evaluate the performance of these transforms. Five different images have been selected to obtain the generalized results. Image compression has been performed for different CRs and the value of optimum *a* that provided best compression results for different CRs has been recorded. Performance of DFrFT is observed to be better than DFrCT for image compression whereas DFrCT provided better results than DFrFT for image encryption.

CHAPTER 6

CONCLUSIONS AND SCOPE FOR FUTURE WORK

6.1 CONCLUSIONS

FT has got significant applications in signal processing. This transform is used both for the signal analysis as well as processing. Apart from signal processing this transform has got multitude of applications in optics, acoustics, heat conduction and diffusion, and statistics. Looking into its versatility a generalized version of this transform, FrFT, has been devised. In this work FrFT has been studied thoroughly and is then applied in certain signal processing applications.

In this study, an effort is made to simplify the complexities associated with the understanding of FrFT and its evaluation. By way of studying the various definitions of FrFT, the software routines developed in Mathematica were listed. Simultaneously, their equivalence, which was established analytically earlier, is also confirmed with the help of simulation results. Similarly, the algorithms developed in MATLAB for calculation of DFrFT got examined by comparing the performance of six available classes of DFrFT. These algorithms are again cross examined by analyzing the fixed and variable window functions in fractional Fourier domain.

In the available literature, there are six definitions of FrFT, namely - linear integral transform, fractional powers of FT, rotation in the time-frequency plane, transformation of coordinate multiplication and differentiation operators, differential equation and hyper

differential operator. These definitions and their equivalence have been examined and verified with the help of simulation results. Usage of linear integral transform is given preference over others in this work, as its closed form expression offers a computational ease. Properties of FrFT have already been reported along with their analytical proofs. Some very basic properties of FrFT that include, integer orders, inverse, unitary, index additivity, Eigen function, Wigner distribution and Parseval have been proved graphically, in this work using Riemann and Hanning function. This is a contribution to the available literature on FrFT. These graphical proofs give a better understanding of these properties of FrFT.

Looking into the computational complexity involved in the FrFT a discrete version of FrFT, i.e., DFrFT, is required. Apart from fast and efficient computation, exactness of DFrFT, that requires satisfaction of FrFT properties, is mandatory. Six classes of DFrFT, direct form type, improved sampling type, linear combination type, group theory type, impulse train type, and eigenvector decomposition type, have been studied. A parameter, deviation factor, has been introduced and used to compare the performance of these DFrFTs. The eigenvector decomposition type DFrFT emerged as the best that puts least possible constraints on the signals, obeys maximum properties of FrFT, can be calculated for all orders with smallest deviation factor. Window functions have then being analyzed using eigenvector decomposition type DFrFT and variations in parameters of a window function like MSLL, SLFOR, and HMLW with DFrFT order a are reported. eigenvector type is thus selected for solving one and two-dimensional signal processing problems included in this study.

Optimal filtering and beamforming are the one-dimensional signal processing applications to which DFrFT has been applied. Application of FrFT for filtering of signals

that overlap in both time and frequency domains is well established. In mobile radio applications apart from this overlap fading is also associated with the received signals. Extending the concepts of optimal filtering, Rayleigh faded signals associated with Gaussian noise have been successfully filtered using DFrFT. MSE has been used as a parameter to determine the optimum fractional Fourier domain. A significant reduction in MSE as compared to the ordinary Fourier domain filtering has been achieved by using the concept of fractional domain. DFrFT offers this benefit at no additional cost and computational complexity.

Beamforming is a useful tool in sensor array signal processing. The FT based method of beamforming is not in use these days because of its inherent shortcoming to handle time varying signals, This shortcoming has been alleviated by using DFrFT. A significant improvement in performance of beamformer in optimum FrFT domain as compared to space and frequency domains has been achieved. The harmonic source used in this work is in far field emitting a frequency of 1 MHz. And the received signal is a Rayleigh faded with additive Gaussian noise. The criterion of optimization used is again minimization of MSE.

In two-dimensional category image compression and encryption have been selected to be accomplished efficiently using fractional transforms. DFrFT provided good results for image compression and performance of DFrCT proved to be better than DFrFT for image encryption. The images selected for this study are Lena, Barbara, Cameraman, Rice, and IC. MSE and PSNR are the parameters used to measure the performance of these transforms. The fractional order a of these transforms offered an extra degree of freedom in image compression. High compression ratio has been achieved by varying a. For same CR, DFrFT gives better decompressed image as compared to FT and DFrCT. The optimum value of a is

observed to be dependent both on the image and the CR. Using simulation results superiority of DFrFT has been established.

In this work DFrCT with random phase masking has been used as a basic cryptographic tool. This double phase encoding scheme encrypts the image into different fractional orders and random distribution so that the unauthorized person by no means can access the image without keys. The image encryption benefits from the extra degree of freedom provided by fractional orders. To compare the performance of DFrCT with DFrFT for image encryption, PSNRs of the images decrypted using wrong keys is compared. The value of PSNR is smaller for DFrCT, thus indicating better performance of DFrCT over DFrFT.

Finally, FrFT or DFrFT is an efficient, more flexible, versatile and powerful tool for application in one or two-dimensional signal processing.

6.2 FUTURE SCOPE OF WORK

After concluding this work following potential problems of significant relevance to signal processing community have emerged-

i) A fast and exact algorithm for DFrFT to be developed for efficient implementation of signal processing applications discussed in this work.

ii) Characterization of window functions establishing analytical relationship between FrFT order and window parameters.

iii) An analytical relationship that can provide the optimum FrFT order for filtering, beamforming and image compression applications.

Solution to these problems shall definitely prove to be beneficial for researchers as well as for the enhancement of technology.

REFERENCES

[1] R. N. Bracewell, "*The Fourier Transforms and Its Applications*", McGraw-Hill, New York, 1986.

[2] N. Wiener, "Hermitian Polynomials and Fourier Analysis", *J. Math Phys*, vol. 8, pp. 70-73, 1929.

[3] H.M. Ozaktas, Z. Zalevsky and M.A. Kutay, "*The Fractional Fourier Transform with Applications in Optics and Signal Processing*", John Wiley & Sons Ltd., New York, 2000.

[4] V. Namias, "The Fractional Order Fourier Transform and Its Applications to Quantum Mechanics", *J. Inst. Math Applications*, vol. 25, pp. 241-265, 1980.

[5] D.Mustard, "*Lie Group Imbeddings of the Fourier Transform*", School of Mathematics Preprint AM87/13, The University of new South Wales, Kensington, Australia, 1987.

[6] D.Mustard, "*The Fractional Fourier Transform and a New Uncertainty Principle*", School of Mathematics Preprint AM87/14, The University of new South Wales, Kensington, Australia, 1987.

[7] D..Mustard, "Lie Group Imbeddings of the Fourier Transform and a New Family of Uncertainty Principles", *Proc. Minicomp Harmonic Analysis Operator Algebra*, Australian National University, Canberra, pp. 211-222, 1987.

[8] E.U.Condon, "Immersion of the Fourier Transform in a Continuous Group of Functional Transformations", *Proc. National Academy Sciences*, vol. 23, pp. 158-164, 1937.

[9] V.Bragmann, "On a Hilbert Space of Analytic Functions and an Associated Integral Transform Part I", *Comm. Pure and Applied Mathematics*, vol. 14, pp. 187-214, 1961.

[10] D. Mendlovic D. and H.M. Ozaktas, "Fractional Fourier Transforms and their Optical Implementation-I", *J. Opt. Soc. of Am.-A*, vol. 10, no. 9, pp. 1875-1881, 1993.

[11] H. M. Ozaktas and D. Mendlovic, " Fractional Fourier Transforms and their Optical Implementation-II", *J. Opt. Soc. of Am.-A*, vol. 10, no. 12, pp. 2522-2531,1993.

[12] H.M. Ozaktas and D. Mendlovic, "Fourier Transforms of Fractional Order and their Optical Interpretation", *Optics Communications*, vol. 101, pp. 163-169, 1993.

[13] A.W. Lohmann, " Image Rotation, Wigner Rotation and The Fractional Fourier Transform", *J. Opt. Soc. of America A*, vol. 10, no. 10, pp. 2181-2186, 1993.

[14] H.M. Ozaktas and D. Mendlovic, " Fractional Fourier Transform as a Tool for Analyzing Beam Propagation and Spherical Mirror Resonators", *Optics Letters*, vol. 19, no. 21, pp. 1678-1680, 1994.

[15] H.M. Ozaktas and D. Mendlovic, "Fractional Fourier Optics", *J. Opt. Soc. of America A*, vol. 12, no. 4, pp. 743-751, 1995.

[16] D. Mendlovic D., H.M. Ozaktas and A.W. Lohmann, "Fractional Correlation", *Appl. Optics*, vol. 34, pp. 303-309, 1995.

[17] L.B. Almedia, "An Introduction to the Angular Fourier Transform", *Proc. IEEE Int. Conf Acoustics, Speech and Signal processing*, IEEE, Piscataway, New Jersey, pp. III-257-III-260, 1993.

[18] S.C. Pei and M.H. Yeh, "Discrete Fractional Fourier Transform", *Proc. IEEE Int. Symp Circuits Syst*., pp. 536-539, 1996.

[19] S.C. Pei and M.H. Yeh, "Improved Discrete Fractional Fourier Transforms", *Optics Letters*, vol. 22, no. 22, pp. 1047-1049, 1997.

[20] S.C. Pei, C.C. Tseng, M.H. Yeh and J.J. Shyu, "Discrete Fractional Hartley and Fourier Transforms", *IEEE Transactions on Circuits and Systems-II: Analog and Digital Signal Processing*, vol. 45, no. 6, pp. 665-675, 1998.

[21] S.C. Pei, C.C. Tseng and M.H. Yeh, "A New Discrete Fractional Fourier Transform Based on Constrained Eigendecomposition of DFT Matrix by Largrange Multiplier Method", *IEEE Transactions On Circuits and Systems—II: Analog and Digital Signal Processing*, vol. 46, No. 9, pp.1240-1246, 1999.

[22] S.C. Pei, M.H. Yeh and C.C. Tseng, "Discrete Fractional Fourier Transform Based on Orthogonal Projections", *IEEE Trans. on Signal Processing*, vol. 47, no. 2, pp. 1335-1348, 1999.

[23] S.C. Pei, M.H. Yeh and T.L. Luo, "Fractional Fourier Series Expansion for Finite Signals and Dual Extension to Discrete-Time Fractional Fourier Transform", *IEEE Trans. on Signal Processing*, vol. 47, no. 10, pp. 2883, 1999.

[24] S.C. Pei and J.J. Ding, "Closed Form Discrete Fractional and Affine Fractional Transforms", *IEEE Trans. on Signal Processing*, vol. 48, no. 5, pp. 1338-1353, 2000.

[25] S.C. Pei and J.J. Ding, "Two-Dimensional Affine Generalized Fractional Fourier Transform", *IEEE Trans. on Signal Processing*, vol. 49, no. 4, pp. 878-897, 2001.

[26] S.C. Pei and J.J. Ding, "Relations between Fractional Operations and Time-Frequency Distributions and Their Applications", *IEEE Trans. on Signal Processing*, vol. 49, no. 8, pp. 1638-1655, 2001.

[27] S.C. Pei and M.H. Yeh, "A Novel Method for Discrete Fractional Fourier Transform Computation", *IEEE International Symposium on Circuits and Systems*, Sydney, Australia, pp. II-585-II-588, 2001.

[28] G. Cariolario, T. Erseghe, P. Kraniauskas and N. Laurenti, "A Unified Framework for the Fractional Fourier Transform", *IEEE Trans. on Signal Processing*, vol. 46, no. 12, pp. 3206-3212, 1998.

[29] H.M. Ozaktas, O. Arikan, M.A. Kutay and G. Bozdagi, "Digital Computation of the Fractional Fourier Transforms", *IEEE Trans. on Signal Processing*, vol. 44, no. 9,pp. 2141-2150,1996.

[30] B. Santhanam and J.H. McClellan, "The Discrete Rotational Fourier Transform", *IEEE Trans. on Signal Processing*, vol. 42, pp. 994-998, 1996.

[31] M.S. Richman and T.W. Parks, "Understanding Discrete Rotations", *Proc. IEEE Inst. Conf. Accoustics, Speech, Signal Processing*, vol. 3, pp. 2057-2060, 1997.

[32] D.F. Huang and B.S. Chen, "A Multi-input Mmulti-output System Approach for the Computation of Discrete Fractional Fourier Transform", *Signal Processing*, vol. 80, pp. 1501-1513, 2000.

[33] Ç. Candan, M.A. Kutay and H.M. Ozaktas, "The Discrete Fractional Fourier Transform", *IEEE Trans. on Signal Processing*, vol. 48, no. 5, pp. 1329-1338, 2000.

[34] N.M. Atakishiyev, L. E. Vicent and K.B. Wolf ,"Continuous vs Discrete Fractional Fourier Transforms", *Journal of Computational and Applied Mathematics*, vol. 107, pp. 73-95, 1999.

[35] M.H. Yeh and S.C. Pei, "A Method for the Discrete Fractional Fourier Transform Computation", *IEEE Trans. on Signal Processing*, vol. 51, no. 3, pp. 889-891, 2003.

[36] A.Sachin, H.M.Ozaktas and D. Mendlovic, "Optical Implementation of Two-dimensional Fractional Fourier Transforms with Different Orders in Two Dimensions", *Optics Communications*, vol. 120, pp. 134-138, 1995.

[37] A. Sachin, H.M. Ozaktas and D. Mendlovic, "Optical Implementation of Two-dimensional Fractional Fourier Transform and Linear Canonical Transforms with Arbitrary Parameters", *Applied Optics*, vol. 37, no. 11, pp. 2130-2141, 1998.

[38] D. Mendlovic, Y. Bitran, R.G. Dorsch and A.W. Lohmann, "Optical Fractional Correlation: Experimental Results", *J. Opt. Soc. of America A*, vol. 12, no.8, pp. 1665-1670, 1995.

[39] H.M. Ozaktas and M.F. Erden, "Relationship Among Ray Optical Gaussian Beam and Fractional Fourier Transform Descriptions of First Order Optical System", *Optics Communications*, vol. 143, pp. 75-86, 1991

[40] H.M. Ozaktas and D. Mendlovic, "Fractional Fourier Transform as a Tool for Analyzing Beam Propagation and Spherical Mirror Resonators", *Optics Letters*, vol. 19, no. 21, pp. 1678-1680, 1994.

[41] H.M. Ozaktas and D. Mendlovic, "Fractional Fourier Optics", *J. Opt. Soc. of America A*, vol. 12, no. 4, pp. 743-751, 1995.

[42] J. Shamir and N. Cohen, "Roots and Power of Transformation in Optics", *J. Opt. Soc. of America A*, vol. 12, no. 11, pp. 2415-2423, November 1995.

[43] L.M.Bernardo and O.D.D.Soares, "Fractional Fourier Transforms and Optical System", *Optics Communications*, vol. 110, pp. 517-522, 1994.

[44] M.E. Marhic, "Roots of Identity Operator and Optics", *J. Opt. Soc. of America A*, vol.12, no. 7, pp. 1448-1459, 1995.

[45] M.F. Erden, H.M. Ozaktas, A. Sachin and D. Mendlovic, "Design of Dynamically Adjustable Anamoprhic Fractional Fourier Transform", *Optics Communications*, vol. 136, pp. 52-60, 1997.

[46] M. Nazarthy and J. Shamir, “First-Order Optics - A Canonocal Operator Representation: Lossless System”, *J. Opt. Soc. of America A*, vol. 72, no. 3, pp. 356-364, 1982.

[47] O. Aytur and H.M. Ozaktas, “Non-Orthognal Domains in Phase Space of Quantum Optics and Their Relation to Fractional Fourier Transforms”, *Optics Communications*, vol. 125, pp. 166-170, 1995.

[48] P. Pellat-finet and G. Bonnet, “Fractional Order Fourier Transform and Fourier Optics”, *Optics Communications*, vol. 111, pp. 141-154, 1994.

[49] P. Pellat-finet, “Fresnel Diffraction and the Fractional Order Fourier Transform”, *Optics Letters*, vol. 19, no. 18, pp. 1388-1393, 1994.

[50] S. Abe and J.T. Sheridan, “Optical Operations on Wave Functions as the Albenian Subgroups of the Special Affine Fourier Transformation”, *Optics Letters*, vol. 19, no. 22, pp. 1801-1803, 1994.

[51] A. W. Lohmann, “Image Rotation, Wigner Rotation and the Fractional Fourier Transform”, *J. Opt. Soc. of America A*, vol. 10, no. 10, pp. 2181-2186, 1993.

[52] A.W. Lohmann, Z. Zalevsky and D. Mendlovic, “Synthesis of Pattern Recognition Filters for Fractional Fourier Processing”, *Optics Communications*, vol. 128, pp. 199-204, 1996.

[53] H.M. Ozaktas and O. Arikan, “Fractional Fourier Domains”, *Signal Processing*, vol. 46, pp. 119-124, 1995.

[54] H.M.Ozaktas, “Repeated Fractional Fourier Domain Filtering Equivalent to Repeated Time and Frequency Domain Filtering”, *Signal Processing*, vol. 54, pp. 81-84, 1996.

[55] I.S.Yetik and A. Nehorai, “Beamforming Using the Fractional Fourier Transform”, *IEEE Trans. on Signal Processing*, vol. 51, no. 6, pp. 1663-1668, 2003.

[56] J.C. Wood and D.T.Barry, “Tomographic Time-Frequency Analysis and its Applications Towards Time-varying Filtering and Adaptive Kernel Design for Multicomponent Linear-FM Signals”, *IEEE Trans. on Signal Processing*, vol. 44, no. 8, pp. 2094-2104, 1994.

[57] L.M. Bernardo and O.D.D.Soares, “Fractional Fourier Transforms and Imaging", *J. Optical Soc. of America A*, vol. 11, no. 10, pp. 2622-2626, 1994.

[58] L. Yu, K.Q. Wang, C.F. Wang and D. Zhang, “Iris Verification based on Fractional Fourier Transform”, *Proc. First International Conf. on Machine Learning and Cybernetics*, Beijing, pp. 1470-1473, 2002.

[59] M..A. Kutay, H.M. Ozaktas, O. Arikan and L. Onural, “Optimal Filtering in Fractional Fourier Domain”, *IEEE Trans. on Signal Processing*, vol. 45, no. 3, pp. 1129- 1143, 1997.

[60] M.A. Kutay and H.M. Ozaktas, “Optimal Image Restoration with Fractional Fourier Transform”, *J. Optical Soc. of America A*, vol. 14, no. 10, pp. 825-833, 1998.

[61] M.A. Kutay, H. Ozaktas, H.M. Ozaktas and O. Arikan, “The Fractional Fourier Domain Decomposition”, *Signal Processing*, vol. 77, pp. 105-109, 1999.

[62] M. Beck, M.G. Raymer, I.A. Walmsley and V.Wong, "Chronocyclic Tomography for Measuring the Amplitude and Phase Structure of Optical Pulses", *Optics Letters*, vol. 18, no. 23, pp. 2041-2043, 1993.

[63] M.F. Edren, M.A. Kutay and H.M. Ozaktas, "Repeated Filtering in Consecutive Fractional Fourier Domains and its Applications to Signal Restoration", *IEEE Trans. on Signal Processing*, vol. 47, no. 5, pp. 1458-1462, 1999.

[64] O. Akay and G.F. Boudreaux-bastel, "Fractional Convolution and Correlation via Operator methods and an Application to Detection of Linear FM Signals", *IEEE Trans. on Signal Processing*, vol. 49, no. 5, pp. 979-993, 2001.

[65] P.W. Hawkes, "*Advances on Imaging and Electron Physics*", Academic Press, vol. 106, pp. 239-291, 1999.

[66] S. Shinde and V. M. Gadre, "An Uncertainty Principle for Real Signals in the Fractional Fourier Transform Domain", *IEEE Trans. on Signal Processing*, vol. 49, no. 11, pp. 2545-2548, 2001.

[67] R.G. Dorsh, A.W. Lohmann, Y. Bitran D. Mendlovic and H.M. Ozaktas, "Chirp Filtering in Fractional Fourier Domain", *Applied Optics*, vol. 33, no. 32, pp. 7599-7602, 1994.

[68] T. Ran, P. Xianjun, Z. Xinghao and W.Yue, "Detection and Estimation of Moving Targets Based on Fractional Fourier Transform", *Proc ICSP'02*, pp. 102-105, 2002

[69] X.G.Xia, "On Bandlimited Signals with Fractional Fourier Transform", *IEEE Signal Processing Letters*, vol. 3, no.3, pp. 72-74, 1996.

[70] Z. Zaievsky and D. Mendlovic, "Fractional Wiener Filter", Applied Optics, vol. 35, no. 5, pp. 3930-3935, 1996

[71] McBride A.C. and Keer F.H., "On Namia's Fractional Fourier Transform", *IMA J. Appl. Math*., vol. 239, pp. 159-175, 1987.

[72] H.M. Ozaktas, B. Billur, D. Mendlovic, and L. Onural, "Convol.ution, Filtering and Multiplexing in Fractional Domains and their Relation to Chirp and Wavelet Transforms", *J. Opt. Soc. of Am.-A*, vol. 11, no. 2, pp. 547-559, 1994.

[73] S. N. Sharma, R. Saxena and S.C. Saxena, " Sharpening the Response of a FIR Filter using Fractional Fourier Transform", *in press Journal of Indian Institute of Sciences*, Bangalore.

[74] I. S. Yetik, M. A . Kutay, H. M. Ozaktas, "Image Representation and Compression with the Fractional Fourier Transform", *Opt. Communications*, vol. 197, pp. 275-278, 2001.

[75] S. Liu, L.Yu and B. Zhu, "Optical Image Encryption by Cascaded Fractional Fourier Transforms with Random Phase Filtering", *Opt. Communications*, vol. 187, pp. 57-63, 2001.

[76] I. Djurovic, S. Stankovic and I. Pitas, "Digital Watermarking in the Fractional Fourier Transformation Domain", *Journal of Network and Computer Applications*, vol. 24, pp. 167-173, 2001.

[77] A. Sachin, H.M. Ozaktas and D. Mendlovic, "Non-separable Two-dimensional Fractional Fourier Transform", *Applied Optics*, vol. 37, pp. 5444-5453, 1998.

[78] L.B. Almedia, "The Fractional Fourier Transform and Time-frequency Representations", *IEEE Trans. on Signal Processing*, vol. 42, pp. 3084-3091, 1994.

[79] K. B. Wolf, "*Integral Transforms in Science and Engineering*", Plenum Press, New York, 1979.

[80] B. Yurke, W. Schieich and D. F. Walls, "Quantum Superpositions Generated by Quantum Nondemolition Measurements", *Phy. Rev. A*, vol. 42, 1703-1711, 1990.

[81] A. Yariv, "*Quantum Electronics*" third edition, Wiley, New York, 1989.

[82] Alieva T. and Bastiaans M.J., "Fractional Cosine and Sine Transforms in Relation to the Fractional Fourier & Hartley Transforms", *IEEE International Symposium on Signal Processing and its applications*, Paris, France, pp. 561-564, 2003.

[83] M.A. Poletti, "The Applications of Linearly Swept Frequency Measurements" *Journal of the Acoustic Scoiety of America*, vol. 84, pp. 599-610, 1988.

[84] M.S. Richman, T.W. Parks and R.G. Shenoy, "Discrete-time Discrete-frequency Time-frequency Representation", *Proc Int. Conf. Acoustic Speech and Signal Processing*, 1995.

[85] J. C. O'Neill and W. J. Williams, " New Properties for Discrete, Bilinear Time-frequency Distributions" *Proc. Third International Symposium on Time-Frequency and Time- Scale Analysis*, 1996.

[86] O. Arikan, M.A. Kutay, H.M. Ozaktas O.K. Akdemir, "The Discrete Fractional Fourier Transform", *IEEE Trans. on Signal Processing*, vol. 48, no. 5, pp.1329-1337,2000.

[87] A. Papoulis, "Signal Analysis", McGraw Hill, New York, 1977.

[88] Dickinson B.W. and Steiglitz K., "Eigenvector and Functions of the Discrete Fourier Transform", *IEEE Trans. on Acoustics, Speech and Signal Processing*, vol. ASSP-30, no. 1, pp. 25-31, 1982.

[89] McClellan J.H. and Parks T.W., "Eigenvalue and Eigenvector Decomposition of Discrete Fourier Transforms", *IEEE Trans. on Audio and Electroacoustics*, vol. AU-20, no.1, pp. 66-74, 1972.

[90] G. Clincotti, F. Gori and M Santarsiero, "Generalised Self-Fourier Functions" *J. Phys*., vol. 25, pp. 1191-1194, 1992.

[91] G. Sansone, *Orthogonal functions*, Interscience, New York, 1959.

[92] S.H. Friedberg, A.J. Insel and L.E. Spence, *Linear Algebra*, Prentice Hall, Englewoods Cliffs, New Jersy, 1989.

[93] G. H. Golub and C.F. Van Loan, *Matrix Computations*, Johns Hopkins Univ. Press, Baltimore, MD, 1989.

[94] A. Bultheel and H. Matreinez-Sulbaran, " *Recent Developments in the Theory of the Fractional Fourier and Linear Canonical Transforms*", Preprint, 2004.

[95] E. C. Ifeachor, *Digital Signal Processing: A Practical Approach*, Pearson Edu., Singapore, 2003.

[96] F. H. Harris, " On the use of Window for Harmonic Analysis with the Discrete Fourier Transform", *Proceedings of IEEE*, vol. 66, no. 1, pp. 51-83, 1978.

[97] J. K. Gautam, A. Kumar and R. Saxena, "Window: A Tool in Signal Processing", *IETE Technical Review*, vol.12, no. 3, pp. 217-226, 1995.

[98] F. L. Lewis, *Optimal Estimation*, John Wiley and Sons Inc., New York.

[99] S. Haykins, *Adaptive Filter Theory*, Pearson Education (Singapore) Pte. Ltd., India Branch, Delhi, 2002.

[100] T. S. Rappaport, *Wireless Communications: Principles and Practices*, Pearson Education (Singapore) Pte. Ltd., India Branch, Delhi, 2003.

[101] K. Fecher, *Wireless Digital Communications: Modulation and Spread Spectrum Applications*, Prentice Hall of India, New Delhi, 2001.

[102] A. K. Jain, *Fundamentals of Digital Image Processing*, Pearson Education (Singapore) Pte. Ltd., Delhi, 2004.

[103] R. C. Gonzalez and R. E. Woods, *Digital Image Processing*, Pearson Education (Singapore) Pte. Ltd., Delhi, 2004.

[104] B. Schneier, *Applied Cryptography*, John Wiley and Sons (Asia) Pvt. Ltd., Singapore, 1996.

LIST OF RESEARCH PAPERS PUBLISHED AND PRESENTED

[P.1] "Fractional Fourier Transform based Beamforming for Next Generation Wireless Communication Systems", *IETE Technical Review*, vol. 21, no. 5, pp. 357-366, 2004.

[P.2] "Fractional Fourier transform : A Novel Tool for Signal Processing", *Journal of Indian Institute of Sciences*, vol. 85, no. 1, pp. 11-26, 2005.

[P.3] "Optimal Beamforming for Rayleigh-faded Time-frequency Channels using Fractional Fourier Transform", *Journal of Indian Institute of Sciences*, vol. 85, no. 1, pp. 27-38, 2005.

[P.4] "Fractional Fourier Transform: A Review" Revised and submitted to *IETE Journal of Research*.

[P.5] "Image Compression by Using Fractional Transforms" submitted to *IEEE Signal Processing Letters*.

[P.6] "Rectangular and Triangular Line Source Amplitude Distribution in Fractional Fourier Domain", *International radar symposium*, India, pp. 308-314, Dec. 3-5, 2003, Bangalore.

[P.7] "A Review on Discrete Fractional Cosine Transforms", pp. 204-206, *National Conference on Electronic Circuits and Communication Systems*, (*ECCS-2004*) Sept. 23-24, 2004, Thapar Institute of Engineering and Technology, Patiala.

[P.8] "Rectangular And Bartlett Window In Fractional Fourier Domain", *National Conference On Mathematical And Computer Applications In Science And*

Engineering (*MCASE –2003*) January 27-28, 2003, Thapar Institute of Engineering and Technology (Deemed University), Patiala.

[P.9] "Fractional Fourier Transforms –An Overview", *National Conference on Signals, Systems And Security* (*NCSSS*) 1-2 March, 2002, PSG College of Technology Coimbatore, TamilNadu.

[P.10] "Discrete Fractional Fourier Transform (DFRFT) – A Tool For Discrete Time Signals ", *National Conference on Mathematical And Statistical Techniques* (*NCMST –2001*) December 6-8, 2001, Thapar Institute of Engineering and Technology (Deemed University), Patiala.